Role of Na+ and K+ in Enzyme Function

Michael J. Page and Enrico Di Cera

Physiol Rev 86:1049-1092, 2006. doi:10.1152/physrev.00008.2006

Physiol Rev 86: 1049–1092, 2006;
doi:10.1152/physrev.00008.2006.

Role of Na^+ and K^+ in Enzyme Function

MICHAEL J. PAGE AND ENRICO DI CERA

Department of Biochemistry and Molecular Biophysics, Washington University School of Medicine, St. Louis, Missouri

Page, Michael J., and Enrico Di Cera. Role of Na^+ and K^+ in Enzyme Function. *Physiol Rev* 86: 1049–1092, 2006; doi:10.1152/physrev.00008.2006.—Metal complexation is a key mediator or modifier of enzyme structure and function. In addition to divalent and polyvalent metals, group IA metals Na^+ and K^+ play important and specific roles that assist function of biological macromolecules. We examine the diversity of monovalent cation (M^+)-activated enzymes by first comparing coordination in small molecules followed by a discussion of theoretical and practical aspects. Select examples of enzymes that utilize M^+ as a cofactor (type I) or allosteric effector (type II) illustrate the structural basis of activation by Na^+ and K^+, along with unexpected connections with ion transporters. Kinetic expressions are derived for the analysis of type I and type II activation. In conclusion, we address evolutionary implications of Na^+ binding in the trypsin-like proteases of vertebrate blood coagulation. From this analysis, M^+ complexation has the potential to be an efficient regulator of enzyme catalysis and stability and offers novel strategies for protein engineering to improve enzyme function.

I. INTRODUCTION

Regulation of activity through metal ion complexation plays a key role in many enzyme-catalyzed reactions. Molecular mechanisms of metal ion coordination and their effects are an important aspect in the characterization of biological macromolecules. Over one-third of known proteins are metalloproteins (46, 154, 320). Conceptual associations with protein-metal complexes tend to favor divalent metals. Examples of Fe^{2+} involvement in redox cycles, Ca^{2+} in structural stability, or Zn^{2+} as electrophile in an enzyme-catalyzed reaction readily come to mind. Significance of divalent metals in protein structure and function has been reviewed in detail (11, 89, 284).

Indeed, many bioinorganic chemistry textbooks are devoted to the description of divalent and polyvalent ions with monovalent cations (M^+) discussed only in the context of membrane potentials. However, a large body of evidence suggests that group I alkali metals Na^+ and K^+ play important roles other than nonspecific ionic buffering agents or mediators of solute exchange and transport. Na^+ is the most abundant metal in human plasma, the backbone of biological fluids, and its occurrence mirrors that found in environmental liquids (Table 1). Molecular evolution has driven incorporation of selective M^+ binding sites to enhance activity, diversity, and/or stability of many enzymes.

A diverse literature spanning more than six decades of scientific investigation directly or indirectly involving M^+-activated enzymes is summarized in this review. The work builds on our recent classification of M^+-activated enzymes (70). Rapid accumulation of macromolecular structures of Na^+- or K^+-bound protein complexes over the past decade permits a broad discussion. For brevity, we focus on enzymes characterized in both kinetic and structural detail. A brief introduction to ion homeostasis provides biological context (sect. I) and is followed by inspection of the chemical properties and coordination of M^+s (sect. II). Emphasis on structural aspects of M^+ coordination in small molecules and larger biological macromolecules highlights similarities and differences observed in the diverse group of M^+-activated enzymes. Theoretical considerations of M^+ activation are dealt with in detail (sect. III). Select examples of type I and II M^+-activated enzymes are used to illustrate key features of processes involved. Focus is placed on Na^+ biochemistry with comparisons drawn to K^+ and divalent cations (M^{2+}). The role of Na^+ on the structure, function, and evolution of serine proteases involved in vertebrate blood coagulation is examined, with focus on the allosteric regulation of thrombin (sect. IV). We conclude with the broader implications on the molecular evolution of M^+-activated enzymes and future perspectives in M^+ biochemistry and protein engineering (sect. V) with a final summary (sect. VI).

TABLE 1. *Inorganic ion content of human plasma, intracellular cytosol, and seawater*

Ion	Concentration, mM		
	Plasma	Cytosol	Seawater
Na^+	135–146	25–35	480
Cl^-	98–108	50–60	559
HCO_3^-	23–31	4–12	2.0
Mg^{2+}	0.8–1.4	4–20	54.0
K^+	3.5–5.2	130–145	10.4
Ca^{2+}	2.1–2.7	<0.01	10.6
PO_4^{2-}	0.7–1.4	90–110	<0.1

Data are from References 14, 21, 100, and 287.

A. Historical Perspective

Earliest evidence for M^+ activation of enzymes was provided by Boyer et al. (30). Further work led to a now classic paper by Kachmar and Boyer (165) showing the absolute requirement of K^+ by an enzyme, pyruvate kinase. Earlier descriptions also demonstrated Na^+-dependent catalytic rate enhancement in β-galactosidase (53). After these discoveries, many enzymes were observed to display increased activity in the presence of M^+ (314). For numerous systems, selectivity for a particular M^+ is low, and a weak increase in activity is achieved by larger cations (i.e., K^+, Rb^+, or NH_4^+). These effects can be understood in terms of kosmotropic effects on the water structure surrounding the protein. Selective activation by K^+ occurs in many instances, yet fewer enzymes have been identified to be selective for Na^+. Dichotomy in the activation profiles likely arises from the unequal distribution of Na^+ and K^+ in cells and extracellular fluids (Table 1). Involvement of M^+ in allosteric regulation is possible through sufficient charge density to drive conformational changes and formation of stable complexes with biological molecules. However, charge density is not adequate to be the causative agent of catalysis as commonly observed with M^{2+}. The biological context of the group IA alkali metals (Li^+, Na^+, K^+, Rb^+, Cs^+) provides the beginning of our discussion.

Sodium chloride lies at the heart of human biology and the roots of human civilization. Abundance or absence of this simple compound has had profound effects on human health and has provided a casus belli in many important milestones in the history of man (for an excellent historical account, see Ref. 182). Several initial forms of economics were based on salt rather than metal coinage and the words *salary* and *soldier* are derived from the Latin *sal* for salt, as is *salus*, the Latin word for "health." Industrial advances have largely eliminated salt as a limiting component of human nutrition or resource. In contrast, current farming practices are leading to significant Na^+ accumulation in soil (94) and have fostered the development of saline-tolerant plants (378). Of the group IA metals, only Na^+ and K^+ are essential for human nutrition despite abundance of Rb^+ and Li^+ in the earth crust. Curiously, Li^+ is noted to be an essential nutrient in rodents and goats. Human health is negatively influenced by excess sodium intake that may result in hypertension and other health problems (69, 101, 212). Naturally occurring organisms have adapted to concentrations of Na^+ far exceeding that of human tolerance.

B. Halophilic and Halotolerant Adaptations

Life can withstand the extremes of ionic conditions found throughout the planet. NaCl concentrations ap-

proach saturation in the Dead Sea, which despite its name supports growth of archaea, bacteria, and fungi, such as *Haloarcula marismortui*, *Dunaliella salina*, and *Eurotium herbariorium* (38, 58, 269). Other bodies of water are known for their high salinity, such as the Sargasso and Red Seas and the Persian Gulf. Salt mines, salt marshes, oil field brines, hydrothermal brines, sodic soils, and drying salt lakes may approach saturation levels of salt (306). The ability to thrive or require salt, halotolerance or halophily, requires a number of energetically expensive cellular adaptations that are typically complemented by photosynthetic metabolism (16, 200). Organisms found in these environs tend to present anionic phospholipid membranes and acidic protein machinery (102, 331, 332). Chelation of cations stabilizes macromolecules in conditions of high ionic strength and provides shielding against the ionic environment (58, 82). Specific ion binding sites and extensive salt bridge networks have also been identified as important structural elements (81, 131). Microorganisms in conditions of high ionic strength may synthesize ectoine, a novel cyclic amino acid, or other small molecules, such as glycerol, sucrose, and glycine betaine, to maintain osmotic balance with the extracellular medium rather than rely on M^+ exchange (368, 369). Alternatively, osmotic balance is achieved with accumulation of high levels of cytosolic K^+ and concomitant adaptation of intracellular machinery to allow higher levels of K^+ (340). Osmotolerance mechanisms have been suggested as putative therapeutic targets to inhibit growth of human pathogens such as *Vibrio cholerae* and *Candida albicans* (135, 259). Furthermore, Na^+ may be employed in extremophilic bacteria as a coupling ion that substitutes for or complements the traditional H^+ cycle (134). Little is known on how the earliest forms of life defended themselves in high ionic conditions, and the defense mechanisms of nonhalotolerant organisms are beginning to be defined.

C. Mechanisms of Salt Homeostasis

Yeast serves as a useful model to dissect fungal and plant responses to saline environments. Ion transport systems, cation detoxification mechanisms, and signal transduction mechanisms are similar in these organisms (108, 188, 248, 283). Ionic strength and/or osmolarity activates mitogen-activated protein (MAP) kinase signaling via a two-component system and the Sho1 membrane protein (201, 202, 266). Upregulated genes include those for synthesis of glycerol and trehalose for osmoprotection and a shift in metabolism to favor protein synthesis. Transcription factors involved in the yeast response are not clearly defined yet overlap other stress response elements (32, 272, 278, 295). A genomic approach to the yeast reaction to saline stress indicated that up to 7% of the yeast genome is upregulated during stress (265). It is surprising that such a large complement of genes is involved, mostly transiently, in response to high ionic strength or osmolarity. High levels of NaCl affect plants through osmotic effects in addition to intracellular accumulation of Na^+. Cellular uptake of essential ions such as K^+ and Ca^{2+} is also inhibited. In turn, imbalanced intracellular M^+ ratios result in substitution of Na^+ for sites requiring K^+. In particular, pyruvate synthesis and protein translation are decreased (196). Regulation of ionic balance in humans is mediated by several mechanisms on a system-wide basis that reduces energetic load on individual cells.

Overall control of water flux plays a key role in regulating the concentration of Na^+ in the human cardiovascular system. Hormone signaling between the hypothalamus, adrenal cortex, heart, and kidney is mediated through vasopressin (antidiuretic hormone), aldosterone, and atrial natriuretic peptide (ANP) to control electrolyte balance. These signals tightly regulate systemic osmotic pressure near a set-point value (29, 68). Vasopressin increases the volume of circulating water by acting on renal collecting ducts via activation of V_2 receptors. Intracellular trafficking of aquaporin channels directs them to cell membranes and increases cell permeability and reabsorption (3, 113, 232). Vasopressin release from the hypothalamus is controlled by osmoreceptors that sense changes in osmolarity of the extracellular fluid (339). Only recently have mechanisms of mechanosensation begun to be unraveled (180, 216). Stretch receptors also control release of ANP in the atrial myocardium, which antagonizes the effects of vasopressin and aldosterone (318). In contrast, aldosterone levels are controlled by the renin-angiotensin system. Aldosterone acts on distal convoluted tubule cells of the kidney through activation of cytoplasmic mineralocorticoid receptors that activate gene expression (103). Of genes expressed, the epithelial Na^+ channel (ENaC) plays a key role in maintaining the proper level of Na^+.

Na^+ transport by the ENaC is a vital component in the maintenance of ion homeostasis (107). Activity of the ENaC channel must vary greatly in response to dietary Na^+ intake. Intracellular trafficking of ENaC proteins is a powerful regulatory mechanism and acts similarly to that observed with aquaporin channels. Trafficking yields a dynamic and large range of response. This contrasts with ligand- or voltage-gated channels that open or close rapidly in response to a stimulus (107). Low serum Na^+ concentration (hyponatremia) is the most common electrolyte disorder and a common medical problem that affects ~1–5% of all hospital inpatients (2, 99, 179). Vigorous exercise, like marathon running, can also cause life-threatening hyponatremia (5). Inherited forms of hypertension and hypotension have been ascribed to several genes involved in ENaC trafficking (192). Like many membrane proteins and channels, structural information regarding the ENaC is lacking. For example, the number

and stoichiometry of the three subunits that heteromultimerize to form the channel is debated (90, 174, 304). A three-residue tract, Gly/Ser-Xxx-Ser, present within all three subunits is suggested to act as the putative selectivity filter where side chain hydroxyl moieties line the channel pore. Such a configuration would contrast with that observed in K^+ channels (79, 224, 296). Although progress has been made in the elucidation of the crystal structures of several M^+ channels and pumps, only a few examples of a potentially diverse class of enzymes have been provided to date. Our best examples of M^+ coordination come from small-molecule studies that provide a useful framework for understanding M^+ binding in proteins and other biological macromolecules.

II. M^+ COORDINATION CHEMISTRY

Sir Humphrey Davy (1807) first isolated sodium by the electrolysis of fused soda (NaOH). Earliest definitions of group IA metals classify them as type A metals and very hard Lewis acids (252). Group IA metals have small ionic radii that bear a strong positive charge with no electron pairs in the valence shell (Table 2). They have low electron affinity and a strong tendency for hydration. Both the strong charge and small ionic radius of group IA metals impart bonding characteristics that are more covalent in nature. However, interaction between M^+ and ligand is based solely on electrostatics and is not technically a "bond" (251). Importantly, ligand exchange rates (k_{ex}) of M^+ are very high and allow rapid association and dissociation kinetics. Charge density of any M^+ is insufficient to be the causative agent of catalysis as the single positive charge is spread over a large volume. However, M^+ coordination can play an important role in rate enhancement or allosteric regulation of an enzyme-catalyzed reaction. From the perspective of organic chemistry, M^+s are typically viewed as counter- or spectator ions to more interesting Lewis bases. The biochemical influence of M^+ is of more considerable scope.

TABLE 2. *Properties of group I alkali metals compared with Ca^{2+} and Mg^{2+} (group IIA). Differences in the charge density of M^+ lead to significant differences in chemical properties*

Group	Ion	Ionic Radius, Å	Charge Density, q^2/r	Approximate k_{ex} (H_2O), s^{-1}	Coordination Numbers
IA	Li^+	0.68	1.67	10^8	4,6
	Na^+	0.97	1.05	10^{10}	6
	K^+	1.33	0.75	10^{10}	6–8
	Rb^+	1.47	0.68	10^{10}	6–8
	Cs^+	1.67	0.60	10^{10}	6–8
IIA	Mg^{2+}	0.72	6.15	10^6	2,4
	Ca^{2+}	0.99	4.04	10^9	6

Data are from Reference 129.

A. M^+ Coordination in Synthetic Molecules

Small molecule chemistry provides a useful introduction to M^+ coordination in biological macromolecules. Lehn, Pederson, and Cram (60, 189, 253) synthesized a series of high-affinity M^+ chelators. Their work led to the development of host-guest chemistry in which a ligand (guest) binds a multidentate macromolecule (host) to drive its synthesis. Cyclic polyethers (crown ethers, Fig. 1*A*) are capable of M^+ coordination through six O atoms, yet conformational flexibility of these molecules requires a significant entropic penalty for complexation (253). Such chelators must significantly alter conformation for M^+ binding. Creation of a bicyclic system (cryptand, Fig. 1*B*) locks the desired conformation and adds dimensionality (189). Rigidification of the system (spherand, Fig. 1*C*) abrogates the need for conformational change and leads to femtomolar affinity and exceptional selectivity (60). Conceptual simplicity, broad applicability, and utility of these designed molecules led to a most deserved Nobel Prize in 1987 for these authors. Chemical coupling of these compounds yields fluorescent M^+ sensors (136, 208, 302). Even larger macrocyclic compounds, such as calixarenes, have been developed more recently for use in M^+-selective electrodes (10, 44). Affinity and selectivity of these synthetic compounds exceed that observed in enzymes.

Synthetic M^+ ionophores demonstrate key aspects of M^+-protein complexation. First, ion coordination is largely mediated by O atoms donated from amino acid side chains and carbonyl O atoms of the polypeptide backbone. Composition of M^+ binding sites is highly variable. Examples involving all of the amino acids are known, yet there is a weak preference for Ala, Gly, Leu, Ile, Val, Ser, Thr, Asp, and Asn (130). Cation-π interactions involving Tyr, Phe, or Trp side chains are rarely found in M^+ binding sites due to the inability of this type of interaction to overcome the large energetic penalty of dehydration (78). However, certain enzymes, such as tagatose-1,6-bisphosphate, feature a cation-π interaction in the coordination shell (124). Inspection of the Cambridge structural database of small molecules demonstrated that O atoms comprise 90% of the interactions with Na^+ and K^+, with N, F^-, and Cl^- found in few instances (130). In contrast, Mg^{2+} and Ca^{2+} binding sites tend to involve carboxyl groups of acidic amino acids and naturally involve a formal charge to compensate for charge density (129). Second, M^+ sites possess a three-dimensional nature with five to eight ligands involved in the coordination shell (70). Hence, geometry of a bound M^+ differs significantly from trigonal planar geometry of the ubiquitous H_2O solvent. Octahedral coordination through six ligands is most commonly observed with Na^+ in known protein structures (Fig. 2). Most M^+ binding sites are mononuclear, yet a second M^{2+} binding site may be thermody-

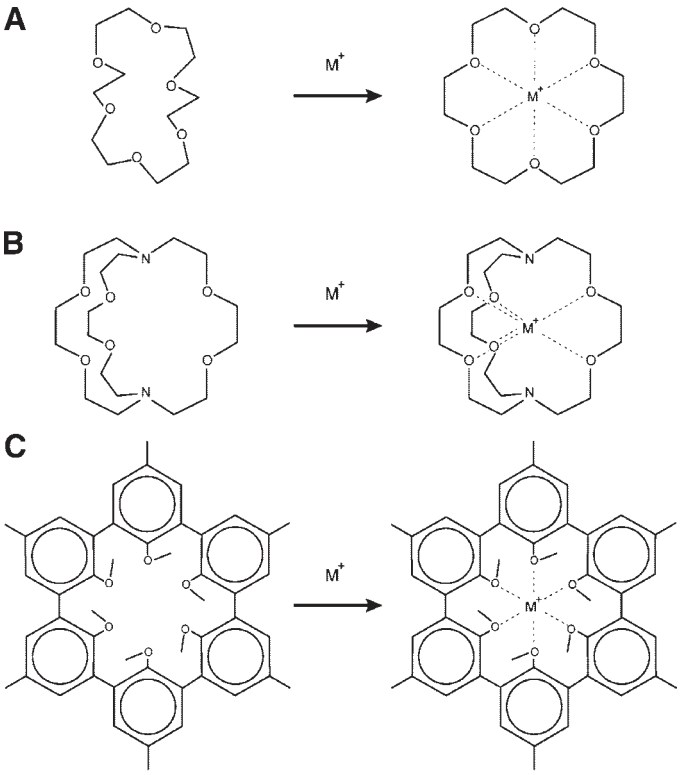

FIG. 1. Principles of M^+ coordination from small molecules. *A*: in crown ethers, significant rearrangement is required for cation binding. *B*: creation of a cryptand adds dimensionality and significantly enhances M^+ selectivity. *C*: rigidification of the system through creation of a spherand provides extreme affinity as the molecule is essentially unchanged upon cation coordination.

namically linked via a bridging water molecule, substrate, cofactor, or other long-range connection. The ion binding site possesses an inner sphere of hydrophilic atoms surrounded by an outer sphere of hydrophobicity (366). Rigidity and preorganization should be present to enhance binding strength as thermodynamic contributions of complexation do not facilitate large-scale rearrangements of the protein. A key feature of several M^+-activated enzymes is selective stabilization of one protein conformation from two or more possibilities. Examination of protein binding sites of M^{2+} suggests that metal ion binding sites undergo rearrangement in ~40% of all proteins and is likely representative of M^+ sites (12). However, observed conformational changes are subtle and typically

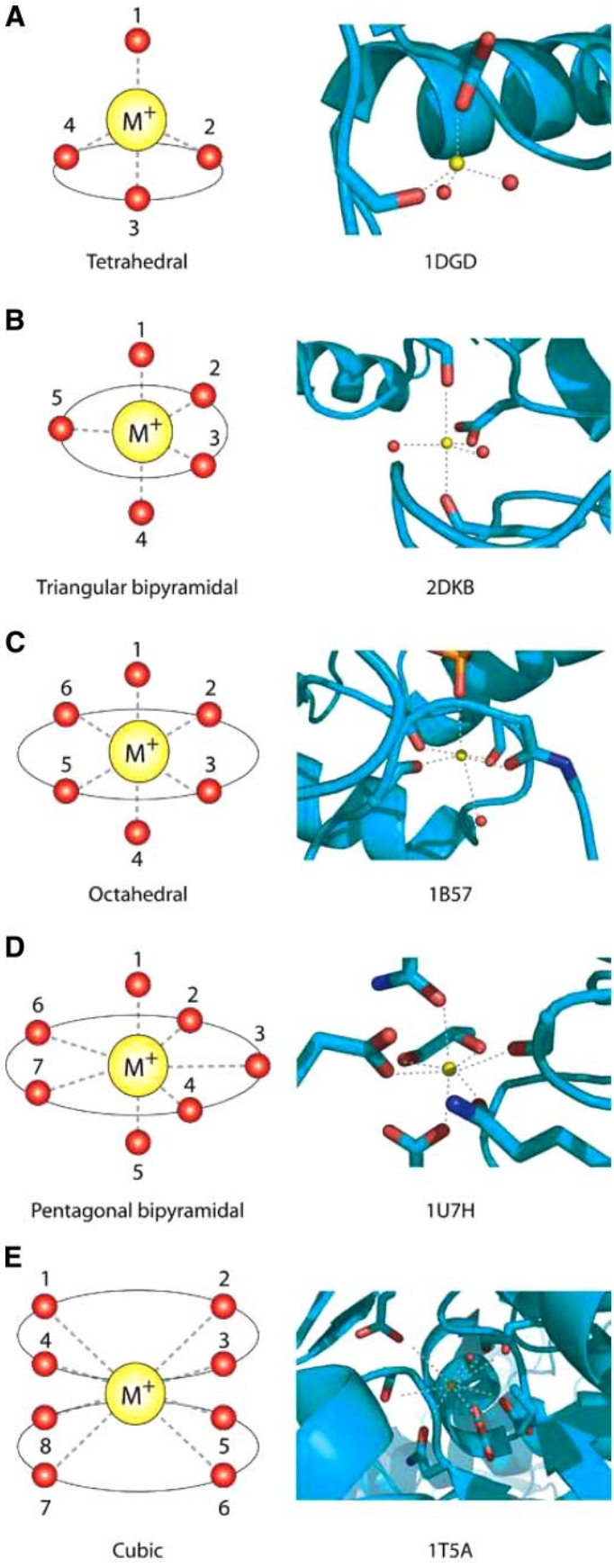

FIG. 2. Examples of coordination shells in proteins. Four to eight ligands may be involved in complexation of M^+ (yellow sphere). Examples shown are from 1DGD, 2DKB, 1B57, 1U7H, and 1T5A. Six ligands in octahedral configuration are most commonly observed. Notably, ideal geometry is rarely observed in M^+-protein complexes and may be compensated by a formal charge. Such distortions may be linked with key mechanistic aspects of M^+ activation. Variable numbers of O atoms donated from the polypeptide and water molecules permit a wide diversity of cation binding sites found in disparate protein families.

involve select ligands of the coordination shell of the ion (46, 320). Finally, complementary geometry of the binding site and ion provides selectivity (319). Despite a wealth of crystallographic data, the mechanism by which M^+ complexation proceeds is largely unknown. Questions remain on whether M^+ complexation involves increasing or decreasing the number of ligands coordinating the cation and the rate constants by which these steps occur. Such processes are more readily understood for divalent metals where ligand exchange rates are slower and allow detection of stable intermediates. Ubiquitous presence of M^+ in nature has led to a variety of cation binding sites and assorted enzymes with concomitant diverse strategies for M^+ utilization. Subtle differences in the electronic properties of M^+ lead to profound differences in coordination chemistry, solvent effects, and catalytic outcome. Ionophores provide further information on the nature of M^+ binding. Unlike large macromolecules, ionophores tend to undergo significant conformational changes upon M^+ complexation.

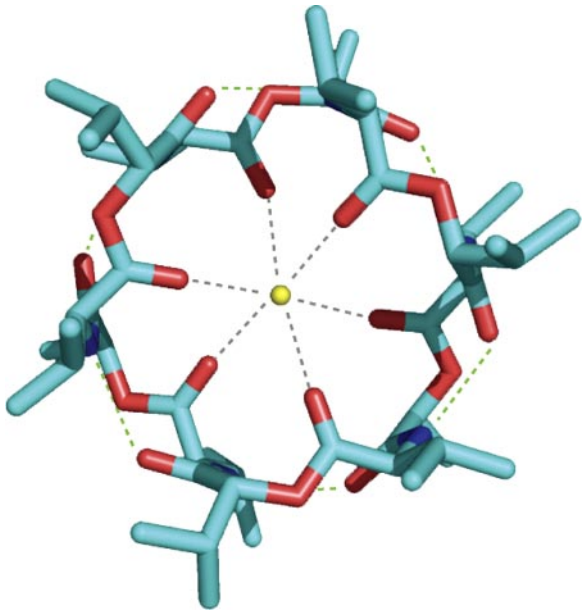

FIG. 3. Valinomycin bound to K^+. An inner sphere of interactions (dashed gray lines) provides near-perfect octahedral coordination of the cation (yellow sphere). Further stability arises from a second shell of intramolecular H-bonds (dashed green lines). In turn, the surface of the complex is hydrophobic and permits facilitated diffusion through a phospholipid bilayer.

B. Naturally Occurring Small Molecules

Many naturally occurring small molecules are well defined for their ability to bind M^+ with high selectivity and affinity (270). Ionophoric antibiotics are produced by several gram-positive bacterial species such as *Streptomyces*, *Streptoverticillium*, *Nocardiopsis*, *Nocardia*, and *Actinomadura* (20). M^+ binding by these compounds involves a conformational change that allows the complex to transport across a membrane through facilitated diffusion. Valinomycin from *Streptomyces fulvissimus* is a 12-membered macrocyclic peptide that prefers larger cations (Rb^+ and K^+). The macrocycle is composed of three repeats of alternating L- and D-amino acids (L-Val-D-Hiv-D-Val-L-Lac, where Hiv is α-hydroxyisovaleric acid and Lac is lactic acid). Crystal structures of valinomycin in the free and bound state provide an elegant example of M^+ complexation. In the free state all six NH groups are intramolecularly H-bonded, four to amide C=O groups with two to C=O from ester moieties (263). Upon complexation with a M^+, the cyclical chain forms a bracelet-like conformation around the ion, and six ester carbonyl groups coordinate the ion in octahedral configuration (Fig. 3). Further stabilization of the complex is achieved through H-bonding between carbonyl O and amide H moieties (230). A Na^+-selective cyclic decapeptide, antamanide, has been described from the poisonous *Amanita* mushroom (350). Interestingly, this ionophore counteracts the effects of other toxic compounds produced by the organism. Noncyclical ionophoric compounds have also been described. Monensin and narasin are polyketides that form stable complexes with Na^+ through conformational changes upon ion complexation (Fig. 4). (47). Monensin, like other antibacterial M^+ ionophores, has been used for many years in the dairy industry for selective reduction of bacterial fauna (40). Most naturally occurring synthetic ionophores prefer K^+ including nonactin (169), monactin (260), dinactin (260), salinomycin (282), and nigericin (195). Several antifungal agents interact with sterols in the cell membrane (ergosterol in fungi, cholesterol in humans) forming ion channels that disrupt cellular concentration gradients such as amphotericin B (25), nystatin (92), and pimaricin (9). Of known small molecule ion permeation channels, gramicidins are the best characterized.

Gramicidins are a group of naturally occurring linear peptides containing alternating L- and D-amino acids that increase cation permeability of bacterial membranes yet do not bind M^+ directly (132). Gramicidins form bilayer-spanning channels that transport M^+ across the membrane by ion permeation, which differs from the M^+-complexation observed in other ionophoric antibiotics. Several structures of gramicidin are available (6, 59, 290, 347). In solution the peptide presents significant flexibility that rigidifies in a phospholipid membrane (333, 334, 341). An antiparallel single-stranded $\beta^{6.3}$-helical dimer forms a channel within the phospholipid bilayer (345, 346). Luminal diameter of the pore (4 Å) is sufficient for nonspecific transport of M^+, H^+, and water (144, 226). Selectivity for M^+ permeation can be influenced by amino acid substitutions in the peptide. However, selectivity is based on electrostatic interactions between permeating ions and

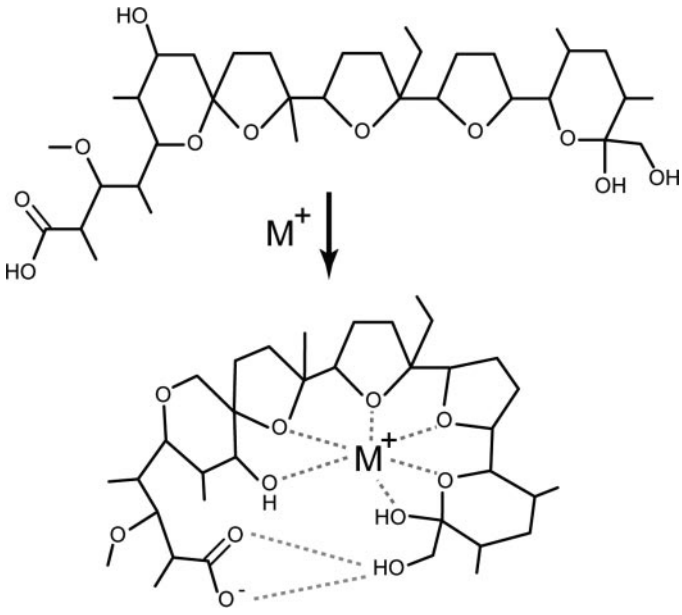

FIG. 4. Monensin selectively binds Na^+, causing a significant change in the conformation. Complexation drives the hydrophilic moieties of the molecule to the core of the complex, leaving a surface of hydrophobic residues. Facilitated diffusion of the molecule through gram-positive bacterial membranes leads to destruction of ionic gradients and the antibiotic effect of the compound.

side chain dipoles. Backbone carbonyl O atoms in gramicidin channels switch between intramolecular H-bonds with the polypeptide backbone or interactions with the permeating ion (159, 160, 170). Rather than a defined positioning of atoms in the coordination shell, diameter of the pore results in selectivity. In turn, permeation decreases with increasing dehydration energy (83). In contrast, K^+ channels present carbonyl groups that lie perpendicular to the direction of ion movement which in addition to the size of the pore dictates ionic selectivity. The nonselective NaK channel from *Bacillus cereus* presents fewer carbonyls in a plane perpendicular to ion motion, with other carbonyl groups parallel to the movement more similar to that observed in gramicidins (Fig. 5).

Conduction by aquaporin channels differs considerably from known M^+ channels. Aquaporins line a hydrophilic pore with O atoms at staggered positions that facilitate selective H-bonding with water and potentially small neutral alditols or CO_2 (224, 342). Hence, pore size does not generate selectivity; rather, the geometry of bonding does. It is unclear whether the putative selectivity filter of ENaC presents hydrophilic side chains or backbone carbonyl O atoms to line the pore and generate selectivity. In Na^+ symporters and antiporters, it is clear that Na^+ binding involves complete dehydration of the ion, thus yielding high selectivity and affinity. Much structural work remains to be done in this field and is likely to yield interesting results in the coming years.

C. M^+ Coordination in Biological Macromolecules

Nucleic acids commonly bind M^+ and M^{2+} to mediate structure, stability, and protein-nucleic acid interactions. Physiological cations bind both the major and minor groove of DNA double helices as demonstrated through experimental (67, 152) and theoretical approaches (50). In particular, Na^+ and other M^+ preferentially bind the minor groove of adenine-rich sequences in A-form of DNA. Ions are thought to bind at similar positions to water molecules yet with considerably longer residence times in the spine of hydration that runs along the groove (126). M^{2+} are thought to bind both the minor and major grooves of DNA also with a preference for the A-form of DNA. Notably, the effect of M^+ binding to DNA structure has met with debate (51). Irrespective of whether M^+ play a role in the A- to B-DNA transition, more definite roles are noted for other nucleic acids. Mg^{2+} and M^+ are well known to be essential for the

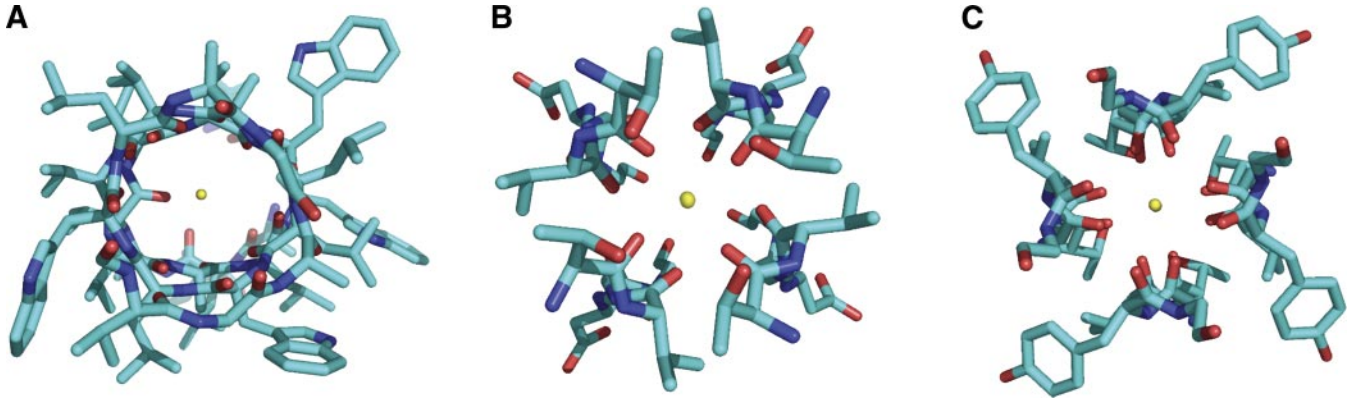

FIG. 5. Pore architecture from K^+ complexes. *A*: ion permeation in gramicidin A (1GMK) is mediated through a dimer of antiparallel single-stranded $\beta^{6.3}$-helix, a structure permitted by the presence of alternating L- and D-amino acids. Carbonyl groups lining the pore orient parallel to the motion of the ion, and low selectivity results. Fewer carbonyl groups line the pore of the nonselective NaK channel from *B. cereus* (2AHZ) (*B*) than the KcsA K^+ channel from *S. lividans* (1K4C) (*C*) and explain the reduced M^+ selectivity.

folding and stability of large RNA molecules. For example, rRNA of the large ribosomal subunit from *Haloarcula marismortui* binds 116 Mg^{2+} and 88 M^+. Similar to DNA, M^+ bind to nucleotide bases in the major groove sides of G-U wobble pairs. The extent to which M^+ bind rRNA is suggestive of a vital role for these ions prior to emergence of proteins.

Coordination of M^+ in a folded polypeptide occurs often through carbonyl O atoms donated from peptide bonds. In the above examples of synthetic M^+ ionophores, ion binding is mediated by ligand O atoms from ketones, esters, or ethers. In fewer instances of M^+ binding, sites employ a negatively charged unidentate carboxyl or phosphoryl group. In contrast, M^{2+} sites often utilize one or more full negatively charged groups to balance the higher charge density of these ions. Peptide bonds possess a useful configuration for allosteric regulation through M^+ complexation. These bonds are planar and extremely stable due to resonance. In turn, increased dipole moment of the carbonyl O atom provides a stronger electrostatic interaction with the ion. Moreover, recruitment of additional regions of the protein is mediated via H-bonding through the amide H (Fig. 6). Signaling through local peptide bonds can occur upon M^+ coordination leading to long-range effects on catalytic properties. Notably, polypeptide segments can communicate through a bound M^+ and its liganding carbonyl O atoms. Conformations not accessible to the polypeptide in aqueous solution alone are stabilized. M^+ sites occur in regions of the polypeptide that do not form secondary structure and frequently between surface-exposed loops (128). Importantly, M^+ complexation is largely achieved by residues separated in the linear sequence of the protein. M^{2+} binding in many proteins occurs often through recognizable sequence and structural motifs. For example, EF-hand motifs and zinc fingers are well known for their ability to selectively complex Ca^{2+} and Zn^{2+}, respectively (22, 207). Lack of sequence similarity in known M^+ binding sites renders bioinformatic analysis impossible in the absence of structural information. However, structural similarities link the selectivity filter of the K^+ channel with the M^+ binding environment of disparate enzyme families (see sect. II*C*).

M^+ complexation can elicit a variety of effects on protein structure and function. Proteins in solution are dynamic entities with significant degrees of freedom afforded to surface-exposed residues (84). Selective stabilization of one conformation of the enzyme through M^+ complexation may produce local and potentially long-range effects on the enzyme structure (Fig. 7). Entropy of these solvent accessible regions can impact kinetic properties of the enzyme (98, 109). Substrate binding to a stabilized enzyme-M^+ complex may be more favorable as the entropic penalty of ordering the enzyme to form the enzyme-substrate complex is paid by the previously bound ion. Divalent metal binding acts similarly in many enzyme systems (203). The variety of reported instances of weak M^+ activation of enzyme activity are possibly the result of global entropic effects rather than a specific M^+ binding site interwoven into the catalytic process of the enzyme. Structural stabilization due to the kosmotropic effects of larger M^+s on the water environment is correlated with enhanced activity in many enzymes (145). However, redistribution of the equilibrium between protein conformational states is a key aspect of allosteric regulation (168). Allostery is defined as the binding of a ligand at one site causing a change in the affinity or catalytic efficiency of a distant site (221). Communication between distal regions in a macromolecule is required to understand protein structure and function. Such allosteric signals can arise from a variety of mechanisms, and growing evidence supports the notion that many, if not all, proteins utilize allostery (123, 209). In certain instances, pathways of communication between allosteric sites are conserved and amenable to detection through bioinformatic analysis (76, 194, 313). However, these approaches have

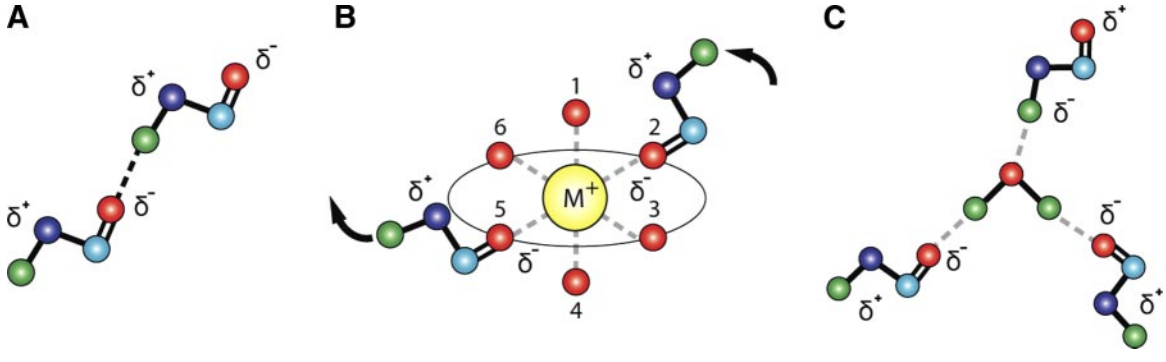

FIG. 6. Allosteric communication mediated through peptide bonds. *A*: in the typical arrangement found in secondary structures, peptide bonds are aligned in parallel. *B*: in contrast, a M^+ binding site allows for antiparallel connections between peptide bonds in regions devoid of secondary structure. H-bonding may be linked to complexation with M^+ through the amide H and provides an efficient mechanism for allosteric signaling. *C*: geometry of water coordination is significantly different from the octahedral configuration typically observed with M^+-protein complexes and highlights the mechanistic diversity facilitated by M^+ binding.

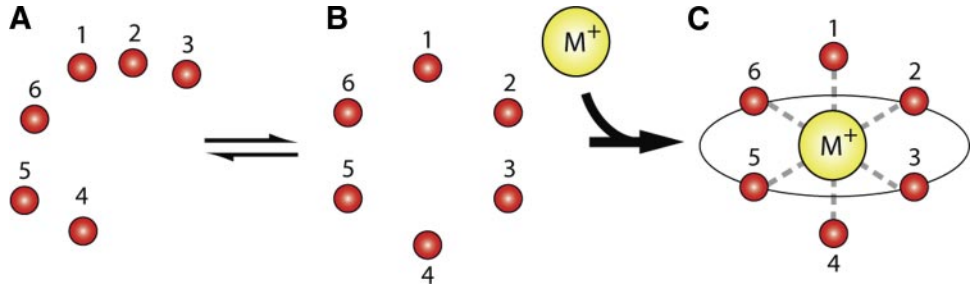

FIG. 7. Stabilization of protein conformational states through M^+ binding. Cation binding may alter the population of protein states leading to improved enzymatic properties. Stabilization of the M^+ binding site may propagate to the active conformation of catalytic machinery, substrate, or cofactor binding sites. Moreover, the cation may provide stability in conditions of high salinity and/or temperature.

been applied to few systems and require large numbers of related protein sequences. Moreover, one may also question whether the close proximity of coevolving residues has structural consequences that have nothing to do with allosteric communication (95, 96).

Introduction of a single positive point charge may act locally to increase the pK_a of a negatively charged group or decrease the pK_a of positively charged moiety. However, pK_a shifts due to M^+ binding are likely to be minor and transient. Binding of a M^+ is distributed among several weakly charged atoms, allowing for the possibility that directional motion of the ion could occur (Fig. 8). Such motion is obvious in the case of M^+ channels. As noted above, fast rates of ligand exchange allow for ion motion to occur with sufficient speed to assist efficient catalysis. Primitive metalloenzymes that bind M^{2+} facilitating additional ligand binding or catalysis have been designed de novo; however, similar results have not been achieved with M^+ (80, 370). Characterization of the allosteric transitions occurring upon M^+ binding is furthered by several new experimental techniques, such as multiple-quantum relaxation dispersion NMR (173) and picosecond time-resolved X-ray crystallography (153). Traditional approaches using X-ray crystallography, NMR, fluorescence, and spectroscopic methods complement kinetic analysis in the majority of reported instances. Numerous M^+-protein complexes have been defined through X-ray crystallography (70).

D. Macromolecular Stability and Solubility

Observed differences in valence parameters of M^+ lead to a host of macroscopic features based on hydration properties of these ions. Group IA alkali metals bear a single positive charge with differing ionic radius (Table 2). Subtle differences in ionic radii correspond with significant alteration of ionic volume, hence charge density, and downstream effects upon bonding parameters. Hydration shells of M^+ are dissimilar, and this extends to secondary and tertiary shells of the ion. Li^+ and Na^+ are small enough to bind three or four water molecules with reasonable affinity and result in a larger apparent size in aqueous solution. K^+ favors four or five water molecules coordinated with weaker strength (54–56, 75, 150). Biological exploitation of this subtle difference is exemplified in the structure of K^+ channels whose selectivity is based on the ability to strip water molecules from the hydration shell of the ion (8, 79). In turn, K^+ channels rather than Na^+ channels form the basis for numerous ionic balance-based transport systems. Universally, intracellular concentrations of K^+ are considerably higher relative to the extracellular environment. Overall, Na^+ balance in all organisms including humans is largely driven through transport of water molecules rather than regulated movement of Na^+ and stems from electronic differences of M^+. A parallel concept is thought to explain why Ca^{2+} and not Mg^{2+} acts as an intracellular messenger. Ligand exchange

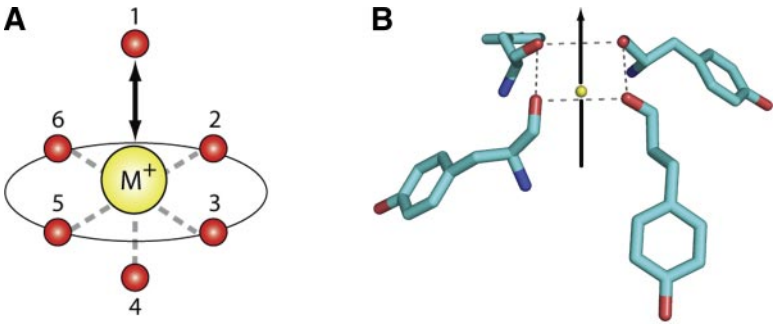

FIG. 8. Coordination of M^+ can influence the pK_a value of ligand atoms. Ligand exchange rates of all group IA M^+s are very high and allow for dynamic interplay with atoms in the coordination shell. *A*: as the distance between ligand atom 1 and M^+ increases, so does the pK_a value. Hence, the plane defined by ligand atoms 2, 3, 5, and 6 plays a key role in octahedral coordination of M^+. *B*: such vertical motion is readily apparent in the K^+ channel, where four carbonyl O atoms are held at fixed distances to one another.

rates of Ca^{2+} are 10,000-fold higher than those of Mg^{2+}, allowing rapid and efficient complexation (286). Hydration shells of M^+ exert dispersive effects on neighboring water molecules through electrostatic interactions and coordination geometry.

Over a century ago, Hofmeister noted the ability of various ions to induce the precipitation of proteins in solution (181). Ionic effects on protein structure have been widely ascribed to their effect on water. Smaller, more strongly hydrated ions are kosmotropic (water structuring) (Li^+, Na^+), whereas larger ions are chaotropic (water disrupting) (K^+, Rb^+, Cs^+) (27, 39, 97, 150). The Hofmeister series bears an important relationship with protein solubility. Chaotropic agents are well known for their ability to cause protein precipitation and formed the backbone of protein chemistry before development of more refined chromatographic techniques. At low concentrations of a given salt, solubility of a macromolecule increases slightly in a process termed salting-in. At high concentrations of salt, the protein solubility drops sharply, termed salting-out, and this phenomenon forms the basis of many protein purification strategies. Debye-Hückel theory can explain certain aspects of this phenomenon by applying continuum electrostatics to simplify ions in solution. The positively or negatively charged ion is represented as a point charge in a solvent of constant dielectric constant. The theory dictates that proteins are surrounded by salt counterions that screen charged groups and results in lower electrostatic free energy of the molecule and increased activity of the solvent, which in turn leads to increasing solubility. However, as the concentration of ions is increased, their solvating power decreases, protein solubility decreases, and precipitation results. For solutions of greater ionic strength, the Pitzer equation should be used (264). Although the Pitzer equation is accurate, many empirical values need to be determined for application. Specific ion interaction theory has been proposed more recently as a simplified, yet accurate, alternative (117). All of the above models for ions in solution suggest ionic influences act over fairly large distances with uniform distribution. Many lines of evidence suggest this simplification may be problematic (26, 55). Inhibition of activity by M^+ at high concentrations has been documented for many enzymes and can be attributed to the chaotropic effect of larger ions. Destabilization of the enzyme structure would then lead to reduced catalytic activity via nonspecific mechanisms. Monovalent anions are more commonly noted for their inhibitory effect on enzyme-catalyzed reactions (374). However, in a large number of systems to be dealt with next, the role of M^+ is highly specific and mediated by binding to the enzyme and or enzyme-substrate complex. In such instances, nonspecific ionic strength effects become of marginal significance, and mass-law binding becomes of the essence.

E. M^+ Selectivity

Several M^+-activated enzymes have been crystallized free or in the presence of Na^+, K^+, or other M^+, and the resulting information has broadened our understanding of M^+ selectivity. In the case of tryptophan synthase, changes between the Na^+-bound and K^+-bound structures are significant (281) but are not matched by differences in the kinetics of activation (357). In pyruvate kinase, replacement of K^+ with Na^+ results in no structural changes (185), although the enzyme is practically inactive without K^+ (30). In thrombin, however, changes in coordination between Na^+ and K^+ propagate to the oxyanion hole and explain the differences in the kinetics of activation (247, 262). In the case of dialkylglycine dehydrogenase (324, 325) and Hsc70 (93, 352), replacement of the essential K^+ with Na^+ drastically changes the geometry of coordination and perturbs residues that control binding of pyridoxal phosphate (PLP) or ATP. These enzymes have evolved K^+ selectivity by imposing geometric constraints on the coordination shell that cannot be obeyed by the smaller ionic radius of Na^+. The linkage with enzyme activation is ensured by the functional connection of these constraints with the optimal orientation of catalytic residues. Rigidity of the coordination shell guarantees selectivity by increasing the entropic cost of any reorganization meant to accommodate a M^+ of different size. Interestingly, an analogous strategy has been exploited successfully in the synthesis of selective chelators (60, 217).

One striking feature of K^+ channels is the GYG signature sequence (residues 77–79) whose backbone O atoms shape part of the selectivity filter that gates access to a pore that transverses the phospholipid membrane. Four carbonyl O atoms define a plane that dictates the size of the pore. B-factors of these O atoms indicate that RMS fluctuations of 0.75–1 Å occur and agree with molecular dynamics simulations (17, 36). In turn, the O atoms are in a fluidlike state, and the size of the channel acts simultaneously to provide fast conduction rates. Indeed, size of the pore allows for near-equal transmission of Rb^+. Naturally occurring nonspecific channels have been identified where the selectivity filter is absent. For example, the NaK channel from *Bacillus cereus* has reduced selectivity similar to cyclic nucleotide-gated channels and possesses a GDG sequence rather than the typical GYG. In turn, carbonyl O atoms adopt a different conformation, yielding a nonspecific binding site (297). Remarkably, conformation of the GYG sequence relative to the bound K^+ in the channel is similar to the GYG sequence (residues 325–327) near the K^+ binding site of pyruvate dehydrogenase kinase (167), the GFG sequence (residues 337–339) near the K^+ binding site of branched-chain α-ketoacid dehydrogenase kinase (197), and the KYG sequence (residues 224–226) near the Na^+ binding site of thrombin (247)

(Fig. 9). Furthermore, mutation of Tyr in this sequence has very similar functional consequences in the K^+ channel (228) and thrombin (121). This unexpected connection is testimony to the basic similarity of M^+ recognition mechanisms that evolution has bestowed on proteins of widely different function.

Other examples are provided by ion transporters for which M^+ selectivity is near absolute. The V-type Na^+-ATPase (225), F-type Na^+-ATPase (211), and bacterial Na^+/Cl^--dependent neurotransmitter homolog (365) cage Na^+ in rigid environments, practically inaccessible to K^+. In the KcsA K^+ channel, backbone O atoms line the channel to maintain distances suitable only for K^+ coordination and provide an exact replica of the coordination shell of K^+ in solution (79). A key feature from currently available structures is the absence of water molecules surrounding the M^+ in antiporters and symporters. Binding sites in channels and pumps are largely composed of O atoms donated by the protein that may or may not possess one formal negative charge. Selectivity in M^+ channels and pumps results from a fairly rigid binding site whose geometry matches the radius of a bound ion. As such, the protein presents carbonyl groups in a similar conformation to that observed in small molecules (Fig. 10). In turn, the energy of ion binding is greater than the energy associated with dehydration of the ion. Ionic selectivity by a macromolecule need not require strict rigidity and may be compensated through entropic terms as evidenced by the numerous ionophores discussed above (236). The structure of the KcsA K^+ channel in the presence of Na^+ demonstrates how the channel may adopt a conformation that permits ion binding yet is not conducive to ion transport (375–377). It is less clear how these observations relate to other systems given the paucity of structures determined in the presence of differing ions. Local conformational dynamics, and potentially larger scale alterations, are central to understanding M^+ coordination and the resulting effect on enzyme-catalyzed reactions.

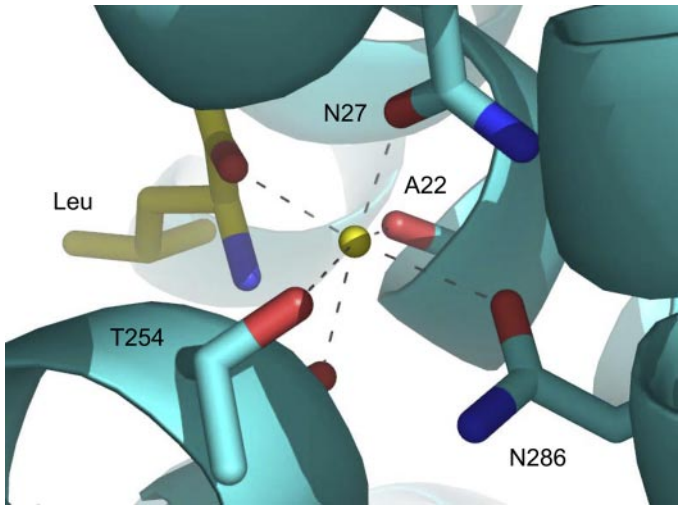

FIG. 10. Na^+ coordination in the $LeuT_{Aa}$ from *Aquifex aeolicus* (2A65) (CPK, C in cyan) involves no water in the rigid coordination shell. In this transporter, two Na^+ are transferred with Leu with antiport of Cl^-, and varying ratios of cations and anions to substrate are known. The amino acid (CPK, C in yellow) has direct contacts that complete the coordination shell of one of the two bound Na^+ (yellow sphere).

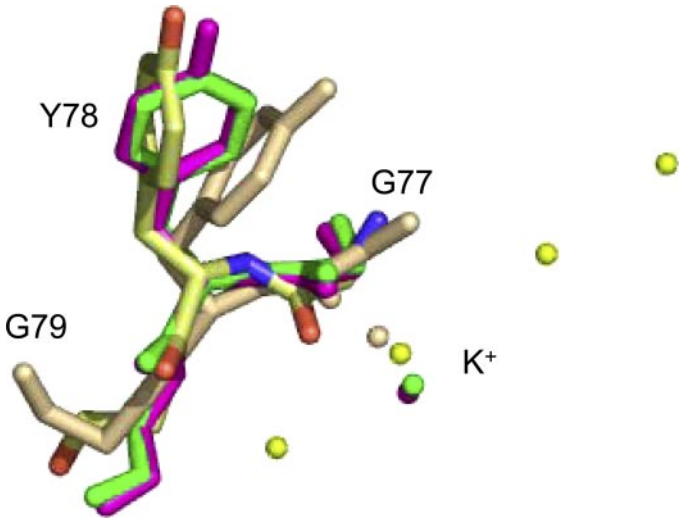

FIG. 9. Overlay of the signature sequence GYG (residues 77–79) in the selectivity filter of the KcsA K^+ channel (CPK, K^+ yellow spheres, 1BL8) with the GYG sequence (residues 325–327) of pyruvate dehydrogenase kinase (magenta, K^+ magenta sphere, 1Y8P), the GFG sequence (residues 337–339) of branched-chain α-ketoacid dehydrogenase kinase (green, K^+ green sphere, 1GJV) and the KYG sequence (residues 224–226) of thrombin (wheat, K^+ wheat sphere, 2A0Q). K^+ sits in equivalent positions relative to the sequence in all cases. [Modified from Di Cera (70).]

III. M^+-ACTIVATED ENZYMES

Over 60 years ago, Boyer et al. (30) reported the groundbreaking observation that pyruvate kinase would only express appreciable catalytic activity in the presence of K^+. A similar effect was soon discovered in other systems, and just a few decades later the field of enzymes requiring M^+ for optimal activity encompassed hundreds of examples from plants and the animal world (86, 314). In general, enzymes requiring K^+ such as kinases and molecular chaperones are also activated by NH_4^+ and Rb^+, but are not activated as well or at all by the larger cation Cs^+ or the smaller cations Na^+ and Li^+. Enzymes requiring Na^+ such as β-galactosidase and clotting proteases are not activated as well by Li^+, or the larger cations K^+, Rb^+, and Cs^+ (Fig. 11). Because the concentration of Na^+ and K^+ is tightly controlled in vivo, M^+s do not function as regulators of enzyme activity. Rather, they facilitate substrate binding and catalysis by lowering energy barriers in the ground and/or transition states. Enzymes activated by M^+ evolved to take advantage of the large avail-

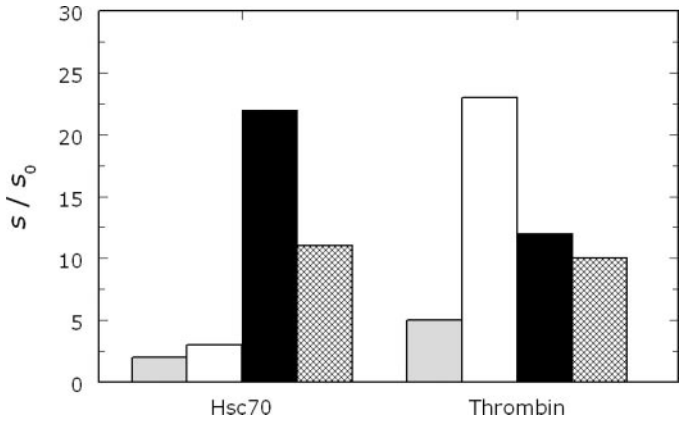

FIG. 11. Enzyme activity in the presence of LiCl (gray), NaCl (white), KCl (black), or RbCl (hatched) for Hsc70 (237) and thrombin (267). Values refer to $s = k_{cat}/K_m$ of ATP hydrolysis for Hsc70 in the presence of 150 mM salt, relative to CsCl, or the hydrolysis of H-D-Phe-Pro-Arg-*p*-nitroanilide by thrombin in the presence of 200 mM salt, relative to choline chloride. The preference for K^+ (Hsc70) or Na^+ (thrombin) is evident from the plot.

ability of Na^+ outside the cell and K^+ inside the cell to optimize their catalytic function. Indeed, a strong correlation exists between the preference for K^+ or Na^+ and the intracellular or extracellular localization of such enzymes. Since the beginning, this rapidly expanding field had to address two basic questions, namely, the molecular mechanism of M^+ activation and the structural basis of M^+ selectivity. Kinetics of M^+ activation are relatively straightforward but often fail to address unequivocally either question. Hence, progress in the field had to await high-resolution crystal structures of M^+-activated enzymes, which have become available over the last decade.

A. Kinetics of M^+ Activation

In the study of enzyme activation by M^+, attention is often focused on the effect of M^+ on the velocity of substrate hydrolysis. The activating effect is readily observed as an increase in the velocity as a function of $[M^+]$. Specificity is detected in this assay by comparing the velocity among different M^+ at the same concentration. Below we show that quantitative information about the energetics and mechanism of M^+ can be obtained by measurements of the independent Michaelis-Menten parameters k_{cat} and $s = k_{cat}/K_m$. In general, these parameters can be defined respectively as the velocity of product formation per unit enzyme under saturating conditions of substrate (k_{cat}) and the velocity of product formation per unit enzyme and substrate when the substrate concentration tends to zero (s). It should be noted that K_m, the concentration of substrate giving half of the maximal velocity of substrate hydrolysis, is not an independent parameter because it requires knowledge of the value of k_{cat}. The values of s and k_{cat}, on the other hand, are independent of each other because they define, respectively, the initial slope and asymptotic value of the velocity curve, expressed in units of enzyme concentration.

We will derive the independent parameters defined above for a basic scheme of M^+ activation (see scheme 1). We will assume that the enzyme E contains a single

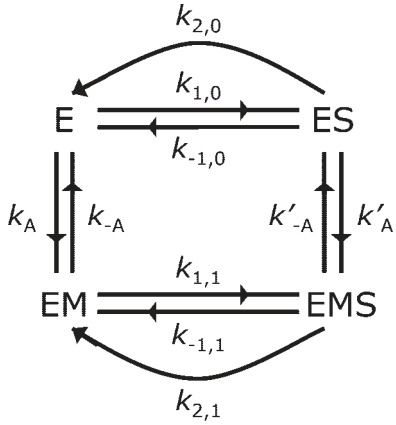

site for substrate and M^+. The scheme also applies to the case where the enzyme has multiple active sites that do not interact, but would not apply to oligomeric enzymes that bind substrate or M^+ at multiple interacting sites. Even in its simple form, scheme 1 finds application in a number of relevant systems and captures the basic features of M^+ activation. Scheme 1 was introduced by Botts and Morales in a different context to analyze the action of a modifier on substrate hydrolysis (28). The enzyme is assumed to exist in two forms, one free (E) and the other bound to M^+ (EM), with different values of kinetic rate constants for binding ($k_{1,0}$, $k_{1,1}$), dissociation ($k_{-1,0}$, $k_{-1,1}$), and hydrolysis ($k_{2,0}$, $k_{2,1}$) of substrate S into product P. $K_A = k_A/k_{-A}$ and $K'_A = k'_A/k'_{-A}$ are the association constants for M^+ binding to E and ES, respectively. Detailed balance imposes a constraint among the rate constants in scheme 1, i.e., $k_{1,0}K'_A k_{-1,1} = k_{-1,0}K_A k_{1,1}$. The exact analytical solution for the velocity of product formation at steady state can be found in a number of different ways. We will use the Hill diagram method (143), because of its elegance and direct connection with the kinetic features of the scheme. Scheme 1 contains four species, of which only three are independent because of mass conservation. Hence, each directional diagram must contain the product of three rate constants. The sum of the trajectories toward each species defines the contribution of that species at steady state. The velocity of product formation is then

$$\frac{v}{e_{tot}} = \frac{k_{2,0}[ES] + k_{2,1}[EMS]}{[E] + [EM] + [ES] + [EMS]} = \frac{k_{2,0}\Sigma_{ES} + k_{2,1}\Sigma_{EMS}}{\Sigma_E + \Sigma_{EM} + \Sigma_{ES} + \Sigma_{EMS}} = \frac{\alpha[S] + \beta[S]^2}{\gamma + \delta[S] + \varepsilon[S]^2} \quad (1)$$

where e_{tot} is the total concentration of active enzyme and Σ_{EX} is the sum of the trajectories toward species EX. Coefficients in *Equation 1* are listed in Table 3 and are polynomial expansions in the variable $[M^+] = x$, with each term mapping into a trajectory in scheme 1. The velocity of product formation for scheme 1 is quadratic in [S], although the enzyme contains only a single site for S. Likewise, polynomial expressions in x are quadratic, although the enzyme contains one binding site for M^+. This consequence arises from the difference in which terms are calculated for equilibrium and steady-state systems (28, 74, 143). Under the influence of M^+, an enzyme containing a single substrate binding site can display cooperativity in substrate binding, and this possibility should be kept in mind when analyzing experimental data. Glucokinase is a relevant example of cooperativity in monomeric enzymes because it isomerizes slowly between two forms, E and EM in scheme 1, that differ in affinity and catalytic competence toward substrate (166).

In the general case, expressions for the independent Michaelis-Menten parameters k_{cat} and $s = k_{cat}/K_m$ are derived as the limits of *Equation 1* for $[S]\rightarrow\infty$ (k_{cat}) and the limit of $v/(e_{tot}[S])$ for $[S]\rightarrow 0$ ($s = k_{cat}/K_m$). The expressions are (see also Table 4)

$$k_{cat} = \frac{\beta}{\varepsilon} = \frac{k_{2,0} + k_{2,1}K'_A x}{1 + K'_A x} \quad (2)$$

$$s = \frac{\alpha}{\gamma} = \frac{s_0 + s_1 K_A x}{1 + K_A x} + (\omega - 1)\frac{K_A x}{1 + K_A x}$$

$$\frac{s_1 - \frac{k_{1,1}}{k_{1,0}}s_0}{1 + \omega\frac{k_{1,1}}{k_{1,0}}K_A x + \frac{k_{2,1} + k_{-1,1}}{K'_{-A}}} = \frac{s_0 + s_1 K_A x}{1 + K_A x} + \Lambda(x) \quad (3)$$

Three independent parameters $k_{2,0}$, $k_{2,1}$, and K'_A can be resolved from measurements of k_{cat} as a function of x. On the other hand, measurements of s as a function of x only resolve two parameters because of the form of *Equation 3*. These parameters are $s_0 = k_{2,0}k_{1,0}/(k_{-1,0} + k_{2,0})$ and $s_1 = k_{2,1}k_{1,1}/(k_{-1,1} + k_{2,1})$ obtained as the values of s in the absence or presence of saturating concentrations of M^+. Resolution of K_A, measuring the affinity of M^+ for the free enzyme, is complicated by the expansion term $\Lambda(x)$ that contains the additional independent parameters

$$\omega = \frac{k_{-1,1} + k_{2,1}}{k_{-1,0} + k_{2,0}}\frac{k_{-1,0}}{k_{-1,1}}$$

and $k_{1,1}/k_{1,0}$. When $\Lambda(x)$ makes a small contribution to the value of s, K_A can be estimated from the value of x at the midpoint transition of s from s_0 to s_1. This appears to be the case under many circumstances (see Fig. 28).

Binding and dissociation of M^+ is fast compared with all other rates in scheme 1. Experimental evidence is known for the case of Na^+ binding to thrombin (183), but this expectation is certainly valid more generally because enzymes activated by M^+ tend to obey Michaelis-Menten kinetics. In fact, when the rate constants k_A, k_{-A}, k'_A, and k'_{-A} become dominant, the only trajectories to be taken into account in the derivation of the kinetic equations are those containing two such constants. In turn, this makes β and ϵ negligible and *Equation 1* reduces to the familiar Michaelis-Menten form

$$\frac{v}{e_{tot}} = \frac{\alpha[S]}{\gamma + \delta[S]} \quad (4)$$

with

$$k_{cat} = \frac{\alpha}{\delta} = \frac{k_{2,0} + k_{2,1}K'_A x}{1 + K'_A x} \quad (5)$$

TABLE 3. *Coefficients in the velocity expression (Eq. 1) for the kinetics of M^+ activation*

$\frac{\alpha}{k_{-A}k'_{-A}}$	$(k_{2,0} + k_{2,1}K'_A x)(k_{1,0} + k_{1,1}K_A x) + k_{2,0}k_{1,0}\left(\frac{k_{2,1} + k_{-1,1}}{k'_{-A}}\right) + k_{2,1}k_{1,1}\left(\frac{k_{2,0} + k_{-1,0}}{k'_{-A}}\right)K_A x$
$\frac{\beta}{k_{-A}k'_{-A}}$	$\frac{k_{1,0}k_{1,1}}{k_{-A}}(k_{2,0} + k_{2,1}K'_A x)$
$\frac{\gamma}{k_{-A}k'_{-A}}$	$[(k_{-1,0} + k_{2,0}) + (k_{-1,1} + k_{2,1})K'_A x](1 + K_A x) + \frac{(k_{-1,0} + k_{2,0})(k_{-1,1} + k_{2,1})}{k'_{-A}}(1 + K_A x)$
$\frac{\delta}{k_{-A}k'_{-A}}$	$(k_{1,0} + k_{1,1}K_A x)(1 + K'_A x) + k_{1,0}(k_{-1,1} + k_{2,1})\left(\frac{1}{k'_{-A}} + \frac{1}{k_{-A}}K'_A x\right) + k_{1,1}(k_{-1,0} + k_{2,0})\left(\frac{1}{k_{-A}} + \frac{1}{k'_{-A}}K_A x\right)$
$\frac{\varepsilon}{k_{-A}k'_{-A}}$	$\frac{k_{1,0}k_{1,1}}{k_{-A}}(1 + K'_A x)$

TABLE 4. *Kinetic parameters of M^+ activation*

Type	v/e_{tot}	$s = \alpha/\gamma$	$k_{cat} = \beta/\varepsilon$ or α/δ
Ia	$\frac{\alpha[S]}{\gamma + \delta[S]}$	$\frac{s_1 K_A x}{1 + K_A x}$	$k_{2,1}$
Ib	$\frac{\alpha[S] + \beta[S]^2}{\gamma + \delta[S] + \varepsilon[S]^2}$	$\frac{s_1 K_A x}{1 + K_A x} + (\omega - 1)\frac{s_1 K_A x}{1 + K_A x}\frac{1}{1 + \omega\frac{k_{1,1}}{k_{1,0}}K_A x + \frac{k_{-1,1} + k_{2,1}}{k'_{-A}}}$	$\frac{k_{2,1}K'_A x}{1 + K'_A x}$
Ib*	$\frac{\alpha[S]}{\gamma + \delta[S]}$	$\frac{s_1 K_A x}{1 + K_A x} + (\omega - 1)\frac{s_1 K_A x}{1 + K_A x}\frac{1}{1 + \omega\frac{k_{1,1}}{k_{1,0}}K_A x}$	$\frac{k_{2,1}K'_A x}{1 + K'_A x}$
II	$\frac{\alpha[S] + \beta[S]^2}{\gamma + \delta[S] + \varepsilon[S]^2}$	$\frac{s_0 + s_1 K_A x}{1 + K_A x} + (\omega - 1)\frac{K_A x}{1 + K_A x}\frac{s_1 - \frac{k_{1,1}}{k_{1,0}}s_0}{1 + \omega\frac{k_{1,1}}{k_{1,0}}K_A x + \frac{k_{-1,1} + k_{2,1}}{k'_{-A}}}$	$\frac{k_{2,0} + k_{2,1}K'_A x}{1 + K'_A x}$
II*	$\frac{\alpha[S]}{\gamma + \delta[S]}$	$\frac{s_0 + s_1 K_A x}{1 + K_A x} + (\omega - 1)\frac{K_A x}{1 + K_A x}\frac{s_1 - \frac{k_{1,1}}{k_{1,0}}s_0}{1 + \omega\frac{k_{1,1}}{k_{1,0}}K_A}$	$\frac{k_{2,0} + k_{2,1}K' x}{1 + K'_A x}$

* M^+ in rapid equilibrium with the enzyme. Type Ia, M^+ absolutely required for substrate binding (no ES intermediate in scheme 1); type Ib, M^+ absolutely required for catalysis ($k_{2,0}$=0 in scheme 1); type II, M^+ as an allosteric effector.

$$s = \frac{\alpha}{\gamma} = \frac{s_0 + s_1 K_A x}{1 + K_A x} + (\omega - 1)\frac{K_A x}{1 + K_A x}\frac{s_1 - \frac{k_{1,1}}{k_{1,0}}s_0}{1 + \omega\frac{k_{1,1}}{k_{1,0}}K_A x} \quad (6)$$

Interestingly, the expression for k_{cat} is not affected by the drastic change in the form of v, and even s changes only slightly. It should be pointed out that the condition $\omega = 1$ was identified by Botts and Morales to ensure Michaelis-Menten kinetics (28). However, the above equations show that such condition is only sufficient, but not necessary, for Michaelis-Menten kinetics. Even when the enzyme obeys Michaelis-Menten kinetics, the value of K_A is difficult to resolve because of the form of *Equation 6*. Measurements of this important parameter must be carried out by means of other techniques, such as enzyme titration through circular dichroism or fluorescence spectroscopy. Alternatively, the value of ω and $k_{1,1}/k_{1,0}$ must be resolved from independent measurements of substrate hydrolysis as done for thrombin (177).

Kinetic signatures of relevant types of activation based on a recent classification of M^+-activated enzymes (70) may differ significantly, and k_{cat} becomes of diagnostic value (Fig. 12). The mechanism of M^+ activation can be established unequivocally from crystal structures as cofactor-like (type I) or allosteric (type II). In the former case, substrate anchoring to the enzyme active site of the enzyme is mediated by M^+, often acting in tandem with a divalent cation like Mg^{2+}. In such a mechanism, M^+ coordination is absolutely required for catalysis or substrate recognition. In the latter, M^+ binding enhances enzyme activity through conformational transitions triggered upon binding to a site where the cation makes no direct contact with substrate. In this case, the M^+ is not expected to be absolutely required for either binding or catalysis. M^+ activation, whether type I or type II, is

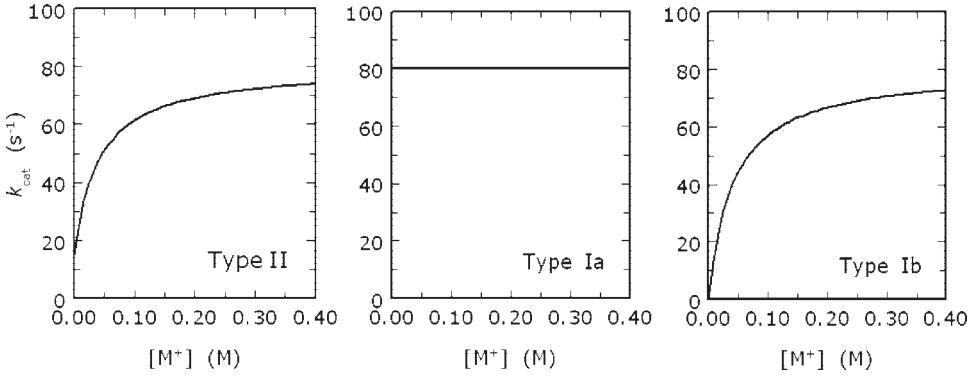

FIG. 12. M^+ dependence of k_{cat} is diagnostic for various cases of M^+ activation based on scheme 1. In type II activation, the value of k_{cat} changes from a finite low value to a higher value. The midpoint of the transition defines K'_A, the binding constant for M^+ binding to ES. In type Ia activation, M^+ is required for S binding and the value of k_{cat} is independent of $[M^+]$. In type Ib activation, M^+ is required for S hydrolysis, and the value of k_{cat} changes like in type II activation, but goes to zero when $[M^+] = 0$.

determined by two events. First, M^+ binds to the enzyme to convert E to EM and, second, the binding triggers changes in EM that produce higher catalytic activity. There are two important implications in this process. First, structural determinants responsible for M^+ binding need not be the same as those responsible for transduction of this event into enhanced catalytic activity. Second, the extent of activation s_1/s_0 is energetically independent from the affinity of M^+ binding. M^+ activation is not possible in the absence of M^+ binding ($K_A = 0$ and $K'_A = 0$). However, absence of M^+ activation can also be caused by absence of transduction when M^+ binding is present but does not change the values of the kinetic rate constants.

Scheme 1 in its general form applies to type II activation, i.e., when M^+ acts as an allosteric effector that promotes substrate binding and catalysis by changing the conformation of the enzyme. In this case, steady-state velocity of substrate hydrolysis should be measured accurately to confirm Michaelis-Menten kinetics. Departure from such behavior is indicative of binding and dissociation of M^+ that take place on the same time scale as substrate binding and dissociation. If the enzyme obeys Michaelis-Menten kinetics, then binding and dissociation of M^+ are fast compared with all other rates. Measurements of k_{cat} and s as a function of $[M^+]$ should reveal an increase in both parameters from finite low values, $k_{2,0}$ and s_0, to higher values, $k_{2,1}$ and s_1. The midpoint of the transition in the k_{cat} versus $[M^+]$ plot yields K'_A, the equilibrium association constant for M^+ binding to the enzyme-substrate complex. The midpoint of the transition in the s versus $[M^+]$ plot yields an approximate measure of K_A, the equilibrium association constant for M^+ binding to the free enzyme. An example of type II activation is offered by thrombin, a Na^+-activated type II enzyme that obeys Michaelis-Menten kinetics (348).

Scheme 1 applies in a reduced form when the M^+ acts as a cofactor in type I enzymes. Two subgroups of type I enzymes can then be distinguished. Type Ia enzymes cannot bind substrate in the absence of M^+ (ES does not exist in scheme 1), whereas type Ib enzymes cannot mediate catalysis in the absence of M^+ ($k_{2,0} = 0$ in scheme 1) yet allow substrate binding. In type Ia activation, scheme 1 is linear and contains only E, EM, and EMS. The enzyme always obeys Michaelis-Menten kinetics, regardless of whether binding and dissociation of M^+ are fast or slow. The relevant expressions for k_{cat} and s are obtained from *Equations 5* and *6* by taking the limits $k_{1,0} \to 0$, $k_{-1,0} \to 0$, $k_{2,0} \to 0$, and $K'_A \to \infty$, so that

$$k_{cat} = k_{2,1} \tag{7}$$

$$s = \frac{s_1 K_A x}{1 + K_A x} \tag{8}$$

Equations 7 and *8* are significantly different from *Equations 5* and *6*. Type Ia activation always leads to Michaelis-Menten kinetics, a value of k_{cat} that is independent of $[M^+]$ and a value of s that increases monotonically with $[M^+]$ from 0 to s_1. Diol dehydratase shows a k_{cat} that does not change among M^+ that produce very different activation (326). This suggests that k_{cat} is constant, although s changes widely, as predicted by *Equations 7* and *8* for type Ia activation. The activating effect of K^+ in this enzyme is therefore to enable substrate binding. In type Ib activation, scheme 1 is the same as in the case of type II activation except for $k_{2,0} = 0$. The enzyme obeys Michaelis-Menten kinetics only if binding and dissociation of M^+ are fast compared with all other rates. The relevant expressions for k_{cat} and s are

$$k_{cat} = \frac{k_{2,1} K'_A x}{1 + K'_A x} \tag{9}$$

$$s = \frac{s_1 K_A x}{1 + K_A x} + (\omega - 1)\frac{K_A x}{1 + K_A x}\frac{s_1}{1 + \dfrac{k_{2,1} + k_{-1,1}}{K'_{-A}} + \omega \dfrac{k_{1,1}}{k_{1,0}} K_A x} \tag{10}$$

Hence, type Ib activation can easily be distinguished from type Ia activation because k_{cat} increases with $[M^+]$ from 0 to s_1. Furthermore, type Ib activation can easily be distinguished from type II activation because both k_{cat} and s are 0 in the absence of M^+. An example of type Ib activation was reported by Kachmar and Boyer (165) for pyruvate kinase, a K^+-activated type I enzyme. More recent measurements of the activating effect of K^+ on pyruvate kinase confirm type Ib activation, with the value of k_{cat} dropping to zero in the absence of M^+ (187, 239). This demonstrates that binding of K^+ in pyruvate kinase is strictly required only for catalysis and not for substrate binding to the active site. Figure 12 shows the different behavior of k_{cat} in the three possible activation cases. The relevant kinetic expressions for the various types of activation are summarized in Table 4.

B. Structural Classification

Although kinetic signatures of M^+ activation are different enough among type I and type II mechanisms, experimental errors often leave the exact mechanism of activation unresolved. For example, a type II enzyme for which $k_{2,0}$ and s_0 are negligible relative to $k_{2,1}$ and s_1 is difficult to distinguish from a type Ib enzyme. This case is approached by inosine monophosphate dehydrogenase from *Tritrichomonas foetus* where K^+ increases the k_{cat}

>100-fold from a very low basal level (106). Likewise, a type I enzyme capable of binding and hydrolyzing substrate at measurable rates even in the absence of M^+ would bear kinetic signatures indistinguishable from type II activation. An example of such enzyme is the Na^+-activated type I enzyme β-galactosidase from *E. coli*. Measurements of s and k_{cat} for the hydrolysis of *para*-nitrophenyl-β-D-galactopyranoside show type II activation with values of $k_{2,0}$ and s_0 that are, respectively, 2- and 16-fold lower than $k_{2,1}$ and s_1 (362). The mechanism of kinetic activation can be resolved unambiguously only by structural investigation. Recent availability of high-resolution crystal structures of M^+-activated enzymes has made it possible to formulate a simple unambiguous classification (70) (Table 5).

M^+-activated enzymes can be further grouped based on the preference for Na^+ or K^+, as established by kinetic studies and mechanism of activation as shown from struc-

TABLE 5. *Classification of M^+-activated enzymes*

Enzyme	PDB entry*	Ligands†	Reference Nos.
	K^+-activated type I		
Branched-chain α-ketoacid dehydrogenase kinase	1GJV, 1GKZ; *Free:* 1GKX	5 (4-0-1)	197
Diol dehydratase	1DIO, 1EEX, 1EGM, EGV, 1UC4, 1UC5; *Free:* 1IWB	7 (5-0-2)	299
Fructose 1,6-bisphosphatase	1FP1	4 (3-0-1)	337
Glycerol dehydratase	1IWP; *Free:* 1MMF	7 (5-0-2)	191
GroEL	1KP8, 1PCQ, 1SVT, 1SX3	7 (2-4-1)	344
Hsc70	1BUP, 1HPM, 1KAX, 1KAY, 1KAZ, 1QQM, 1QQN, 1QQO; *Na^+ bound:* 1BA0, 1BA1, 1UD0, 3HSC	8 (2-3-3) 7 (5-1-1)	93, 352
MvRadA	1XU4; *Free:* 1T4G	4 (2-1-1)	358
Pyridoxal kinase	1LHR, 1RFT, 1RFU; *Free:* 1LHP	6 (4-1-1)	190
Pyruvate dehydrogenase kinase	1Y8N, 1Y8O, 1Y8P	5 (4-0-1)	167
Pyruvate kinase	1A3W, 1A3X, 1A49, 1AQF, 1F3W, 1F3X, 1LIU, 1LIW, 1LIX, 1LIY, 1PKN, 1T5A; *Na^+ bound:* 1A5U	6 (4-1-1)	185
S-adenosylmethionine synthase	1MXA, 1MXB, 1MXC, 1O90, 1O92, 1O93, 1O9T, 1P7L, 1QM4, 1RG9, 1XRA, 1XRB, 1XRC	4 (3-0-1)	172
	K^+-activated type II		
Branched-chain α-ketoacid dehydrogenase	1DTW, 1OLS, 1OLU, 1OLX, 1U5B, 1V11, 1V16, 1V1M, 1V1R, 1X7W, 1X7X, 1X7Y, 1X7Z, 1X80	5 (5-0-0)	87
Dialkylglycine decarboxylase	1D7R, 1D7S, 1D7U, 1D7V, 1DKA, 1M0N, 1M0O, 1M0P, 1M0Q; *Na^+ bound:* 1D7R, 1D7S, 1D7U, 1D7V, 1DGD, 1DKA, 1M0N, 1M0O, 1M0P, 1M0Q, 2DKB	6 (5-1-0)	324, 325
MutL	1NH1; *Na^+ bound:* 1NHJ	5 (4-1-0)	151
Ribokinase	1GQT, 1TYY, 1TZ3, 1TZ6	6 (6-0-0)	7, 373
Ser dehydratase	1PWH; *Free:* 1PWJ	6 (6-0-0)	363
Tryptophanase	1AX4	7 (4-3-0)	156
Tyrosinase	1TPL, 2TPL	7 (4-3-0)	316
	Na^+-activated type I		
β-Galactosidase	1DP0, 1HN1, 1JYN, 1JYV, 1JYW, 1JYX, 1JYY, 1JYZ, 1JZ0, 1JZ1, 1JZ2, 1JZ3, 1JZ4, 1JZ5, 1JZ6, 1JZ7, 1JZ8, 1PX3, 1PX4, 1TG7, 1XC6	5 (3-1-1)	161, 162
Fructose 1,6-bisphosphate aldolase	1B57, 1RV8, 1RVG	6 (4-1-1)	125
Tagatose 1,6-bisphosphate aldolase	1GVF	6 (5-0-1)	124
	Na^+-activated type II		
Factor Xa	1P0S, 2BOK	6 (4-2-0)	291
Thrombin	1A2C, 1A46, 1A4W, 1A5G, 1A61, 1AD8, 1B5G, 1BB0, 1C1U, 1C1V, 1C1W, 1C4U, 1C4V, 1C5L, 1C5N, 1C5O, 1CA8, 1D3D, 1D3P, 1D3Q, 1D3T, 1D4P, 1D6W, 1D91, 1DE7, 1DOJ, 1DX5, 1GHV, 1GHW, 1GHX, 1GHY, 1GJ4, 1GJ5, 1JM0, 1JOU, 1K21, 1K22, 1O2G, 1O5G, 1OYT, 15B1, 1SFQ, 1SG8, 1TBZ, 1VZQ, 1XMN, 1Z8I, 1Z8J, 2THF, 7KME, 8KME; *K^+ bound:* 2A0Q; *Free:* 1SGI, 1SHH, 2AFQ, 2A0Q	6 (2-4-0)	247, 262
Trp synthase	1A50, 1A5S, 1BKS, 1C29, 1C8V, 1C9D, 1CW2, 1CX9, 1FUY, 1K3U, 1K7E, 1K7X, 1K8X, 1K8Y, 1K8Z, 1KFC, 1KFE, 1KFJ, 1KFK, 1QOP, 1UBS, 1V8Z, 2TRS, 2TSY, 2TYS, 2WSY; K^+bound: 1A5A, 1A5B, 1BEU, 1TTQ	5 (3-2-0)	281, 349

* From a total of over 1,500 structures containing Na^+ or K^+, deposited in the PDB as of April 12, 2006. † The format is *N* (p-w-s), where *N* is the sum of ligands from the protein (p), water (w), and substrate (s). Only the most relevant references are listed.

tural analysis. Crystallographic assignment of Na^+ or K^+ is nontrivial, even for high-resolution structures. Na^+ has a small ionic radius (0.97 Å) and the same number of electrons as a water molecule. K^+ has a higher electron density but an ionic radius (1.33 Å) almost identical to that of a water molecule. Hence, correct assignment of Na^+ and K^+ must be based on several criteria: presence of a spherical electron density peak at a σ level in the F_0-F_c map considerably above that of all other water molecules, number of surrounding O atoms and B-value comparable to neighboring atoms. Anomalous scattering often provides unequivocal evidence of K^+ and larger M^+. Additional important criteria involve proper M^+-O distances, on the average 2.4 Å for Na^+-O and 2.8 Å for K^+-O pairs (130), and valence values close to unity (229). Valence of an ion was originally defined by Pauling (251) as a measure of bond strength. Brown and Wu (33) parameterized this basic concept in terms of a simple force field that depends on the M^+-O distance and an empirical exponent. This force field has been implemented into the WASP algorithm to screen solvent molecules in protein crystals and to identify bound cations (229). The original formula introduced by Brown and Wu has been recently redefined (219). Figure 13 shows the ideal M^+-O distance based on Brown's formula for Na^+ and K^+ as a function of coordination geometry. Average Na^+-O and K^+-O distances found from analysis of high-resolution structures databases (130) are in excellent agreement with the prediction of the valence theory and single out an optimal coordination of six or seven ligands for K^+ and five or six ligands for Na^+.

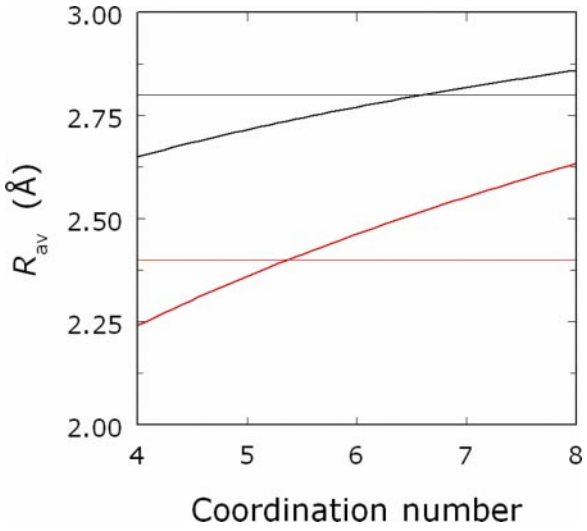

FIG. 13. Predicted average M^+-O distances as a function of coordination geometry for Na^+ (red) and K^+ (black). The relationship is derived from Brown's force field (33) by imposing a value of unity for the valence of Na^+ and K^+ and solving for the average distance (R_{av}) in a symmetrical coordination shell where all ligands are equidistant from M^+. The equation used is $R_{av} = Rc^{-1/N}$, where c is the coordination number, R is the specific distance, and N is the power law exponent. The values of R are 1.622 Å (Na^+) and 2.276 Å (K^+). The values of N are −4.29 (Na^+) and −9.1 (K^+). Horizontal thin lines depict the average M^+-O distances for Na^+ (red) and K^+ (black) determined from analysis of structures in the Cambridge Database (130). The intersections between the curves and the horizontal lines define the optimal coordination geometry. The values of 5–6 for Na^+ and 6–7 for K^+ are in excellent agreement with the observed coordination in available protein crystal structures (see Table 5).

C. K^+-Activated Type I Enzymes

Diol and glycerol dehydratases provide the simplest example of type I enzymes (191, 299). Diol dehydratase is a coenzyme B_{12}-dependent enzyme with an absolute requirement for K^+ (326). The requirement is explained eloquently by the crystal structure of the enzyme bound to propanediol (Fig. 14). K^+ is coordinated by five ligands from the protein and acts as a "bait" for two hydroxyl O atoms of the substrate (299), thereby explaining how absence of K^+ would make binding of substrate impossible. In the free form, the enzyme retains K^+ in essentially the same coordination yet replaces two substrate ligands with water molecules (298). Practically the same result is observed for glycerol dehydratase, which binds the essential K^+ in the same coordination shell in the absence of glycerol (191) by replacing the glycerol hydroxyl O atoms as ligands (364) with water. Involvement of M^+ is commonly applied to overcome substrate charge rather than neutral substrates.

A crucial role for M^+ is observed in several phosphoryl transfer enzymes such as pyruvate kinase, ribokinase, and class II aldolases (discussed below). It is tempting to speculate that K^+ involvement in phosphoryl transfer reactions in kinases evolved from proteins recognizing K^+ bound to the phosphate backbone of nucleic acids. Indeed, several large RNA polymers apply selective coordination of a K^+ with the phosphoryl group to ameliorate unfavorable energetics of buried phosphate groups, thus allowing more complex structures and ribozyme catalysts to form (57, 127). Compensation for charge density in combination with rapid association and dissociation kinetics allows M^+ to play vital roles in enzyme-catalyzed reactions involving electrostatic interactions.

Enzymes involved in phosphoryl transfer reactions were long recognized to be the dominant group among M^+-activated enzymes (86, 314), and this early observation is confirmed by the entries in Table 5. In addition to K^+, these enzymes have an absolute requirement for a divalent cation, typically Mg^{2+} (30, 223, 237, 336, 359). The mechanism of activation typically involves K^+ and Mg^{2+} acting in tandem to provide optimal docking for the phosphate moiety of substrate into the protein active site. Pyruvate kinase is a crucial enzyme of the glycolytic pathway that catalyzes production of the second of two ATP molecules by converting phospho*enol*pyruvate and ADP to pyruvate and ATP. This was the first enzyme to be

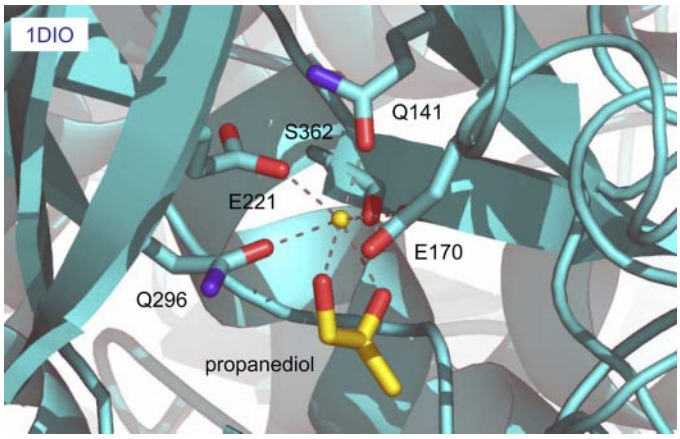

FIG. 14. Structural basis of type I K^+ activation of diol dehydratase (1DIO, see also Table 5). Shown are substrate (CPK, C in yellow), relevant residues (CPK, C in cyan), and K^+ (yellow sphere). K^+ is coordinated by five ligands from the protein and acts as a "bait" for the two hydroxyl O atoms of propanediol.

identified to require K^+ for optimal catalytic activity (30). The requirement is absolute, along with two Mn^{2+} or Mg^{2+} (214, 215). Recent structural work has provided a molecular framework to understand the crucial role of K^+ in this key enzyme (163, 186). Pyruvate kinase is allosterically regulated and features a tetrameric structure where each subunit is arranged in four separate domains. The NH_2-terminal N domain is a short helical stretch. The active site is formed by the A domain (residues 19–88 and 189–360) capped by a nine-stranded β-barrel B domain (residues 89–188). Two segments of the A domain fold into a parallel $(\alpha/\beta)_8$ barrel with two additional α-helices. The COOH-terminal C domain is the locale for regulatory interactions and folds as an α/β open sheet. A structure of the yeast enzyme solved in the presence of the substrate analog phosphoglycolate (163) reveals close interaction between K^+ and Mn^{2+} with groups of the active site and substrate (Fig. 15). Substrate binds in the active site cleft between domains A and B formed by residues Arg-49, Asn-51, Asp-84, Ser-213, Lys-240, Glu-242, Asp-266, and Thr-298. The phosphate of substrate is in a favorable electrostatic coupling with Arg-49 and Lys-240 within the pocket. However, coupling is influenced and controlled by the presence of Mn^{2+} and K^+. The divalent cation anchors the substrate via its carboxylate and phosphoester O atoms to the carboxylate O atoms of Glu-242 and Asp-266. On the other hand, K^+ increases electrostatic coupling of the phosphate group by screening the carboxylate O of Asp-84, which is engaged in the coordination shell along with carbonyl O of Thr-85, the Oγ of Ser-53, and the Oδ1 of Asn-51. Capping the shell is the phosphate group itself that resides 3.3 Å away from K^+. This creates very favorable conditions for the transfer of the phosphate group from substrate to ATP, using Arg-49, Lys-240, Mn^{2+}, and K^+ and perhaps Ser-213 as activators and protonation contributed by Lys-240 or Thr-298. In such a scenario, it is easy to appreciate the absolute requirement of K^+ for catalytic activity. In the absence of K^+, the phosphate group of phospho*enol*pyruvate would lack a key ligand, and the favorable contributions from Arg-49 and Lys-240 would be weakened by the side chain of Asp-84. Hence, K^+ acts to electrostatically optimize substrate binding by participating in direct interaction and influencing the environment of the active site in pyruvate kinase. Although Na^+ activates pyruvate kinase only 8% relative to K^+, the crystal structures of Na^+- and K^+-bound pyruvate kinase are almost indistinguishable (185). The tandem of K^+ and Mg^{2+} is observed in other phosphoryl transfer enzymes.

GroEL is an allosteric tetradecameric protein composed of two stacked heptamers that define a large central cavity when in complex with GroES (149). Activity of GroEL is influenced by Mg^{2+} and has an absolute requirement for K^+ (336). NH_4^+ and Rb^+ partially substitute for K^+, but Li^+, Na^+, or Cs^+ are poor activators. The apparent K^+ affinity of GroEL is in the 0.08–0.6 mM range (336), by far the highest ever reported for a M^+ activated enzyme. The crystal structure of GroEL bound to ATP reveals Mg^{2+} and K^+ acting in tandem to assist binding of ATP to the protein (Fig. 16). K^+ is hepta-coordinated, with one ligand coming from Pα, two carbonyl O atoms from Thr-30 and Lys-51, and four water molecules (344). Nucleophilic attack on the Pγ of ATP is mediated by Asp-52. K^+ fixes both groups in place through some of its ligand water molecules and is assisted by Mg^{2+}, which anchors all three P groups of ATP.

Branched-chain α-ketoacid dehydrogenase (BCKD) kinase (197) and pyruvate dehydrogenase kinase (167) use a similar K^+-Mg^{2+} tandem. These mitochondrial

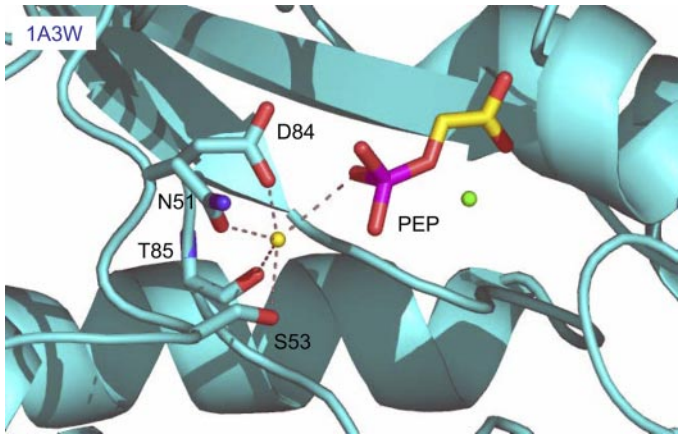

FIG. 15. Structural basis of type I K^+ activation of pyruvate kinase (1A3W, see also Table 5), the first enzyme to be identified to require K^+ for optimal catalytic activity (30). Shown are substrate (CPK, C in yellow), relevant residues (CPK, C in cyan), K^+ (yellow sphere), and Mn^{2+} (green sphere). The substrate phospho*enol*pyruvate (PEP) binds in the active site cleft in a favorable electrostatic coupling within the pocket that is optimized by Mn^{2+} and K^+.

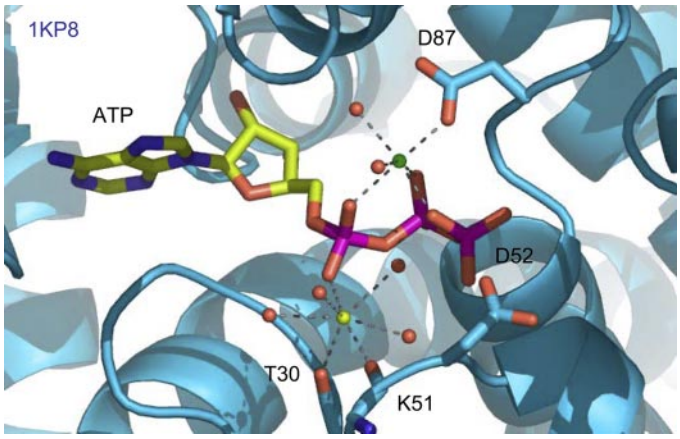

FIG. 16. Structural basis of type I K^+ activation of GroEL (1KP8, see also Table 5). Shown are substrate (CPK, C in yellow), relevant residues (CPK, C in cyan), K^+ (yellow sphere), and Mg^{2+} (green sphere). Nucleophilic attack on the Pγ of ATP is mediated by Asp-52. K^+ fixes both groups in place through some of its ligand water molecules and is assisted by Mg^{2+}, which anchors all three P groups of ATP.

serine protein kinases belong to the GHKL ATPases that also comprise gyrase (351), Hsp90 (271), bacterial histidine kinase CheA (23, 24), and the DNA mismatch repair protein MutL (151). These proteins share sequence motifs essential for ATP binding and play crucial roles in DNA metabolism, protein folding, and signal transduction. As expected for phosphotransferases, they require Mg^{2+} and K^+ for optimal catalytic activity. BCKD kinase is also activated by Rb^+, but not Na^+. All crystal structures available for this class of enzymes show Mg^{2+} bound to the Oδ1 atom of a conserved Asn and to the triphosphate moiety of ATP. In addition, K^+ is situated on the opposite side of ATP relative to Mg^{2+}, rather than in *cis* as in pyruvate kinase or Hsc70, and bridges one O atom of the phosphate moiety of ATP to typically four protein atoms. BCKD kinase has been crystallized in the presence of ATP and K^+, as well as in the apo form. Comparisons of the two structures reveal drastic changes induced by K^+ binding that explain the requirement for this cofactor. Binding of K^+ involves the carbonyl O atoms of Val-298, Asp-300, Phe-303, and Gly-337, as well as the Pα O atom of ATP (Fig. 17). Binding produces substantial ordering of the region between His-302 and Phe-336 not visible in the apo form crystal structure. Ordering of His-302 and Phe-336 produces quadruple aromatic stacking with Tyr-301 and Phe-338 to stabilize architecture of three neighboring helices and contributes to stability of the entire protein fold. A similar architecture has been observed in the recent crystal structure of pyruvate dehydrogenase kinase bound to ATP (167).

Two K^+ in tandem with Mg^{2+} are observed in the molecular chaperone Hsc70 (352) and the Rad51 recombinase homolog from *Methanococcus voltae* (358). Hsc70 belongs to the heat shock family of proteins involved in binding and release of polypeptides linked to ATP hydrolysis (110). Similar to GroEL, ATPase activity of Hsc70 is optimal in the presence of K^+ (Fig. 11), with NH_4^+ and Rb^+ showing nearly half as much activity and minimal activity in Na^+, Li^+, and Cs^+ (237). Detailed kinetic analysis of ATP hydrolysis reveals that K^+ stimulates turnover rate, with almost no effect on the equilibrium binding properties of the enzyme toward ADP. The crystal structure of a fragment of Hsc70 retaining the M^+ activation of wild-type was solved in the presence of Na^+ (93) and K^+ (352). The K^+ structure shows two K^+ bound to the active site, together with a Mg^{2+} that is required for optimal catalysis (Fig. 18). Mg^{2+} anchors the substrate to the active site residues as seen for Mn^{2+} in pyruvate kinase. Octahedral coordination of the divalent cation is mediated by four water molecules that work as extensions of Asp-10 and Asp-199, by one Pβ O atom of ADP and one O atom of P_i. The first K^+ is coordinated by eight ligands. Three ligands are provided by two O atoms of Pβ and the Pα-Pβ bridging O atom of ADP. Three additional ligands are water molecules, of which two are shared with the Mg^{2+} coordination shell. Only two ligands are donated by the protein from the carbonyl O atoms of Asp-10 and Tyr-15. The second K^+ is coordinated by seven ligands; only one water molecule is shared with the Mg^{2+} shell and another is an O atom of P_i. Remaining ligands come from the Oδ1 and Oδ2 atoms of Asp-199, Oδ1 atom of Asp-206, and the carbonyl O and Oγ atoms of Thr-204. The structure of Hsc70 bound to K^+ documents a cofactor role for the M^+ analogous to that seen in pyruvate kinase. Likewise, K^+ provides optimal electrostatic coupling for the

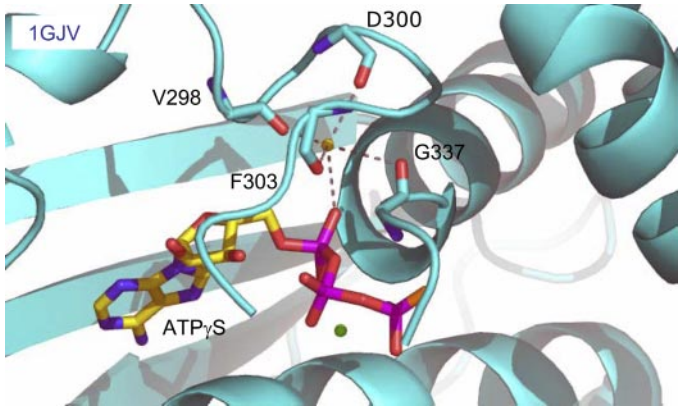

FIG. 17. Structural basis of type I K^+ activation of BCKD kinase (1GJV, see also Table 5). Shown are substrate (CPK, C in yellow), relevant residues (CPK, C in cyan), K^+ (yellow sphere), and Mg^{2+} (green sphere). BCKD kinase and pyruvate dehydrogenase kinase belong to the GHKL ATPases that also comprise gyrase, Hsp90, bacterial histidine kinase CheA, and the DNA mismatch repair protein MutL (see Fig. 21). All crystal structures available for this class of enzymes show Mg^{2+} bound to the Oδ1 atom of a conserved Asn and to the triphosphate moiety of ATP. In addition, K^+ is situated on the opposite side of ATP relative to Mg^{2+}, rather than in *cis* as in pyruvate kinase (see Fig. 16) or Hsc70 (see Fig. 19), and bridges one O atom of the phosphate moiety of ATP to typically four protein atoms.

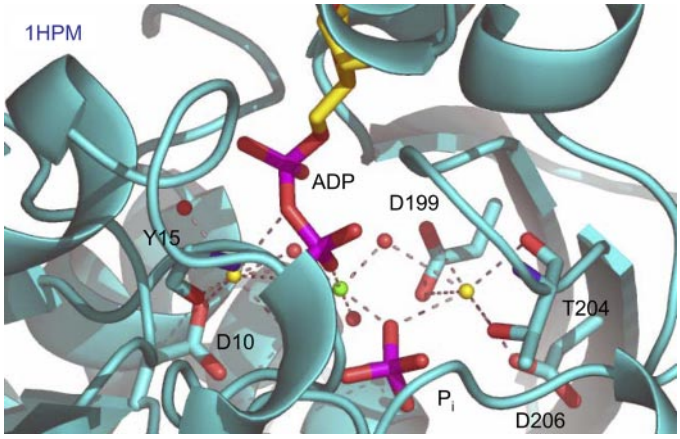

FIG. 18. Structural basis of type I K^+ activation of Hsc70 (1HPM, see also Table 5). Shown are substrate (CPK, C in yellow), relevant residues (CPK, C in cyan), and two K^+ (yellow sphere) in tandem with Mg^{2+} (green sphere). As for pyruvate kinase (see Fig. 16), K^+ provides optimal electrostatic coupling for the phosphate moiety of substrate and optimizes the register for docking in the enzyme active site and formation of the transition state. The function is assisted by a divalent cation, Mg^{2+} in this case, whose likely function is formation of a β,γ-bidentate complex with ATP favoring nucleophilic attack on the Pγ.

phosphate moiety of substrate and optimizes the register for docking in the enzyme active site and formation of the transition state. The function is assisted by a divalent cation, Mg^{2+} in this case, whose likely function is formation of a β,γ-bidentate complex with ATP favoring nucleophilic attack on the Pγ. The structure of Hsc70 solved in the presence of Na^+ reveals important changes around the M^+ binding sites (93). Most notably, Na^+ at site 1 is octahedrally coordinated and loses contacts with one of the Pβ O atoms and the Pα-Pβ bridging O atom of ADP. Na^+ at site 2, on the other hand, is tetrahedrally coordinated and loses Asp-199, Asp-206, and the carbonyl O atom of Thr-204 as ligands. These changes are very significant and cause Pβ of ADP to reposition in the active site. Hence, exact coordination of substrate depends on the ionic radius of the M^+ present, offering a sound explanation for the kinetic preference of K^+ over Na^+. Such changes have been observed in the structure of the human Hsp70 chaperone solved in the presence of Ca^{2+} and Na^+ (307). Of particular interest is the tertiary fold of Hsc70, which is almost identical to that of actin. However, requirement for a M^+ to bridge the Pα and Pβ of ADP is fulfilled by the Nζ atom of Lys-18 (164). Simple replacement of Asp-206 with Lys in Hsc70 abolishes the M^+ requirement and structurally substitutes for K^+. However, the mutant enzyme only has 5% of the activity of wild-type (353). The M^+ may facilitate product release while a positively charged side chain cannot.

Repair of double-stranded DNA breaks or stalled replication forks and homologous gene recombination involves several M^+ activated members of the recombinase superfamily. Activity of bacterial RecA, archael RadA or Rad51, and eukaryal Rad51 depends on ATP and Mg^{2+} and in the case of human and yeast, but not *E. coli*, on the presence of K^+ or NH_4^+. The Rad51 homolog from *Methanococcus voltae* has a peculiar requirement for K^+ and is practically inactive in the presence of any other M^+ (359). The crystal structure of MvRadA has been solved in the presence of an ATP analog and Mg^{2+}, in the absence and presence of K^+ (358, 359). The structures reveal a typical arrangement of Mg^{2+} and two K^+ in the active site that polarize the Pγ of ATP. Each K^+ is ligated by an O atom from the Pγ and a carboxylate from the protein, Asp-302 or Glu-151. Extensive contacts made by K^+ with the dimer interface formed upon assembly of the MvRadA filament explain the absolute requirement for the M^+. Furthermore, presence of cationic side chains in remote RecA homologs in the region surrounding K^+ in MvRadA may explain how other recombinases have constitutively replaced K^+ and are no longer activated by M^+. Interestingly, binding of K^+ in the active site causes a long-range conformational ordering of the 220–227 and 258–272 regions that form the putative single-stranded DNA binding domain. Hence, MvRadA is another example of molecular switch that has evolved to utilize a physiologically abundant M^+.

Several other important enzymes are activated by K^+. K^+ in tandem with two Mg^{2+} is observed in fructose 1,6-bisphosphatase (337) and *S*-adenosylmethionine synthase (172). Fructose 1,6-bisphosphatase is a key enzyme of gluconeogenesis and catalyzes the conversion of α-D-fructose 1,6-bisphosphate to α-D-fructose 6-phosphate. The enzyme has an absolute requirement for Mg^{2+}, but the activity is further enhanced by K^+ and inhibited by Li^+ (206). The structure of the enzyme bound to a substrate analog and several combinations of M^+ and M^{2+} have revealed the molecular basis of these effects. K^+ anchors the substrate to the active site via the 1-phosphate group and assists the role of two neighboring Mg^{2+} located in *cis*, as for other enzymes catalyzing phosphoryl transfer. K^+ replaces the guanidinium group of Arg-276 and may facilitate polarization of the phosphate group for nucleophilic attack. The inhibitory role of Li^+ is due to binding to one of the two Mg^{2+} sites (337). *S*-adenosylmethionine synthase catalyzes the formation of *S*-adenosylmethionine from ATP and Met and provides the most widely used methyl donor in biology. The enzyme has an absolute requirement for Mg^{2+} and K^+, with NH_4^+ and Rb^+ giving comparable activity, but not Li^+, Na^+, or Cs^+ (223). Substantial crystallographic work has been carried out on this enzyme in complex with various substrates, cofactors, and inhibitors (112, 321, 322). In the presence of an ATP analog and the substrate Met, the structure reveals two Mg^{2+} and a K^+ in the active site anchoring the phosphate moiety of the cofactor (172). The architecture is similar to that of pyruvate kinase and BCDK and explains the absolute requirement of K^+ in the activation of

this enzyme. Pyridoxal kinase is a member of the ribokinase superfamily involved in the ATP-dependent phosphorylation of pyridoxal to provide pyridoxal-5′-phosphate (PLP), a widely used coenzyme. The enzyme requires K^+ and Zn^{2+} as absolute cofactors (184), and the crystal structure bound to ATP has revealed the molecular basis of the activation (190). Again, the K^+ assists formation of the enzyme-substrate complex through interactions with a negatively charged phosphate moiety. All of the above examples demonstrate the vital role M^+, particularly K^+, play in enzyme-catalyzed reactions involving phosphate groups. Notably, the dynamic nature of the interaction with the M^+ in addition to electrostatic factors enable efficient catalysis. Furthermore, this highly similar role for the M^+ has evolved within multiple protein folds.

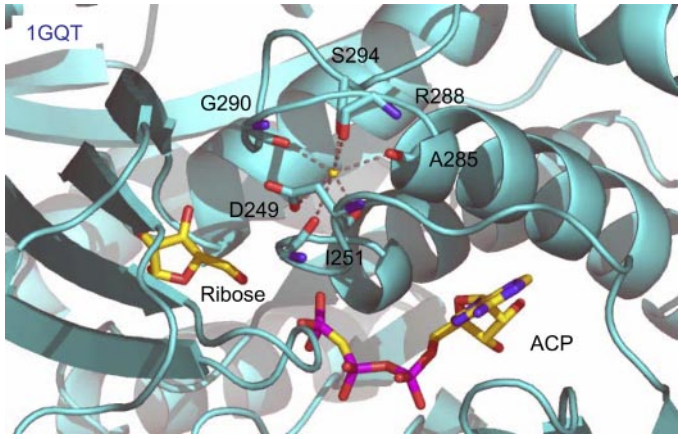

FIG. 19. Structural basis of type II K^+ activation of ribokinase (1GQT, see also Table 5). Shown are substrate (CPK, C in yellow), relevant residues (CPK, C in cyan), and Cs^+ (yellow sphere) that plays a functional role analogous to K^+. The M^+ binding site completely sequesters the M^+ from solvent and contact with substrate, the ATP analog phosphomethylphosphonic acid adenylate ester (ACP).

D. K^+-Activated Type II Enzymes

Some kinases are type II activated enzymes as the K^+ does not directly contact ATP. In this case, K^+ exerts its influence by perturbing the conformation of active site residues. Ribokinase (7) breaks the K^+-Mg^{2+} tandem by embracing the M^+ in a β-turn adjacent to the active site. The enzyme catalyzes the phosphorylation of ribose using ATP and Mg^{2+}, with the ancillary requirement of K^+. Unlike other carbohydrate kinases and the examples dealt with above, ribokinase is also activated by Cs^+ to an extent comparable to K^+, but not at all by Na^+ or Li^+ (7). Ribokinase is a homodimer with each subunit composed of two domains, a larger domain providing most of the binding interactions for substrate and a smaller domain that provides the dimer interface and a lid for the ribose. The crystal structure of ribokinase bound to Cs^+ reveals an unexpected architecture of the M^+ binding site which completely sequesters the cation from solvent and contact with substrate (Fig. 19). Cs^+ is coordinated by five carbonyl O atoms from residues Asp-249, Ile-251, Ala-285, Arg-288, and Gly-290, the carboxylate of Asp-294, and the Oγ of Ser-294. The 249–251 turn contributing to the Cs^+ coordination shell separates the M^+ from the nucleotide. Essentially the same architecture has been observed for the K^+ binding site of aminoimidazole riboside kinase (373). Although a structure of the apo form is not available, it has been proposed that binding of K^+ alters the conformation of the 249–251 sequence. In turn, the architecture of backbone N atoms of residues 252–255 are positioned for interactions with the phosphate moiety of the nucleotide and at the end of which resides the catalytic Asp-255.

MutL is similarly activated by Na^+, K^+, Rb^+, or Cs^+ but not at all by Li^+ (151). The crystal structure of MutL indicates that K^+ is penta-coordinated as in BCKD kinase and pyruvate dehydrogenase kinase, with four ligands coming from carbonyl O atoms of the protein. However, contact between K^+ and the Pα O atom of ATP has been mediated by a water molecule (Fig. 20). Why such a change would cause MutL to respond similarly to M^+ from Na^+ to Rb^+, however, is not clear, and a structure of MutL in the apo form would be very useful. Interestingly, when residue Ala-100 close to the M^+ binding site is replaced by Pro, to mimic the environment found in gyrase and BCKD kinase, MutL acquires exclusive specificity toward Na^+, which is coordinated by four carbonyl O atoms and the Pα O atom of ATP, similar to K^+ in BCKD kinase. MutL represents an intriguing intermediate between typical ATPases where K^+ directly contacts the triphosphate moiety of ATP and ribokinase that evolved a complete separation of K^+ from ATP. Here, one can almost envision the transition between type I enzymes utilizing K^+ as a cofactor into type II enzymes utilizing K^+ as an allosteric effector.

Two K^+ binding sites have been identified in BCKD. One site controls binding of thiamine diphosphate, and the other, also found in pyruvate dehydrogenase (52), stabilizes the quaternary structure (87). The BCKD catalytic machine is a member of the highly conserved mitochondrial α-ketoacid dehydrogenase complexes including the BCKD complex (BCKDC), the pyruvate dehydrogenase complex (PDC), and the α-ketoglutarate dehydrogenase complex (277). The BCKDC contains multiple copies of BCKD, as well as a dihydrolipoyl transacylase, the BCKD kinase and phosphatase. Activity of BCKD and BCKDC is completely shut off by phosphorylation of Ser-292, which results in an order-disorder transition in the phosphorylation loop of BCKD (360). BCKD is a thiamine diphosphate-dependent enzyme and is arranged as a $\alpha_2\beta_2$-heterotetramer (87). Structural work reveals that BCKDC

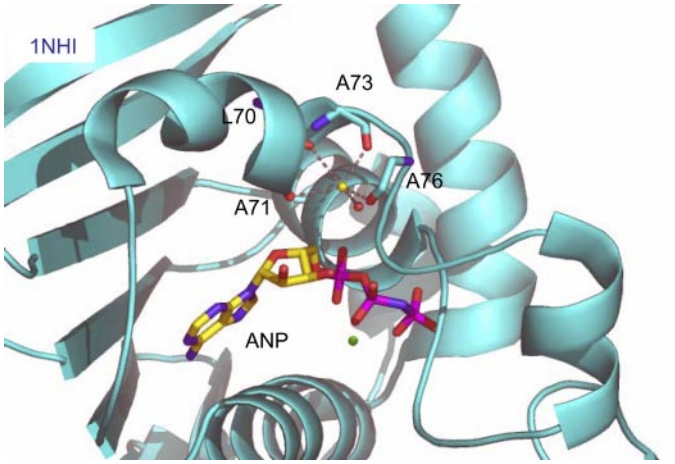

FIG. 20. Structural basis of type II K^+ activation of MutL (1NHI, see also Table 5). Shown are substrate (CPK, C in yellow), relevant residues (CPK, C in cyan), K^+ (yellow sphere), and Mg^{2+} (green sphere). MutL represents an intriguing intermediate between typical ATPases where K^+ contacts directly the triphosphate moiety of ATP (see Fig. 18) and ribokinase (see Fig. 20) that evolved a complete separation of K^+ from ATP. Substrate is the ATP analog phosphoaminophosphonic acid adenylate ester (ANP). The A100P replacement converts MutL into a Na^+-specific enzyme with Na^+ bound like K^+ in BCKD kinase (see Fig. 18). Hence, MutL is a borderline type II enzyme that can easily convert into a type I enzyme as other GHKL ATPases.

utilizes the entire repertoire of K^+ binding sites found in BCKD (87) and its kinase (197). The crystal structure of BCKD bound to ThDP shows two K^+ binding sites in crucial positions (Fig. 21). One is located within the 160-loop of the α-subunit that stabilizes cofactor binding and may explain the role of K^+ in enzyme activation. A naturally occurring mutation, T166M, has been linked to severe maple syrup urine disease and may cause disruption of this K^+ binding site with a resulting inability to bind the cofactor in a proper conformation for activity. The second site is in the β-subunit and stabilizes contacts within the $\alpha\beta$-dimer interface, explaining the role of K^+ in maintaining the tetrameric structure of BCKD (87). This second site is also found in pyruvate dehydrogenase, where the role of K^+ in site 1 is constitutively replaced by a pair of H-bonds (52). It is obvious from the architecture of site 1 that K^+ does not contact the cofactor or substrate and therefore acts allosterically on enzyme activity.

Dialkylglycine decarboxylase is a PLP-dependent enzyme endowed with both decarboxylation and transamination activities. Activity of this enzyme depends on K^+, with Li^+, Na^+, or Cs^+ displaying at most 5% of the total activity in K^+ (147). The enzyme is a tetramer composed of four identical subunits. Each monomer contains a PLP binding domain, an NH_2-terminal domain, and a COOH-terminal domain. Active sites in the tetramer are close to each other and formed from residues contributed by both monomers in a tightly assembled dimer. The resulting tetramer is formed by two such dimers associated symmetrically. Crystal structures of the enzyme solved in the presence of K^+ and Na^+, with PLP bound to the active site, have revealed the mechanism through which the enzyme utilizes K^+ for activation (324, 325). Figure 22 shows the coordination shell of K^+ near the dimer interface where PLP binds. The coordination is octahedral with K^+ bound to Oδ1 of Asp-307, the Oγ of Ser-80 and the carbonyl O atoms of Leu-78, Thr-303, and Val-305. A water molecule completes the coordination shell. When Na^+

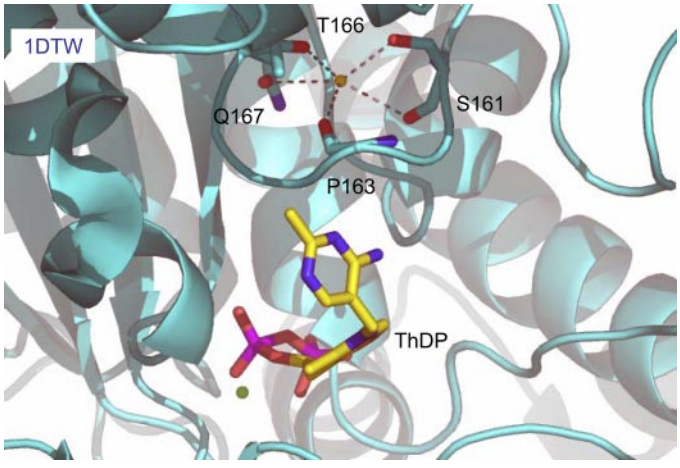

FIG. 21. Structural basis of type II K^+ activation of BCKD (1DTW, see also Table 5). Shown are substrate (CPK, C in yellow), relevant residues (CPK, C in cyan), K^+ (yellow sphere), and Mg^{2+} (green sphere). Of the two K^+ binding sites of BCKD, one controls binding of thiamine diphosphate (ThDP). A naturally occurring mutation, T166M, has been linked to severe maple syrup urine disease and may cause disruption of this K^+ binding site with a resulting inability to bind the cofactor in a proper conformation for activity.

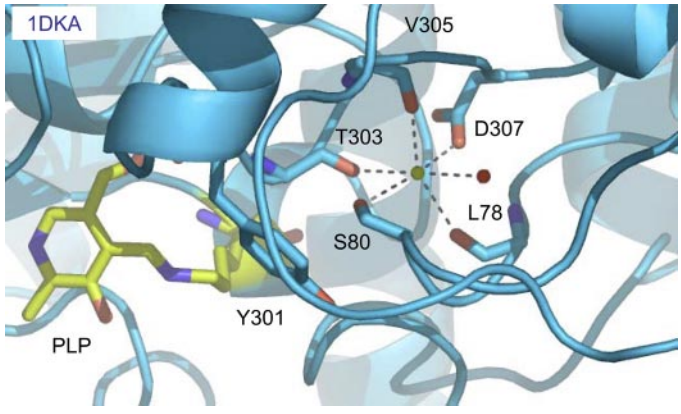

FIG. 22. Structural basis of type II K^+ activation of dialkylglycine decarboxilase (1DKA, see also Table 5). Shown are substrate (CPK, C in yellow), relevant residues (CPK, C in cyan), and K^+ (yellow sphere). Dialkylglycine decarboxylase is a pyridoxal phosphate (PLP)-dependent enzyme endowed with both decarboxylation and transamination activities. The enzyme is a beautiful example of M^+-dependent molecular switch. When Na^+ replaces K^+ in the site, the contribution from Thr-303 and Ser-80 is lost, the Oγ of Ser-80 repositions itself and clashes with the phenyl ring of Tyr-301 that adopts a new conformation incompatible with substrate binding.

replaces K^+ in the site, contribution from Thr-303 and Ser-80 is lost, and the two ligands are replaced by a water molecule. Differences in ionic radius between Na^+ and K^+ cause this drastic change and create more room for a water molecule to displace the carbonyl O atom of Thr-303 and the Oγ of Ser-80 from their coordinating position. As a result, the Oγ of Ser-80 repositions itself to clash with the phenyl ring of Tyr-301, a residue in the active site, located immediately downstream to the M^+ binding site. In turn, Tyr-301 adopts a new conformation that compromises substrate binding in the active site.

A clear allosteric role for K^+ is documented in Ser dehydratase, another PLP-dependent enzyme. Here, K^+ binds near the active site but does not contact the substrate or cofactor. Binding of K^+ induces a large conformational change that organizes the active site (363). Similar effects of K^+ have been observed in the structures of the highly homologous PLP-dependent enzymes tryptophanase and tyrosinase, for which K^+ is absolutely required for activity and Na^+ acts as a poor activator (146, 317). As for dialkylglycine decarboxylase and Ser dehydratase, the K^+ binding site makes no contact with substrate or PLP but helps organize proper architecture of the binding site (156, 316).

E. Na^+-Activated Type I Enzymes

Several class II aldolases employ a different M^+-M^{2+} tandem. Fructose-1,6-biphosphate aldolase (125) and tagatose-1,6-bisphosphate aldolase (124) apply a similar strategy observed in K^+-activated type I kinases where substrate complexation is assisted by the M^+. However, in these enzymes a pairing of Na^+-Zn^{2+} is present rather than the typical configuration of K^+-Mg^{2+}. Zn^{2+} is the catalytic agent in class II aldolases. In contrast, class I aldolases are metal-independent through application of a Schiff base forming Lys active site residue, and no M^+-activated members have been noted. Notably, tagatose-1,6-bisphosphate is unique as the coordination shell involves a cation-π interaction.

β-Galactosidase hydrolyzes lactose to galactose and glucose. The enzyme is the gene product of the lacZ operon in *E. coli* and occupies a prominent place in the history of molecular biology (162). Enzyme activity is greatly influenced by Mg^{2+} and enhanced by Na^+ or K^+, an effect discovered by Cohn and Monod in 1951 (53). Recent structural work has elucidated in exquisite detail the role of metal ions in the mechanism of β-galactosidase activity (161, 162). The interplay between Na^+ and Mg^{2+} differs from the partnership observed in kinases. Na^+ directly contacts the galactosyl 6-hydroxyl, and Mg^{2+} binds distal to the substrate (Fig. 23). Three protein atoms and two water molecules coordinate Na^+ in the free enzyme, and lactose binding replaces one of the water molecules in the coordination shell. Change in the Na^+ coordination triggers a conformational transition of the 794–804 loop linked to the repositioning of Phe-601, one of the Na^+ ligands, induced by substrate binding.

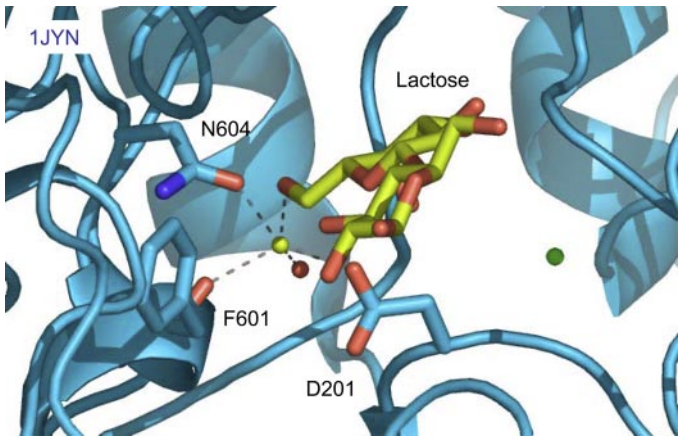

FIG. 23. Structural basis of type I Na^+ activation of β-galactosidase (1JYN, see also Table 5). Shown are substrate (CPK, C in yellow), relevant residues (CPK, C in cyan), Na^+ (yellow sphere), and Mg^{2+} (green sphere). The interplay between Na^+ and Mg^{2+} differs from the partnership observed in kinases. Na^+ directly contacts the galactosyl 6-hydroxyl, and Mg^{2+} binds distal to the substrate.

F. Na^+-Activated Type II Enzymes

Among enzymes involving PLP-mediated catalysis, Trp synthase has been studied in great detail both structurally and kinetically. Trp synthase is an $\alpha_2\beta_2$-tetramer with the subunits arranged in a linear $\alpha\beta\beta\alpha$ fashion. The α-subunit catalyzes cleavage of IGP to G3P and indole, which is then tunneled to a neighboring β-subunit that catalyzes condensation of indole with L-Ser to give L-Trp (356, 357). The enzyme requires Na^+ or K^+ for optimal catalysis (254, 356, 357). Both ground and transition states of the enzyme are influenced by M^+ binding (354–357). M^+ coordination increases catalytic activity 30-fold by changing distribution of the various intermediates along the kinetic pathway (effect on the ground state) and enhancing the rate of catalytic conversion (effect on the transition state). Crystal structures of Trp synthase bound to Na^+ or K^+ show that the M^+ does not contact substrate or PLP (Fig. 24), in agreement with the lack of absolute requirement for catalysis, and binds the β-subunit near the tunnel which shuttles the indole for complexation with L-Ser (281). Allosteric communication between subunits occurs through a set of interactions at the dimer interface, ensuring coordination of the reactions taking place at both active sites. Presence of M^+ influences the nature of these interactions including the salt bridge between Asp-56 in the α-subunit and Lys-167 in the β-subunit, which is critical for allosteric communication. When

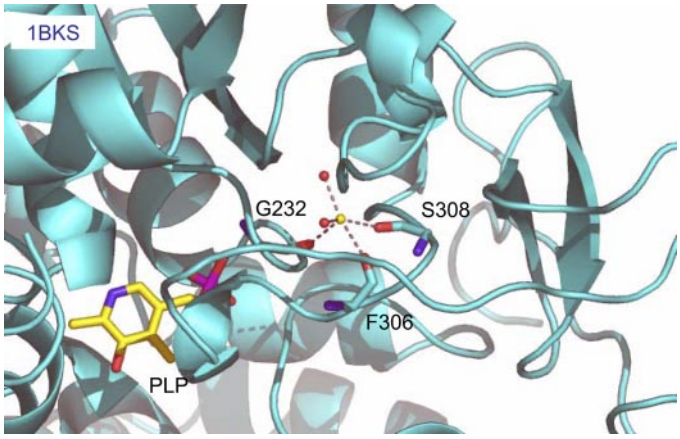

FIG. 24. Structural basis of type II Na^+ activation of Trp synthase (1BKS, see also Table 5). Shown are substrate (CPK, C in yellow), relevant residues (CPK, C in cyan), and Na^+ (yellow sphere). Na^+ does not contact substrate or PLP and binds the β-subunit near the tunnel which shuttles the indole for complexation with L-Ser.

Na^+ is bound, Asp-305 in the β-subunit exists in two orientations, one forming an ion pair with Lys-167 and the other rotated away from this residue. In the K^+ structure, Lys-167 is flipped 180° and forms an ion pair with Asp-56 in the α-subunit, thereby establishing a critical communication within the $\alpha\beta$-dimer. Changes are propagated to the tunnel partially blocked by residues Phe-280 and Tyr-279 in the Na^+ form and more open in the K^+ form. A further testimony to the long-range allosteric communication in Trp synthase comes from the structural observation that binding to the active site in the α-subunit can displace Na^+ from its site in the β-subunit (349).

In clotting proteases, the allosteric effect of Na^+ arises from optimization of substrate recognition and subtle conformational changes affecting the catalytic machinery. Na^+ binds to thrombin close to the primary specificity pocket and orients the critical Asp-189 for correct engagement of the substrate Arg side chain (Fig. 25). Therefore, Na^+ binding directly influences a critical enzyme-substrate interaction found in all trypsin-like enzymes. Furthermore, long-range effects induced by Na^+ binding propagate through a network of buried water molecules that connects up to the catalytic Ser-195 some 15 Å away (262). A similar architecture of Na^+ recognition is observed in clotting factor Xa yet does not involve the extensive water connectivity between the Na^+ site and catalytic machinery (291). A detailed discussion of the role of Na^+ in clotting proteases and implications for evolution of the family is given in section IV.

G. Other Examples of M^+ Activation

Inspection of the RCSB PDB database of molecular structures identifies many enzymes with a bound M^+ whose effect has not been investigated. Complexes involving Na^+ are most abundant (>1,100), with fewer structures containing K^+ (>400). Other M^+ are far less represented with only 10–50 structures reported. Caution must be taken when visually inspecting structures in the database as many ions are the result of crystallization conditions and not indicative of catalytic relevance. Numerous ions are modeled on the sole basis of electron density and have poor geometry. Moreover, low-resolution models may contain cations but not water molecules, and hence may confuse the viewer. Binding sites on the surface of proteins are common and are likely to play no role in enzyme catalysis, yet may influence stability. Notably, the number of water molecules compared with protein O atoms in the coordination shell of M^+ is not a good indicator of site validity. Valence and bond geometry must be considered (discussed in sect. III*B*). For a large number of enzymes, the link between structural and functional evidence of M^+ activation is less compelling than in the cases listed in Table 5. However, these enzymes deserve attention because future investigation may resolve some of the outstanding issues about the mechanism and extent of M^+ activation.

In certain instances, M^+ are found close to the catalytic residues of the enzyme, but their influence has not been addressed or shows a minimal kinetic effect. Inosine monophosphate dehydrogenase is a NAD^+-dependent enzyme that catalyzes the rate-limiting step in guanine nucleotide biosynthesis. The enzyme is activated by K^+, with an affinity of 12 mM, although the requirement is not absolute (106). The crystal structure of the enzyme from Chinese hamster reveals the presence of a K^+ binding site almost on the surface of the molecule, but with K^+ in contact with the carbonyl O atom of the catalytic residue Cys-331 (301). Structures of the enzyme from

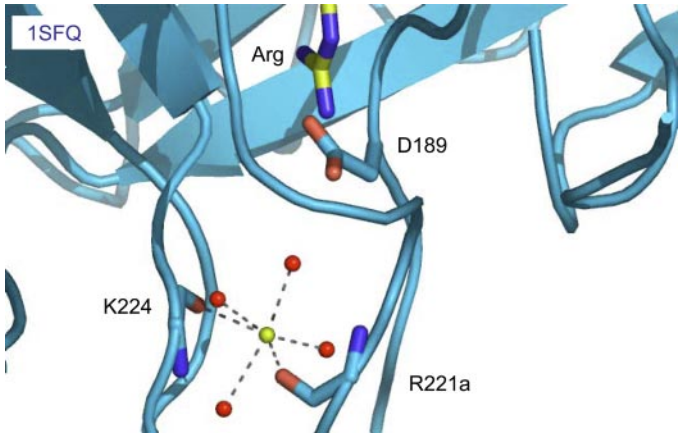

FIG. 25. Structural basis of type II Na^+ activation of thrombin (1SFQ, see also Table 5). Shown are substrate (CPK, C in yellow), relevant residues (CPK, C in cyan), and Na^+ (yellow sphere). Na^+ binding orients the critical Asp-189 for correct engagement of the substrate Arg side chain.

Tritrichomonas foetus have identified an additional K^+ binding site near the NAD^+ binding site at the dimer interface (106, 273, 274). In both cases, K^+ does not contact the substrate or cofactor, which could explain the lack of absolute requirement for catalysis. Most likely, K^+ acts as an allosteric effector (type II activation) in this system by modulating the conformation of the active site Cys-331 and the NAD^+ binding site, but further studies seem necessary to sort out the role of each K^+ binding site in this enzyme. Similarly, the recent structure of the Smurf2 ubiquitin ligase HECT domain identifies Na^+ bound adjacent to the catalytic Cys-746 but with poor geometry (238). Structural roles for M^+ complexation are also readily apparent.

Crystal structures of several enzymes demonstrate M^+ binding at the interface between dimers or stabilizing other structural elements. In the case of uridine phosphorylase, a K^+ is found at the dimer interface, but a twofold enhancement of catalytic activity is not compelling (43). Likewise, the structure of a bifunctional transformylase/cyclohydrolase enzyme documents a role for K^+ not convincingly matched by functional data (116). Structural roles for a bound Na^+ are also likely in D-ribose-5-phosphate isomerase from *Pyrococcus horikoshii* (155), 1-pyrroline-5-carboxylate reductase from *Streptococcus pyogenes* (233), and a mutated member of the C-type animal lectin family (171). Structures of lysozyme (104), rhodanese (193), and aldehyde dehydrogenase (255) with documented M^+ are not matched by kinetic or functional effects. Kex2 is a highly selective, Ca^{2+}-dependent transmembrane protease of the subtilisin family involved in the processing of neuropeptides, hormones, coagulation and growth factors. The enzyme is influenced by K^+ in a biphasic manner, with activation at concentrations <1 M followed by inhibition at higher concentrations (285). Three K^+ binding sites are observed in the crystal structure of Kex2 along with three Ca^{2+} sites (148). However, none of the three K^+ sites seems to be involved in the kinetic effect, and the activation of Kex2 by K^+ remains unresolved at the molecular level. An interesting dual role of K^+ as enzyme activator and thermostabilizing agent is observed in the archaea *Methanosarcina kandleri*. The formyltransferase from this archaea requires high concentrations of K^+ for activity and thermostability (204). The requirement is consistent with the high (>1 M) concentration of cyclic 2,3-diphosphoglycerate K^+ in the cytoplasm. Salt drives a monomer-dimer-tetramer equilibrium where only the dimer is active and tetramer thermostable.

Novel constellations of M^+ and M^{2+} have also been reported with unclear effects. Amylases catalyze the hydrolysis of glycosidic bonds. In addition to an absolute requirement for Ca^{2+}, some members of this class of enzymes feature activation by M^+ (235). The crystal structure of α-amylase from *Bacillus licheniformis* has documented the presence of an unusual Ca^{2+}-Na^+-Ca^{2+} triad that stabilizes the folding of the active site region without making contact with substrate (198, 199). The role of Na^+ in such triad is uncertain given the modest effect on catalytic activity. The structure of α-amylase AmyK38 from another *Bacillus* strain shows three Na^+ sites, consistent with the lack of Ca^{2+} requirement of this enzyme (235). The Na^+ effect is more significant, although it is reproduced by Li^+ and K^+ which calls into question its specificity. Likewise, hemopexin domains from various enzymes have been crystallized with a novel linear arrangement of two to three M^+ or M^{2+} located at the center of the four-bladed propeller characteristic of this domain. In gelatinase A, a Na^+-Ca^{2+} tandem is found (222), whereas in human promatrix metalloprotease-1, an additional Cl^- anion is included (158). In the free and heme-bound form of hemopexin, two Na^+ and one Cl^- are suggested in a similar position (246). Although unclear, it is surprising to find such similarity in structural models from disparate proteins.

Other distantly related homologs demonstrate similarity in identified binding sites with no role noted for M^+. Homoserine dehydrogenase (66) reveals a Na^+ binding site that has been suggested to be important for enzyme activity, but further functional studies are necessary. This enzyme belongs to the large superfamily of proteins containing the NAD(P)-binding Rossmann-fold domain. Remarkably, other enzymes in this family have an identified Na^+ binding site including an archaeal Ala dehydrogenase (105), rhodococcal L-Phe dehydrogenase (34, 330), malic enzyme from pigeon liver (371), and ornithine cyclodeaminase (114). Similarly, human mitochondrial aldehyde dehydrogenase binds Na^+ separated from the NAD^+ by a single stretch of protein residue on a different polypeptide fold (255). Many common metabolic intermediates and cofactors have also interwoven over evolutionary time with M^+ playing a potential role. A hyperthermophilic aldehyde ferredoxin oxidoreductase from *Pyrococcus furiosus* (48) is an all α protein where Na^+ coordinates the tungstopterin cofactor through extensive contacts including one of the phosphate moieties. Coenzyme A is coordinated by Na^+ in the Esa1 histone acetyltransferase from yeast (367). Moreover, Na^+ sites have been identified in other histone-modifying enzymes such as human HDAC8 (305).

These findings demonstrate how readily a protein scaffold can incorporate M^+ to optimize structure or function. Despite the ease at which such sites evolve, there remains difficulty in linking these binding sites to functional significance. In particular, many of the above enzymes lack convenient assays that can conclusively identify a functional role. Moreover, issues may arise as many proteins do not respond well to ionic concentrations greatly exceeding that of their natural habitat. Proteolytic enzymes have provided a wealth of information

on the energetic influences of M^+ coordination. Notably, these studies have combined kinetic analysis using different chromogenic and fluorogenic oligopeptide substrates in combination with a plethora of small molecule inhibitors and comparatively investigated through biophysical techniques.

IV. Na^+-ACTIVATED PROTEOLYTIC ENZYMES

Among M^+-activated enzymes, chymotrypsin-like proteases deserve special mention in view of the very important role played by Na^+ binding in their function and evolution (72, 176). This large family of enzymes catalyzes the hydrolytic cleavage of peptide bonds to facilitate diverse physiological and cellular functions. Over 2,000 proteases are included in the S1A family of peptidases, and they are most abundant within the animal kingdom (276). A catalytic triad of residues acts to yield a Ser that engages the substrate through nucleophilic attack followed by hydrolysis (137). The majority of S1A family members are trypsin-like enzymes that cleave polypeptide chains on the COOH-terminal side of Arg or Lys residues. Schecter and Berger (292) nomenclature terms this residue the P1 or primary "peptide" residue. Substrate residues on the NH_2-terminal side of the scissile bond are termed P2, P3, and so forth, and residues on the COOH terminus are deemed P1′, P2′, and onward. Substrate binding pockets, or "subsites," on the enzyme are labeled S and then according to the substrate residue they bind. For example, the P4 substrate residue is bound in the S4 pocket of the enzyme. Much effort has been placed on understanding mechanisms of regulation and substrate selectivity within this large family of enzymes (13, 133, 328). The primary specificity pocket (S1 site) plays a dominant role in trypsin-catalyzed reactions. However, the large surface area involved in formation of the enzyme-substrate complex has allowed multiple routes for allosteric regulation to evolve in various trypsin-like proteases to meet biological requirements. Na^+ coordination near the S1 binding pocket activates a select few trypsin-like enzymes, and binding is allosterically linked with distant and distinct regions on the protease surface.

Two β-barrels lie perpendicular to one another in addition to a COOH-terminal α-helix to comprise the chymotrypsin fold and form the basic unit of a number of key physiological processes (Fig. 26*A*). Catalytic residues (His-57, Asp-102, and Ser-195) are present in both β-barrels as well as two hot spots involved in protein-protein and protein-glycosaminoglycan interactions. These additional sites of interaction are termed exosite I and II and are well characterized in coagulation proteases (178), but sparingly in other members of the family. Each β-barrel bears functional symmetry, where one end is catalytic and the other regulatory (244). Most trypsin-like enzymes also possess a Ca^{2+} binding site adjacent to exosite I. Allosteric relationships between exosites, Na^+ site, Ca^{2+} sites, active site, and catalytic triad vary within the family and provide the underlying mechanisms for complex pathways to evolve (Fig. 26*B*). For example, sequential activation of zymogen protease precursors mediates digestion (343), immune responses (35), developmental patterning (49), blood coagulation (205), and fibrinolysis (15). Blood coagulation proteases are unique among these examples as they present a plethora of allosteric relationships within the catalytic domain in conjunction with associated protein interacting domains (EGF, kringle) and protein cofactor enhancement. Further localization to a phospholipid surface adds another level of rate enhancement through apparent increases in concentrations. Delineation of the allosteric mechanisms within clotting proteases is further complicated by the evolutionary demand for a rapid and controlled process, two features that are rarely found together in other trypsin-like enzymes.

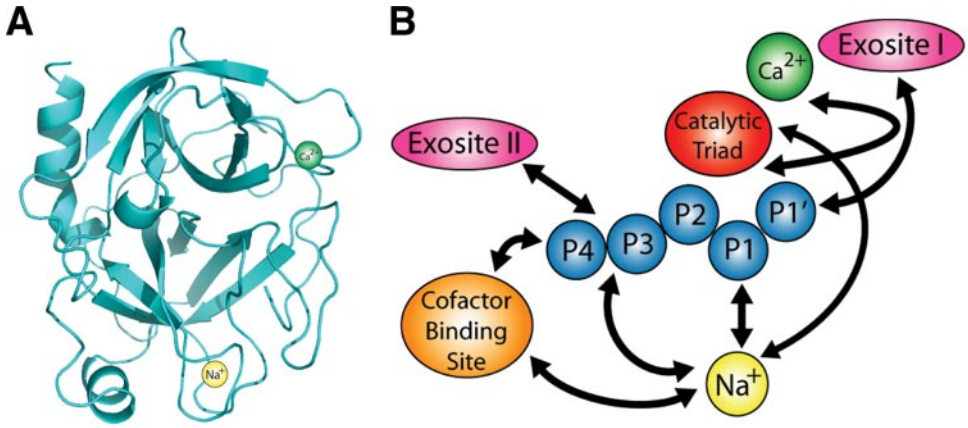

FIG. 26. Overview of S1A peptidases. *A*: two β-barrels comprise the overall fold with the Na^+ and Ca^{2+} binding sites found on different barrels. *B*: known relationships between cation and protein (exosites I and II) binding sites facilitate the rapid and controlled blood coagulation. The schematic representation superimposes on the cartoon model of the structure. The Na^+ site lies immediately adjacent to Asp-189 in the S1 pocket of the enzyme and establishes a direct link with substrate. Furthermore, Na^+ binding influences the extended binding site of the enzyme.

A. Coagulation Factors IXa, Xa, and Activated Protein C

In coagulation proteases, Na^+ binding yields several thermodynamic consequences. All members of the vitamin K-dependent family of clotting proteases, to which thrombin belongs, are endowed with type II Na^+ activation (62). As for thrombin (241, 348), the activity of activated protein C (aPC) (293, 309–312) as well as coagulation factors VIIa (FVIIa) (258), IXa (FIXa) (294), and Xa (FXa) (220, 240, 279) is enhanced significantly by the presence of Na^+. In aPC, FXa, and FIXa, Na^+ binding directly acts on the S1 pocket through local stabilization of the site and potentially influences the pK_a of Asp-189. There is no evidence of Na^+ bound to the currently available structures of aPC, FVIIa, and FIXa, although models of the Na^+ binding environment have been proposed (293, 294, 300). The coordination shell of the bound Na^+ is well defined in the 1.64 Å structure of FXa complexed with a small molecule inhibitor (291). There are six ligands in the coordination shell with one water molecule bridging Na^+ to Asp-189 (Fig. 27). Notably, bond distances of this bridging water molecule are the longest interactions. Fluctuation of Na^+ and/or the bridging water from their observed positions closer to the carboxyl group may act to attenuate the pK_a of Asp-189. A transient increase in pK_a could assist substrate dissociation.

Na^+ binding stabilizes the extended S4 binding pocket of coagulation proteases through a series of interactions that run underneath the active site and contribute to the hydrophobicity of the primary specificity pocket (300). Recently, we demonstrated that introduction of the Na^+ activation mechanism into a digestive trypsin-like enzyme required removal of a buried hydrophobic residue, Tyr-172. Further optimization of the H-bonding network of this buried water network enhanced the effect of Na^+ catalytic rate enhancement (245). These results suggest an entropic effect is involved in Na^+ activation. Destabilization of the enzyme structure due to loose packing is reconstituted in part through M^+ complexation. Dramatic conformational rearrangements are a vital feature of the entire family. For example, activity of every S1 peptidase is controlled by zymogen activation via site-specific proteolysis (231). Carbamylation studies have shown that the critical NH_2-terminal residue that defines the active state of the enzyme is more accessible in FXa and FIXa in the absence of Na^+ (293, 294, 329). In thrombin, there is a strong linkage between the protonation of the NH_2 terminus and Na^+ binding, demonstrating a role for Na^+ in stabilization of the fold (118). Thermal and chemical denaturation studies also suggest a more rigid structure in the presence of Na^+ (64). Importantly, abrogation of Na^+ binding in FXa, FIXa, and aPC through site-directed mutagenesis influences activity of the enzyme in solution, yet these effects are fully restored by complexation with their natural cofactor (41, 294).

B. Thrombin Allostery

Thrombin is the pivotal member of the blood coagulation cascade and fulfills procoagulant and anticoagulant functions (61, 348). In vivo, thrombin switches from a procoagulant to an anticoagulant enzyme upon binding to thrombomodulin, a receptor on the surface of endothelial cells (85). Thrombomodulin binds to exosite I of thrombin (261) and precludes binding of fibrinogen and the thrombin receptor PAR1. The thrombin-thrombomodulin complex provides an optimal docking surface for the productive diffusion of protein C into the active site (361). Unlike other coagulation proteases, the effect of Na^+ on thrombin function has clear and profound physiological implications. Na^+ significantly enhances cleavage of the procoagulant substrates fibrinogen and PAR1, but has no effect on the activation of the anticoagulant substrate protein C (61, 63). Na^+ also enhances activation of factors V (227), VIII (234), and XI (372). Hence, the Na^+-bound form of thrombin is responsible for the procoagulant, prothrombotic, and signaling functions of the enzyme. The Na^+-free form, on the other hand, is anticoagulant because it retains normal activity toward protein C but is unable to promote physiologically acceptable cleavage of fibrinogen or PAR1. The degree of Na^+ saturation of thrombin dictates the procoagulant or anticoagulant fate

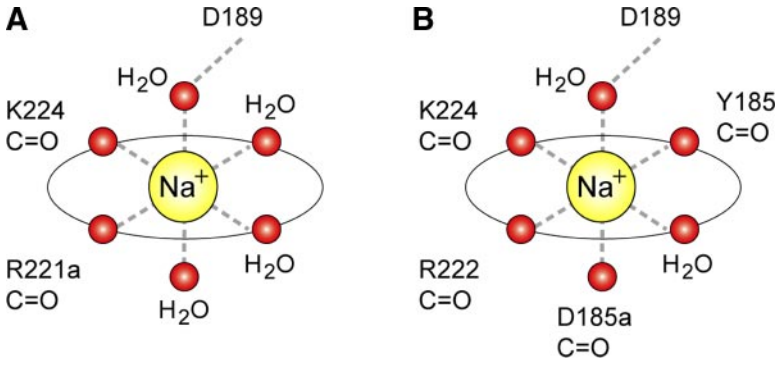

FIG. 27. Schematic of coagulation factor protease Na^+ binding sites. *A*: in thrombin (1SG8), four water molecules are found in the coordination shell and underscore the crucial role solvation plays in the allosteric transduction of Na^+ binding. *B*: in contrast, FXa (2BOK), like aPC and FIXa, has fewer water molecules involved in Na^+ complexation.

of the enzyme. Under physiological conditions of [Na^+] (140 mM), pH, and temperature, the K_d for Na^+ binding is 110 mM (118, 122, 348), and thrombin is 60% bound to Na^+. This feature makes thrombin ideally poised for allosteric regulation in vivo, perhaps by molecules that remain to be identified (183). Destabilization of Na^+ binding to thrombin invariably results in an anticoagulant effect. Naturally occurring mutations in prothrombin Frankfurt (65), Salakta (218), Greenville (142), Scranton (315), Copenhagen (308), and Saint Denis (288) affect residues important for Na^+ recognition and often cause bleeding. Engineered thrombin molecules defective for Na^+ binding produce significant anticoagulant responses both in vitro (42, 63, 327) and in vivo (111, 119, 120). Changes in the Na^+ concentration of plasma resulting in hypernatremia ([Na^+] >145 mM) or hyponatremia ([Na^+] <135 mM) are among the most common electrolyte disorders encountered by primary care providers, nephrologists, and pediatricians (1, 2) and are often associated with thrombosis or bleeding, respectively (71, 115). The Na^+ concentration of plasma has been reported to drop drastically and reversibly around platelet thrombi in vivo (242), suggesting that under certain conditions Na^+ may directly regulate the activity of thrombin in the microenvironment of blood vessels.

Kinetic signatures of Na^+ activation in thrombin obey the allosteric scheme 1 and follow type II activation. When values of s and k_{cat} for the hydrolysis of a small chromogenic substrate are measured as a function of [Na^+], significant hyperbolic increases are observed (Fig. 28). An important feature of this effect is that s and k_{cat} have low but finite values at [Na^+] = 0, regardless of whether the experiment is run at constant ionic strength (37) or not (45). Thrombin has significant activity even at an ionic strength of I = 0 M (45). This property immediately rules out type I activation. The strong dependence of k_{cat} on [Na^+] also proves the existence of two alternative conformations in equilibrium with finite catalytic activity (45), an important condition first noted by Botts and Morales in their general theory of enzyme modifiers (28). Hence, Na^+ activation of thrombin cannot be explained in terms of an equilibrium between an active and inactive conformations, with Na^+ pulling the equilibrium in favor of the active form, as recently suggested (157). Such an active-inactive equilibrium model predicts a k_{cat} independent of [Na^+], which is inconsistent with more than 20 years of enzymatic studies (45, 241, 348) (see also Fig. 28). Earlier kinetic data have suggested the existence of inactive forms of thrombin (183), that can be readily incorporated into an extension of scheme 1 (45), but their population is minuscule compared with the active conformations of the enzyme and are unlikely to play any physiological role (45).

Dissection of the Michaelis-Menten parameters in terms of the underlying kinetic rate constants in scheme 1 shows that Na^+ promotes substrate binding (higher k_1, lower K_m) and substrate hydrolysis (higher k_2, higher k_{cat}) (177). Binding of Na^+ optimizes both substrate binding and catalysis to influence the enzyme in both the ground and transition state. Measurements of s in the presence of different M^+, at the same ionic strength, reveal that thrombin is activated preferentially by Na^+ (Fig. 11) and that this preference is also seen in the equilibrium binding properties of the enzyme (267). The structure of thrombin has therefore been optimized for preferential binding of Na^+ and for allosteric transduction of Na^+ binding into enhanced catalytic activity. M^+ selectivity seen in thrombin and other M^+-activated enzymes is reminiscent of that featured by ion channels. It is therefore remarkable that such selectivity can be redesigned by rational engineering. Thrombin can be converted into a K^+-specific or Li^+-specific enzyme by site-directed mutagenesis (267, 268) (Fig. 29). Thermodynamic signatures of Na^+ binding are noteworthy. Ionic strength dependence of Na^+ binding to thrombin shows only a small effect, but temperature-dependence studies show a marked curvature in the van′t Hoff plot conducive to a large and negative heat-capacity change (122, 268). This peculiar temperature dependence is also observed for K^+ binding to thrombin (268) and for Na^+ binding to aPC (118).

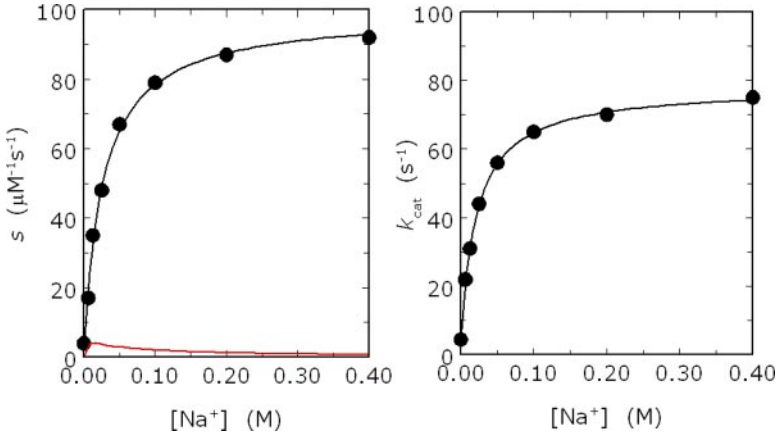

FIG. 28. Na^+ dependence of the kinetic constants $s = k_{cat}/K_m$ (*left*) and k_{cat} (*right*) for the hydrolysis of H-D-Phe-Pro-Arg-*p*-nitroanilide by thrombin. Experimental conditions are as follows: 50 mM Tris, 0.1% PEG, pH 8.0 at 25°C. The [Na^+] was changed by keeping the ionic strength constant at 400 mM with choline chloride. The data illustrate the signatures of type II activation with both s and k_{cat} showing a marked Na^+ dependence and changing from low, finite values to significantly higher values. Curves were drawn with the equations listed in Table 4 for type II* activation, with best-fit parameter values as follows: (data at *left*) $s_0 = 2.3 \pm 0.1\ \mu M^{-1} \cdot s^{-1}$, $s_1 = 99 \pm 3\ \mu M^{-1} \cdot s^{-1}$, $K_A = 38 \pm 1\ M^{-1}$; (data at *right*) $k_{2,0} = 4.7 \pm 0.2\ s^{-1}$, $k_{2,1} = 78 \pm 2\ s^{-1}$, $K_A' = 45 \pm 2\ M^{-1}$. Also shown is the contribution of the expansion term in *Eq. 6* (red line, *left*) calculated from the reported values of kinetic rate constants (177). This term contributes at most a 3% correction at low [Na^+].

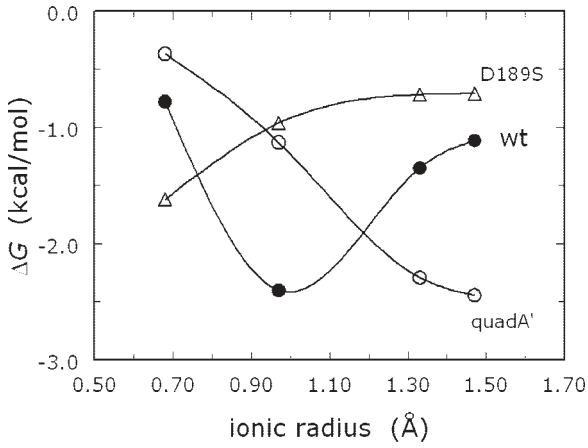

FIG. 29. M^+ specificity profile for wild-type thrombin (●) and the mutants quadA′ (○) and D189S (△). Shown are the values of the binding free energy ΔG determined for Li^+, Na^+, K^+, and Rb^+ by fluorescence titrations under experimental conditions of 5 mM Tris, 0.1% PEG, pH 8.0 at 10°C, I = 800 mM. Note how the specificity of quadA′ (268) and D189S (267) is shifted toward M^+ values of larger and smaller ionic radius, respectively. Continuous curves are spline interpolations of the data.

Site-directed mutagenesis and structural studies have provided insight into the molecular origin of Na^+ activation (262). Na^+ binding in thrombin occurs in close proximity to the primary specificity pocket of the enzyme between the 220 and 186 loops that contribute to substrate specificity in serine proteases (Fig. 30) (137, 256, 257). The bound Na^+ is octahedrally coordinated by two backbone O atoms from the protein residues Arg-221a and Lys-224 and four buried water molecules anchored to the side chains of Asp-189, Asp-221, and the backbone atoms of Gly-223 and Tyr-184a. In contrast, Na^+ binding sites of FXa (291) and aPC (293) are similarly located and arranged structurally yet involve four ligands from the polypeptide backbone and two water molecules. Extensive Ala-scanning mutagenesis of thrombin has revealed the allosteric core of residues energetically linked to Na^+ binding (262). Practically all residues of the allosteric core cluster around the Na^+ site. Na^+ binding is severely compromised (>30-fold increase in K_d) upon mutation of Asp-189, Glu-217, Asp-222, and Tyr-225 that reside within 5 Å from the bound Na^+. Asp-189 assists the orientation of one of the four water molecules ligating Na^+ and provides an important link between the Na^+ site and the P1 residue of substrate (267). Glu-217 makes polar contacts with Lys-224 and Thr-172 that help stabilize the intervening 220 loop in the Na^+ site. The ion pair between Arg-187 and Asp-222 latches the 186 loop onto the 220 loop to stabilize the Na^+ site and the pore of entry of the cation to its binding site (262). Tyr-225 plays a crucial role in determining the Na^+-dependent allosteric nature of serine proteases (62) by allowing the correct orientation of the backbone O atom of residue 224 (121), which contributes to the coordination of Na^+. The side chain of Tyr-225 also secures the integrity of the water channel surrounding the primary specificity pocket required for correct substrate recognition (121), and the backbone around Tyr-225 is oriented like the selectivity filter of the K^+ channel (70, 79) (see Fig. 9). The allosteric core is assisted by another set of residues whose Ala substitution affects Na^+ binding >10-fold. These residues are Thr-172, Tyr-184a, Arg-187, Ser-214, and Gly-223 and, together with the residues of the allosteric core, link the Na^+ binding site to the S3-S4 specificity pocket and the S1 specificity site. Ala-scanning mutagenesis of thrombin also revealed residues important for allosteric transduction. Asp-189 and Asp-221 are key residues promoting substrate binding to the Na^+-bound form and hence allosteric transduction. Asp-189 is part of the allosteric core and defines the primary specificity of the enzyme by directly coordinating the guanidinium group of Arg at P1 of substrate. Asp-221 is a crucial component of the Na^+ binding site, with its side chain anchoring one of the four water molecules ligating Na^+ and also H-bonding to Asp-189. Mutation of Asp-221 does not affect Na^+ binding, but almost abrogates the Na^+-induced enhancement of substrate hydrolysis or the preferential recognition of inhibitors (213).

Mutagenesis of the allosteric core suggests that binding of Na^+ to thrombin influences residues in the immediate proximity to the cation binding site, namely, Asp-189, Glu-217, Asp-222, and Tyr-225. Other residues making contact with the ligating water molecules in the coordination shell are Tyr-184a, Asp-221, and Gly-223, and their mutation to Ala reduces Na^+ binding >10-fold (Tyr-184a, Gly-223), or affects the allosteric transduction of this event into enhanced catalytic activity (Asp-221). Available structures of the Na^+-free and Na^+-bound forms of thrombin have largely confirmed the role of these important residues (262) and are highly similar overall, but there are five notable differences that help explain several kinetic and thermodynamic signatures of Na^+ binding to thrombin. These differences influence the following (Fig. 30): *1)* ion pairing of Arg-187:Asp-222, *2)* orientation of Asp-189 in the primary specificity pocket, *3)* conformation of Glu-192 at the entrance of the active site, *4)* orientation of the catalytic Ser-195, and *5)* architecture of the water network spanning >20 Å from the Na^+ site to the active site. A change in the conformation of the pore of entry to the Na^+ binding site is also observed between the two forms, with the pore shrinking upon Na^+ binding. Such local interactions propagate throughout the protein structure and are clearly observed in the K^+-bound form of the enzyme. Thrombin coordination of K^+ produces a reduced enzyme activation compared with Na^+ because of rearrangement of the disulfide bond between Cys-191 and Cys-220. In turn, these changes disrupt the oxyanion hole leading to lower k_{cat} for substrate hydrolysis (45).

Electrostatic interaction between Arg-187:Asp-222 connects the 220 and 186 loops that define the Na^+ site.

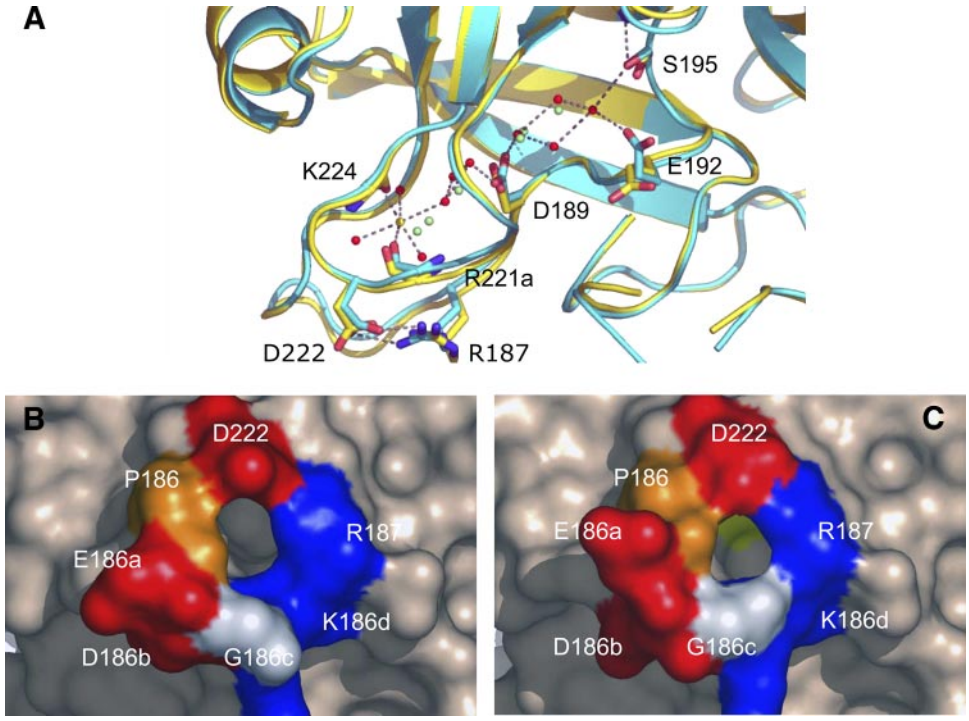

FIG. 30. Structural changes induced by Na^+ binding to thrombin depicted by the structures of the Na^+-free (1SGI, yellow) and Na^+-bound (1SG8, cyan) forms (*A*). The main changes induced by Na^+ (yellow sphere) binding are as follows: formation of the Arg-187:Asp-222 ion-pair that causes a shift in the backbone O atom of Arg-221a, reorientation of Asp-189 that accounts for the change in substrate binding, shift of the side chain of Glu-192, and shift in the position of the Oγ atom of Ser-195 that accounts for the change in k_{cat}. Also shown are the changes in the water network connecting the Na^+ site to the active site Ser-195. The water molecules in the Na^+-bound form (red spheres) are organized in a network that connects Na^+ to the side chain of Asp-189 and continues on to reach the Oγ atom of Ser-195. A critical link in the network is provided by a water molecule that H-bonds to Ser-195 and Glu-192. This water molecule is removed in the Na^+-free form, causing a reorientation of Glu-192. The connectivity of water molecules in the Na^+-free form (green spheres) is further compromised by the lack of Na^+ and proper anchoring of the side chain of Asp-189. H-bonds are shown by broken lines and refer to the Na^+-bound form. The drastic ordering of the water network in the Na^+-bound form explains the large heat capacity change linked to Na^+ binding. Mutation of Glu-192 to Ala abolishes this heat capacity change, lending support to the crucial anchoring role of this residue in the water network. The pore of entry to the Na^+ binding site is also affected by the conformational transition. The pore is wider in the Na^+-free form (*B*) compared with the Na^+-bound form (*C*) as a result of the shift in the carbonyl O atom of Gly-186c. Residues lining the pore are labeled and colored according to their chemical properties. Mutations in this region of the enzyme result in significant changes in M^+ specificity (268). Residue Asp-222 is Lys in murine thrombin. The replacement causes a loss of Na^+ activation, but retention of high catalytic activity (37).

Asp-222 belongs to the allosteric core, and the mutant D222A has drastically impaired Na^+ binding, a property mirrored to a smaller extent by the R187A mutant. The ion pair breaks when Na^+ is released, bringing about a concomitant shift in the backbone O atom of Arg-221a that directly coordinates Na^+. In the Na^+-bound form, Asp-189 is optimally oriented for electrostatic coupling with the P1 Arg residue of substrate, but its orientation changes when Na^+ is released. The change reduces affinity toward the substrate and offers an explanation for the reduced k_1 observed in the Na^+-free form. Structural changes around Asp-189 are also consistent with mutagenesis data as the D189A mutation abrogates most of the allosteric transduction of Na^+ binding. The side chain of Glu-192 relocates when Na^+ is released and no longer supports a key water molecule that links the network to the catalytic Ser-195. This residue, in turn, reorients when Na^+ is released and breaks the H-bond with the catalytic His-57. The energetic cost of realigning Ser-195 for H-bonding with His-57, which is required for the nucleophilic attack of the amide bond of substrate, contributes to the lower k_{cat} in the Na^+-free form. In the Na^+-bound form of thrombin, relative to the Na^+-free form, these residues are in a conformation more prone to interact with substrate and explains why Na^+ binding optimizes thrombin for its procoagulant, prothrombotic, and signaling functions (61, 71, 72). Orientation of Glu-192 in the Na^+-free form, however, compensates for the deleterious changes around Asp-189 and Ser-195 and reduces the electrostatic clash with the acidic residues at position P3 and P3′ of protein C. A conformation that retains activity toward protein C explains the intrinsic anticoagulant nature of the Na^+-free form of thrombin (61, 71, 72).

Conformational differences of Asp-222, Asp-189, and Ser-195 offer a plausible explanation for the reduced substrate binding and conversion in the Na^+-free form. The hallmark of allosteric proteins is the ability to couple structural domains that are separated in space. In throm-

bin, communication between the Na^+ site, Asp-189, and Ser-195 requires a network of linked processes that span more than 20 Å. Remarkably, this network is provided by a cluster of H-bonded water molecules that embed the Na^+ site, primary specificity pocket, and enzyme active site (Fig. 30). Na^+ binding organizes a network of 11 water molecules that connect through H-bonds up to side chain of Ser-195. These water molecules link β-strands involving residues 191–193, 215–219, and 225–227, which define the Na^+ site, walls of the primary specificity pocket, and fine tune substrate docking into the active site. In the Na^+-free form, only seven water molecules occupy positions in the network equivalent to those seen in the Na^+-bound form, and the connectivity is significantly altered. Change in the number and long-range ordering of water molecules linked to Na^+ binding offers an explanation for the large and negative heat capacity change measured upon Na^+ binding to thrombin (118, 122, 268). The change is likely the result of the formation of water binding sites connecting strands and loops of the Na^+ site. The network provides the long-range connectivity needed to allosterically communicate information from the Na^+ site to the active site Ser-195 and to residues involved in substrate recognition, like Asp-189 and Glu-192. Interestingly, the E192A mutation abolishes the heat capacity change linked to Na^+ binding, providing further support to the anchoring role of Glu-192 to the water network.

C. Na^+ Binding and the Evolution of Serine Proteases

Na^+ activation of thrombin and related serine proteases has contributed to our understanding of the evolution of these enzymes. Signatures of watershed events linked to evolutionary transitions in protein families can be identified from sequence comparisons and analysis of amino acid occurrences at any given position along the sequence. Evolutionary markers can be defined as dichotomous choices at given amino acid positions mapping to codons that cannot interconvert by single nucleotide mutations (31, 176). Because of their very nature, such markers identify decisive evolutionary transitions that are best understood after reading the whole section.

Analysis of over 600 sequences of serine proteases of the chymotrypsin family returns codon usage dichotomies only at three positions: residues 195, 214, and 225 (176). Sequence dichotomies used to categorize chymotrypsin-like proteases are TCN (N = any base) or AGY (Y = C or T) codon usage for the active site nucleophile Ser-195, TCN, or AGY codon usage for the highly conserved Ser-214, which is adjacent to the active site Asp-102 (177), and Pro or Tyr usage for residue 225 which determines whether a chymotrypsin-like protease can undergo catalytic enhancement mediated by Na^+ binding (62). Na^+ binding requires Tyr-225 (or Phe-225) because Pro-225 reorients the backbone O atom of residue 224 in a position incompatible with Na^+ coordination (62, 121). Primordiality of TCN compared with AGY and of Pro compared with Tyr establishes the relative age of the lineages with respect to each other. Thus Ser-195:TCN/Ser-214:TCN/Pro-225 is the most primordial marker configuration, and Ser-195:AGY/Ser-214:AGY/Tyr-225 is the most modern (176). Profiling selected proteases involved in a number of physiologically relevant processes reveals distinct evolutionary transitions (Table 6). Notably, the primordial proteases are engaged in degradative processes, with trypsin, chymotrypsin, and elastase being the best-known examples. In these early enzymes, substrate

TABLE 6. *Segregation of function and evolutionary markers in serine proteases*

	Residue 225	Codon 195	Codon 214
	Degradative		
Chymotrypsin	*Pro*	*TCN*	*TCN*
Elastase	*Pro*	*TCN*	*TCN*
Enterokinase	*Pro*	*TCN*	*TCN*
Trypsin	*Pro*	*TCN*	*TCN*
	Development		
Easter	*Pro*	*TCN*	*TCN*
Snake	*Pro*	*TCN*	*TCN*
Gastrulation defective	**Tyr**	*TCN*	*TCN*
Nudel	**Phe**	*TCN*	**AGY**
	Fibrinolysis		
tPA	*Pro*	*TCN*	**AGY**
uPA	*Pro*	*TCN*	**AGY**
Plasmin	*Pro*	**AGY**	*TCN*
	Complement		
Factor D	*Pro*	*TCN*	**AGY**
Factor I	*Pro*	*TCN*	**AGY**
Factor B	Gln*	*TCN*	**AGY**
Factor C2	Lys*	*TCN*	**AGY**
MASP-1	**Tyr**	*TCN*	*TCN*
MASP-2	**Tyr**	**AGY**	*TCN*
C1r	**Phe**	**AGY**	*TCN*
C1s	**Tyr**	**AGY**	*TCN*
	Coagulation		
Factor XIa	*Pro*	*TCN*	**AGY**
Factor XIIa	*Pro*	*TCN*	**AGY**
Thrombin	**Tyr**	**AGY**	*TCN*
Activated protein C	**Tyr**	**AGY**	**AGY**
Factor VIIa	**Phe**	**AGY**	**AGY**
Factor IXa	**Tyr**	**AGY**	**AGY**
Factor Xa	**Tyr**	**AGY**	**AGY**

Proteases are coded by font based on their evolutionary distance from the ancestral Ser-195:TCN/Ser-214:TCN/Pro-225 marker profile as italic (one marker change), bold (two marker changes), or underline (three marker changes). All proteases are human, except developmental that are from fruit fly. Markers are coded by font based on their chronology as italic (ancient) or bold (modern). * Human complement factors B and C2 have an insertion in the 220 region that makes identification of residue 225 ambiguous. Listed are the residues located 12 positions upstream of the highly conserved Trp-237.

selectivity and allosteric regulation are absent, and they fulfill a simple biological niche.

Changes in molecular markers start to appear with the developmental proteases of the fruit fly or fibrinolytic proteases. Interestingly, pressure to change residue 225 to a Na^+ accommodating residue like Tyr or Phe first emerged with developmental proteases. Dorsal-ventral polarity in *Drosophila* is controlled by a cascade of proteases involving nudel, gastrulation defective (gd), snake, and easter. These proteases generate a concentration gradient of the activated toll ligand spätzle (49). Of these proteases, nudel and gd possess Phe or Tyr, whereas snake and easter possess the typical Pro (Table 6). It is with the complement system that pressure to mutate the molecular markers becomes conspicuous. Complement appears as an evolutionary battleground for such markers where factors in the alternative pathway retain Pro-225 and factors in the lectin and classical pathways show pressure to introduce Na^+ binding. It is well known that the alternative pathway predated the lectin and classical pathways (88, 303). Interestingly, within the deuterostome lineage that gave rise to the vertebrates, the ancestor of complement factor B found in the sea urchin has Tyr-225, with Ser-195:TCN/Ser-214:AGY. It is in the sea urchin, where a primitive complement system only included the ancestors of factor B, C3, and MASP, that evolution started to explore alternative codons for Ser-214 and Na^+ binding residues like Tyr-225. That trend is revealed in the vertebrates MASPs and the proteases C1r and C1s in the classical pathway. The final stage of transition for the codons is witnessed in the blood coagulation system that evolved as a specialization of the classical pathway of the complement.

Proteases of blood coagulation are clearly split in two evolutionary groups, with FXI and FXII showing a distinct codon usage for Ser-195 and Ser-214 compared with the vitamin K-dependent FVII, FIX, FX, prothrombin, and protein C. FXI and FXII therefore evolved from a different lineage compared with the other clotting factors (249). However, an important difference in the codon usage of Ser-214 is seen between prothrombin and the other vitamin K-dependent factors. Prothrombin appears more ancestral and of a different evolutionary origin compared with the other vitamin K-dependent factors. Prothrombin possesses kringle domains and not EGF domains, whereas all other vitamin K-dependent clotting proteases carry EGF domains but not kringles. Changes in such auxiliary domains through exon shuffling were quite common during evolution (250), and it is not possible to specify a chronology for such transition. However, we surmise that prothrombin predated all other coagulation factors and was recruited in the coagulation cascade from another system, perhaps involved in immune response. The similarity of marker profiles between prothrombin, MASP-2, C1r, and C1s is particularly striking.

Evolutionary markers trace the origin of Na^+ binding to serine proteases within the complement system along the deuterostome lineage and within the developmental proteases along the protostome lineage (Table 6). Perhaps the need for Na^+ binding emerged independently during evolution along the two main branches of the animal kingdom (175). Alternatively, Na^+ binding might have emerged much earlier, before the protostome-deuterostome split. Indeed, carbonic anhydrase of the halotolerant alga *Dunaliella salina* carries an added loop for specific Na^+ binding that confers enhanced halotolerance and stability (269). The loop closely resembles the Na^+ binding loop of thrombin (Fig. 31). Allosteric activation by Na^+ in serine proteases is likely quite ancient and certainly predated vertebrates and the onset of sophisticated mechanisms of defense, like immunity and blood clotting. Type II activation by Na^+ may have evolved as a variation of halotolerance, and the Na^+ binding site morphed from a purely structural determinant of protein stability to a functional component of ligand recognition. The transition could have been triggered by the need to respond to injury caused to the cell and exposure to an extracellular environment rich in Na^+, perhaps seawater (see Table 1). Activation of a primordial enzyme could have been linked to repair of the injury. The cytoplasm of certain algae undergoes a sol→gel transition at the site of puncture of the cell, as though a Na^+-activated intracellular protease were at work (275). K^+ activation has different origins and likely evolved from mechanisms aimed at recognizing the polyphosphate backbone of nucleic acids rich in counterions like Mg^{2+} and K^+. The need for both cations acting in tandem in several kinases and phosphotransferases (see sect. III*C*) bears striking similar-

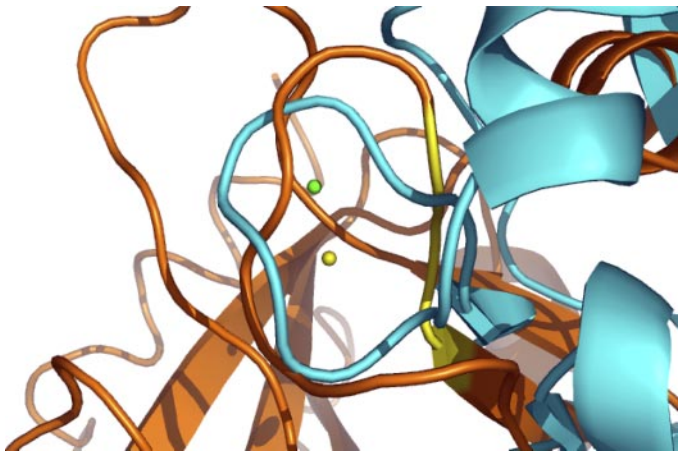

FIG. 31. Overlay of the Na^+ binding loops of carbonic anhydrase from *Dunaliella salina* (1Y7W, cyan, Na^+ as yellow sphere) and thrombin (1SFQ, brown, Na^+ as green sphere). The loop defined by the GAQADG 67–72 sequence in the carbonic anhydrase structure overlaps very well with the loop defined by the GCDRDGK 219–224 sequence in thrombin. The sequence 224–226 in the thrombin loop that overlaps with the GYG sequence in the K^+ channel (see Fig. 9) is highlighted in yellow.

ities at the molecular level with the determinants of recognition of DNA by proteins.

V. M^+ AS AGENTS OF STABILITY

M^+ coordination can stabilize macromolecules at high temperatures or ionic strength. The PDB database currently contains numerous crystal structures of proteins from thermophilic organisms, such as *Thermophilus maritima*, that possess reasonably well-defined ion binding sites on the basis of resolution, electron density, and ion valence (244, 323). Little experimental evidence exists to suggest that ion binding in these proteins substantially influences the enzyme-catalyzed reaction. Ion binding may stabilize surface-exposed residues to increase overall thermal stability with little effect or no effect on catalysis. M^+ binding is noted to enhance the stability of a number of enzymes of mesophilic origin (4, 77). Insight into halotolerance was recently provided by the crystal structure of a carbonic anhydrase II (dCA II) from *Dunaliella salina*. dCaII is an extracellular protein that retains function over a wide range of salinities and acts to provide the cell with CO_2 (91). Like other proteins from halophilic organisms, dCA II presents a uniform negatively charged surface. However, the binding pocket of the catalytic zinc is considerably more electronegative than mesophilic homologs of this enzyme. Extension of one surface-exposed loop hosts Na^+ in octahedral coordination with six ligands, two backbone carbonyl O atoms, and one Gln side chain (269). Such binding of a M^+ with residues from a single surface-exposed loop is rarely observed in other M^+-protein complexes (see Fig. 31 for a comparison with thrombin). Examples of M^+ binding sites are known in many protein folds and suggest simple mimicry through protein engineering may yield increased resistance to saline conditions and/or additional thermal stability in the presence of a bound M^+.

VI. PROTEIN ENGINEERING AND MOLECULAR MIMICRY OF M^+ ACTIVATION

Importance and widespread occurrence of enzymes activated by M^+ is testimony to the requirement for high catalytic activity under physiological conditions. Recent structural investigation, together with decades of careful kinetic analysis of such enzymes, has contributed a coherent framework on how enzyme activity is enhanced via type I and type II activation (70). The efficiency of the activation raises the possibility to engineer de novo the mechanism into enzymes devoid of such property or to mimic it by alternative molecular strategies. In either case, substantial advantages can be expected for enzymes involved in key biomedical and biotechnological applications. For example, enhancement of catalytic activity may boost the fibrinolytic efficacy of tissue-type plasminogen activator (338) or other trypsin-like enzymes.

Because the majority of serine proteases are devoid of Na^+ binding and activation, significant efforts have been devoted to introducing such property into any member of the family. Soon after the structural identification of the first Na^+ binding site in a serine protease (73), it became obvious that the single most important difference between proteases activated by Na^+ and those devoid of such property was due to the nature of residue 225 (62, 121). Residue 225 is either a Pro or Tyr in the vast majority of serine proteases (62, 176), and such dichotomous distribution is all the more remarkable because the amino acid codons of Pro and Tyr cannot interconvert by a single nucleotide substitution. Pro is found in more ancestral proteases and practically all chymotrypsin-like proteases. Tyr is found in more modern lineages, such as the complement system and the vitamin K-dependent proteases of blood coagulation (see Table 6). Tyr-225 ensures an optimal architecture for Na^+ binding (121) and is part of a conserved KYG motif that shares striking similarities with the GYG sequence of the selectivity filter in the K^+ channel (70, 79). The presence of Pro-225 in proteases like trypsin and chymotrypsin forces the carbonyl O atom of residue 224, one of the Na^+ ligands, in a direction incompatible with Na^+ coordination. The Y225P replacement in thrombin (62, 63), aPC (293), and coagulation FVIIa (258) and FXa (220) abrogates Na^+ activation. However, the reverse substitution P225Y in tissue-type plasminogen activator does not result in Na^+ binding or activation (338). Hence, Na^+ binding and activation depend on the nature of residue 225 as a necessary but not sufficient condition, just like the nature of residue 189 in the primary specificity pocket is a necessary but not sufficient condition for enzyme specificity (141). Mutagenesis studies on thrombin have shown that residues located up to 15 Å away from the Na^+ site influence the binding of Na^+, with residues in the 170, 186, and 220 loops playing a dominant role (262). Similar conclusions have been drawn for FXa (280).

Streptomyces griseus trypsin (SGT) is one of only a few trypsin-like enzymes of bacterial origin (276) and was recently turned into a Na^+-activated protease when residue Tyr-172 and the 186 and 220 loops of the enzyme were replaced with those of FXa (245). Simple substitution of Pro-225 to Tyr similarly failed to elicit Na^+ activation in SGT, similar to observations with tissue-type plasminogen activator (338), as did replacement of the 186 and 220 loops to reproduce the complete Na^+ binding environment of factor Xa (245). Further replacement of Tyr-172, a residue not in direct contact with Na^+, was necessary to achieve Na^+ activation. Inspection of the crystal structures of FXa (243), aPC (210), and thrombin (262) reveals a key difference in the residues surrounding the Na^+ binding site relative to other trypsin-like enzymes. Most

trypsin-like proteases possess Tyr-172, whose side chain buries within the core of the enzyme (19). In turn, the phenolic hydroxyl moiety of Tyr-172 forms a potential H bond with the amide backbone of Pro-225. Previous mutagenesis studies have demonstrated that residue 172 is an important determinant of primary substrate specificity (140). Conversion of Tyr-172 to Trp was crucial for engineering chymotrypsin-like specificity into trypsin. Overlap between residues controlling substrate specificity and Na^+ binding in clotting proteases (262, 267) proves that residue 172 also plays a key role in Na^+ activation. These results are strikingly similar to those observed in the conversion of trypsin into a chymotrypsin-like enzyme (138–141, 335). In both instances, mutagenesis of the 186 and 220 loops was initially suspected to introduce the desired catalytic property, yet further work identified a crucial role for residue 172. Further mimicry of the entire 170 loop of FXa resulted in an enzyme that is potently activated by Na^+, with the value of $s = k_{cat}/K_m$ increasing almost 60-fold relative to the inert cation choline (Fig. 32). Titration of the constructed Na^+-activated proteases demonstrated weak cation binding characteristics, with values of K_d for Na^+ binding significantly higher than those reported for thrombin (K_d = 14 mM) (262) or FXa (K_d = 39 mM or 9.5 mM in the presence of Ca^{2+}) (329). Nonetheless, the activating effect of Na^+ is pronounced, proving that essential determinants for Na^+ binding and allosteric transduction have been introduced for the first time in a serine protease. The importance of engineering Na^+ activation in SGT should be appreciated as a proof of principle and placed in the context of the large number of proteases that have intrinsically poor activity toward substrate, like tissue-type plasminogen activator or several complement enzymes. Future engineering studies will reveal if the strategy used for SGT has wider applicability and may indeed increase the catalytic activity of poor enzymes. In the absence of enhanced catalytic activity, Na^+ activation provides a mechanism for allosteric regulation that many proteases including SGT lack. Such regulation may bring about changes in specificity and drastic shifts in biological activities as demonstrated by thrombin (71).

Molecular mimicry by substitution of an amino acid side chain for M^+ provides an alternative strategy to rationally engineer more proficient enzymes (70). The task is a difficult one, as demonstrated by attempts to mimic Na^+ or K^+ activation in thrombin (289), pyruvate kinase (187), and the molecular chaperone Hsc70 (353). In all cases the ability of the enzyme to bind M^+ was successfully reproduced by introduction of a Lys side chain. However, that did not lead to high catalytic activity. These observations suggest that replacement of a bound M^+ is relatively straightforward, but the events that transduce M^+ complexation into enhanced catalytic activity cannot be recapitulated by single amino acid substitutions. Additional changes in and around the M^+ binding environment are necessary to provide crucial functional links between M^+ binding and catalytic enhancement.

Clues of what such changes might entail have come from the recent observation that murine thrombin is devoid of Na^+ activation but retains high catalytic activity (37). In human thrombin, Na^+ binding is severely compromised (>30-fold increase in K_d) upon mutation of Asp-189, Glu-217, Asp-222, and Tyr-225. Of these four residues, Glu-217 and Tyr-225 are conserved in thrombin in all species sequenced to date from hagfish to human (18). Asp-189 is a Ser in the sturgeon, and the D189S mutant of human thrombin has impaired Na^+ binding and substrate recognition (267). Asp-222 is the least conserved residue among the four. It is Ser in the sturgeon, Lys in the mouse, and Asn in the rat (18). The substitution in the mouse is particularly interesting,

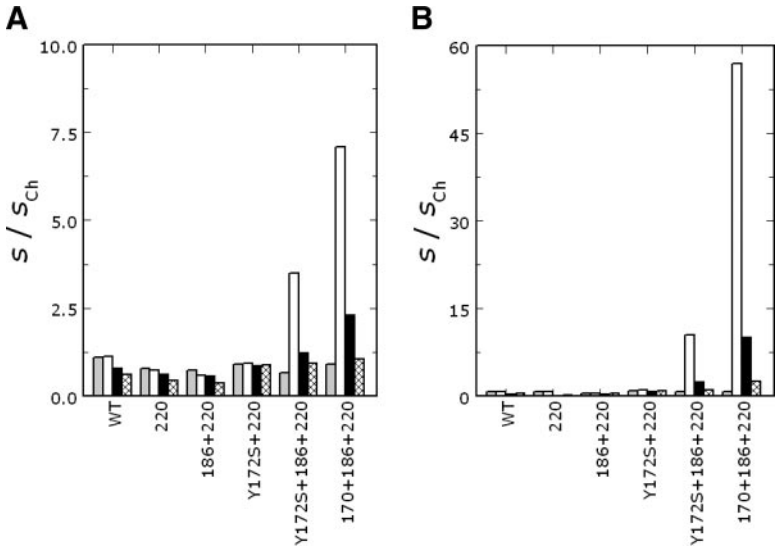

FIG. 32. Specificity constant $s = k_{cat}/K_m$ of loop mutants of SGT in the presence of LiCl (gray), NaCl (white), KCl (black), or RbCl (hatched), relative to the value in choline chloride at 200 mM (*A*) and 800 mM concentrations (*B*). The Y172S mutation results in a Na^+-dependent trypsin-like enzyme only when both the 186- and 220-loops of FXa have been introduced. Further mimicry of the 170-loop of FXa leads to significant Na^+ activation.

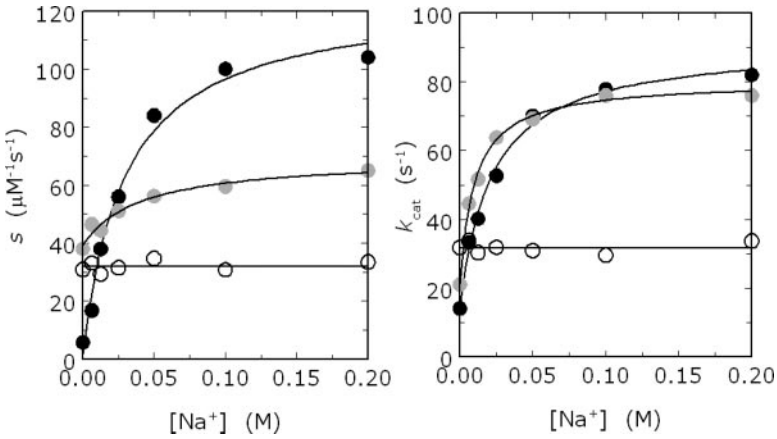

FIG. 33. Na^+ dependence of the kinetic constants $s = k_{cat}/K_m$ (*left*) and k_{cat} (*right*) for the hydrolysis of Spectrozyme TH by human (black circles) and murine (white circles) thrombin. Also shown are the data pertaining to the murine K222D mutant (gray circles). The profiles are flat for wild-type murine thrombin, as opposed to the sharp Na^+ dependence seen for human wild-type (see also Fig. 28). The K222D mutation restores most of the Na^+ effect. Experimental conditions are 50 mM Tris, 0.1% PEG, pH 8.0 at 25 °C. The $[Na^+]$ was changed keeping the ionic strength constant at 200 mM with choline chloride. Curves were drawn with the equations listed in Table 4 for type II* activation, with best-fit parameter values: (data at *left*) $s_0 = 1.8 \pm 0.1$ $\mu M^{-1} \cdot s^{-1}$, $s_1 = 125 \pm 8$ $\mu M^{-1} \cdot s^{-1}$, $K_A = 33 \pm 1$ M^{-1} (black circles); $s_0 = 32 \pm 1$ $\mu M^{-1} \cdot s^{-1}$, $s_1 = 32 \pm 1$ $\mu M^{-1} \cdot s^{-1}$, $K_A = 0$ M^{-1} (white circles); $s_0 = 39 \pm 1$ $\mu M^{-1} \cdot s^{-1}$, $s_1 = 69 \pm 2$ $\mu M^{-1} \cdot s^{-1}$, $K_A = 25 \pm 1$ M^{-1} (gray circles); (data at *right*) $k_{2,0} = 15 \pm 1$ s^{-1}, $k_{2,1} = 91 \pm 2$ s^{-1}, $K_A' = 45 \pm 2$ M^{-1} (black circles); $k_{2,0} = 32 \pm 1$ s^{-1}, $k_{2,1} = 32 \pm 1$ s^{-1}, $K_A' = 0$ M^{-1} (white circles); $k_{2,0} = 21 \pm 1$ s^{-1}, $k_{2,1} = 80 \pm 2$ s^{-1}, $K_A' = 100 \pm 2$ M^{-1} (gray circles). [From Bush et al. (37), copyright the American Society for Biochemistry and Molecular Biology.]

because it involves a charge reversal in the 220 loop that has the potential to destabilize the Na^+ binding environment. The D221A/D222K mutant of human thrombin is devoid of Na^+ activation (73) due to complete disruption of the Na^+ binding site (262). However, the mutant has functional properties intermediate between those of the Na^+-free and Na^+-bound forms of wild-type (73), which suggests that murine thrombin can retain significant catalytic activity even in the absence of Na^+ activation. Indeed, values of s and k_{cat} for the hydrolysis of a chromogenic substrate by murine thrombin are constant over the entire $[Na^+]$ range and fall in between those of the Na^+-free and Na^+-bound forms of the human enzyme. Cleavage of other chromogenic and physiological substrates occurs with values of s similar to those of the Na^+-bound form of human thrombin (37). Interestingly, the K222D mutation in murine thrombin significantly restores Na^+ activation, as revealed most eloquently by the k_{cat} (Fig. 33). Affinity of this mutant for Na^+ is very close to that of human thrombin. Hence, murine thrombin represents a successful example of molecular mimicry of M^+ activation. Constitutive replacement of Na^+ activation in murine thrombin has an important evolutionary advantage. Several mutations of human thrombin, e.g., Frankfurt (65), Salakta (218), Greenville (142), Scranton (315), Copenhagen (308), and Saint Denis (288), occur naturally at residues important for Na^+ recognition and often cause bleeding. It is therefore possible that pressure to constitutively replace Na^+ activation arose in the mouse to counter the effect of such mutations or more disruptive ones. Studies with anticoagulant mutants in human and murine thrombin support this conclusion and show that the same construct in the murine enzyme is less anticoagulant compared with the human construct (37). Investigation of the molecular determinants of Na^+ activation mimicry in the murine enzyme should reveal useful information to enhance the catalytic activity of many proteases.

VII. SUMMARY

M^+ lie at a conceptual crossroads between modifier of solvent and metal-cofactor assisting enzyme function. Unlike organic solvents that affect solvent properties, M^+ are ubiquitous components of fluids that bath biological macromolecules. Regulated intracellular and extracellular ionic composition provided the consistency of conditions that led to incorporation of M^+ into protein structure to increase stability, function, activity, and diversity. Charge density of M^+ is not sufficient to drive catalysis. Rather, M^+ stabilizes catalytic intermediates and enzyme structure or provides optimal positioning of substrate. Vertebrate blood coagulation is an excellent example of how Na^+ has interwoven into the activity and evolution of an enzyme family to facilitate a complex biological process. The knowledge emerged from studies on enzymes activated by Na^+ and K^+ should now enable the rational design of more proficient enzymes.

ACKNOWLEDGMENTS

We are indebted to Dr. Paul Boyer for valuable discussions and to Drs. David Davies, Liz Hedstrom, Eugene Huber, Thomas

Hurley, Yu Luo, Mischa Machius, George Reed, Barry Stoddard, Michael Toney, Jimin Wang, and Wei Yang for helpful exchanges of information.

Address for reprint requests and other correspondence: E. Di Cera, Dept. of Biochemistry and Molecular Biophysics, Washington University School of Medicine, St. Louis, MO 63110 (e-mail: enrico@wustl.edu).

GRANTS

This work was supported by a postdoctoral fellowship from the American Heart Association (to M. J. Page) and National Heart, Lung, and Blood Institute Research Grants HL-49413, HL-58141, and HL-73813.

REFERENCES

1. **Adrogue HJ and Madias NE.** Hypernatremia. *N Engl J Med* 342: 1493–1499, 2000.
2. **Adrogue HJ and Madias NE.** Hyponatremia. *N Engl J Med* 342: 1581–1589, 2000.
3. **Agre P and Nielsen S.** The aquaporin family of water channels in kidney. *Nephrologie* 17: 409–415, 1996.
4. **Ahmad A, Akhtar S, and Bhakuni V.** Monovalent cation-induced conformational change in glucose oxidase leading to stabilization of the enzyme. *Biochemistry* 40: 1945–1955, 2001.
5. **Almond CS, Shin AY, Fortescue EB, Mannix RC, Wypij D, Binstadt BA, Duncan CN, Olson DP, Salerno AE, Newburger JW, and Greenes DS.** Hyponatremia among runners in the Boston Marathon. *N Engl J Med* 352: 1550–1556, 2005.
6. **Andersen OS, Koeppe RE II, and Roux B.** Gramicidin channels. *IEEE Trans Nanobiosci* 4: 10–20, 2005.
7. **Andersson CE and Mowbray SL.** Activation of ribokinase by monovalent cations. *J Mol Biol* 315: 409–419, 2002.
8. **Antson AA, Demidkina TV, Gollnick P, Dauter Z, von Tersch RL, Long J, Berezhnoy SN, Phillips RS, Harutyunyan EH, and Wilson KS.** Three-dimensional structure of tyrosine phenol-lyase. *Biochemistry* 32: 4195–4206, 1993.
9. **Aparicio JF, Colina AJ, Ceballos E, and Martín JF.** The biosynthetic gene cluster for the 26-membered ring polyene macrolide pimaricin: a new polyketide synthase organization encoded by two subclusters separated by functionalization genes. *J Biol Chem* 274: 10133–10139, 1999.
10. **Arimori S, Davidson MG, Fyles TM, Hibbert TG, James TD, and Kociok-Kohn GI.** Synthesis and structural characterisation of the first bis(bora)calixarene: a selective, bidentate, fluorescent fluoride sensor. *Chem Commun* 14: 1640–1641, 2004.
11. **Armstrong RN.** Mechanistic diversity in a metalloenzyme superfamily. *Biochemistry* 39: 13625–13632, 2000.
12. **Babor M, Greenblatt HM, Edelman M, and Sobolev V.** Flexibility of metal binding sites in proteins on a database scale. *Proteins Struct Funct Genet* 59: 221–230, 2005.
13. **Backes BJ, Harris JL, Leonetti F, Craik CS, and Ellman JA.** Synthesis of positional-scanning libraries of fluorogenic peptide substrates to define the extended substrate specificity of plasmin and thrombin. *Nat Biotechnol* 18: 187–193, 2000.
14. **Bacon S, Snaith HM, and Yelland MJ.** An evaluation of some recent batches of IAPSO standard seawater. *J Atmospheric Oceanic Technol* 17: 854–861, 2000.
15. **Bajzar L, Morser J, and Nesheim M.** TAFI, or plasma procarboxypeptidase B, couples the coagulation and fibrinolytic cascades through the thrombin-thrombomodulin complex. *J Biol Chem* 271: 16603–16608, 1996.
16. **Baliga NS, Bjork SJ, Bonneau R, Pan M, Iloanusi C, Kottemann MC, Hood L, and DiRuggiero J.** Systems level insights into the stress response to UV radiation in the halophilic archaeon Halobacterium NRC-1. *Genome Res* 14: 1025–1035, 2004.
17. **Ban F, Kusalik P, and Weaver DF.** Density functional theory investigations on the chemical basis of the selectivity filter in the K^+ channel protein. *J Am Chem Soc* 126: 4711–4716, 2004.
18. **Banfield DK and MacGillivray RT.** Partial characterization of vertebrate prothrombin cDNAs: amplification and sequence analysis of the B chain of thrombin from nine different species. *Proc Natl Acad Sci USA* 89: 2779–2783, 1992.
19. **Bartunik HD, Summers LJ, and Bartsch HH.** Crystal structure of bovine beta-trypsin at 1.5 A resolution in a crystal form with low molecular packing density. Active site geometry, ion pairs and solvent structure. *J Mol Biol* 210: 813–828, 1989.
20. **Bauer F and Dost G.** Moenomycin in animal nutrition. *Antimicrob Agents Chemother* 5: 749–752, 1965.
21. **Berner YN and Shike M.** Consequences of phosphate imbalance. *Annu Rev Nutr* 8: 121–148, 1988.
22. **Bhattacharya S, Bunick CG, and Chazin WJ.** Target selectivity in EF-hand calcium binding proteins. *Biochim Biophys Acta* 1742: 69–79, 2004.
23. **Bilwes AM, Alex LA, Crane BR, and Simon MI.** Structure of CheA, a signal-transducing histidine kinase. *Cell* 96: 131–141, 1999.
24. **Bilwes AM, Quezada CM, Croal LR, Crane BR, and Simon MI.** Nucleotide binding by the histidine kinase CheA. *Nat Struct Biol* 8: 353–360, 2001.
25. **Bolard J.** How do the polyene macrolide antibiotics affect the cellular membrane properties? *Biochim Biophys Acta* 864: 257–304, 1986.
26. **Bostrom M, Kunz W, and Ninham BW.** Hofmeister effects in surface tension of aqueous electrolyte solution. *Langmuir* 21: 2619–2623, 2005.
27. **Boström M, Williams DRM, and Ninham BW.** Why the properties of proteins in salt solutions follow a Hofmeister series. *Curr Opin Colloid Interface Sci* 9: 48–52, 2004.
28. **Botts J and Morales M.** Analytical description of the effects of modifiers and of multivalency upon the steady state catalyzed reaction rate. *Trans Faraday Soc* 49: 696–707, 1953.
29. **Bourque CW.** Osmoregulation of vasopressin neurons: a synergy of intrinsic and synaptic processes. *Prog Brain Res* 119: 59–76, 1998.
30. **Boyer PD, Lardy HA, and Phillips PH.** The role of potassium in muscle phosphorylations. *J Biol Chem* 146: 673–681, 1942.
31. **Brenner S.** The molecular evolution of genes and proteins: a tale of two serines. *Nature* 334: 528–530, 1988.
32. **Brewster JL, de Valoir T, Dwyer ND, Winter E, and Gustin MC.** An osmosensing signal transduction pathway in yeast. *Science* 259: 1760–1763, 1993.
33. **Brown ID and Wu KK.** Empirical parameters for calculating cation-oxygen bond valence. *Acta Crystallogr B* 32: 1957–1959, 1976.
34. **Brunhuber NMW, Thoden JB, Blanchard JS, and Vanhooke JL.** Rhodococcus L-phenylalanine dehydrogenase: kinetics, mechanism, and structural basis for catalytic specifity. *Biochemistry* 39: 9174–9187, 2000.
35. **Budayova-Spano M, Lacroix M, Thielens NM, Arlaud GJ, Carlos Fontecilla-Camps J, and Gaboriaud C.** The crystal structure of the zymogen catalytic domain of complement protease C1r reveals that a disruptive mechanical stress is required to trigger activation of the C1 complex. *EMBO J* 21: 231–239, 2002.
36. **Burykin A, Kato M, and Warshel A.** Exploring the origin of the ion selectivity of the KcsA potassium channel. *Proteins* 52: 412–426, 2003.
37. **Bush LA, Nelson RW, and Di Cera E.** Murine thrombin lacks Na^+ activation but retains high catalytic activity. *J Biol Chem* 281: 7183–7188, 2006.
38. **Butinar L, Zalar P, Frisvad JC, and Gunde-Cimerman N.** The genus *Eurotium:* members of indigenous fungal community in hypersaline waters of salterns. *FEMS Microbiol Ecol* 51: 155–166, 2005.
39. **Cacace MG, Landau EM, and Ramsden JJ.** The Hofmeister series: salt and solvent effects on interfacial phenomena. *Q Rev Biophys* 30: 241–277, 1997.
40. **Callaway TR, Edrington TS, Rychlik JL, Genovese KJ, Poole TL, Jung YS, Bischoff KM, Anderson RC, and Nisbet DJ.** Ionophores: their use as ruminant growth promotants and impact on food safety. *Curr Issues Intest Microbiol* 4: 43–51, 2003.
41. **Camire RM.** Prothrombinase assembly and S1 site occupation restore the catalytic activity of FXa impaired by mutation at the sodium-binding site. *J Biol Chem* 277: 37863–37870, 2002.

42. **Cantwell AM and Di Cera E.** Rational design of a potent anticoagulant thrombin. *J Biol Chem* 275: 39827–39830, 2000.
43. **Caradoc-Davies TT, Cutfield SM, Lamont IL, and Cutfield JF.** Crystal structures of *Escherichia coli* uridine phosphorylase in two native and three complexed forms reveal basis of substrate specificity, induced conformational changes and influence of potassium. *J Mol Biol* 337: 337–354, 2004.
44. **Carden DE, Diamond D, and Miller AJ.** An improved Na^+-selective microelectrode for intracellular measurements in plant cells. *J Exp Bot* 52: 1353–1359, 2001.
45. **Carrell CJ, Bush LA, Mathews FS, and Di Cera E.** High resolution crystal structures of free thrombin in the presence of K^+ reveal the basis of monovalent cation selectivity and an inactive slow form. *Biophys Chem* 121: 177–184, 2006.
46. **Castagnetto JM, Hennessy SW, Roberts VA, Getzoff ED, Tainer JA, and Pique ME.** MDB: the Metalloprotein Database and Browser at the Scripps Research Institute. *Nucleic Acids Res* 30: 379–382, 2002.
47. **Caughey B, Painter G, Pressman BC, and Gibbons WA.** The solvent polarity dependent conformational equilibrium of the carboxylic ionophore narasin: a proton NMR study. *Biochem Biophys Res Commun* 113: 832–838, 1983.
48. **Chan MK, Mukund S, Kletzin A, Adams MWW, and Rees DC.** Structure of a hyperthermophilic tungstopterin enzyme, aldehyde ferredoxin oxidoreductase. *Science* 267: 1463–1469, 1995.
49. **Chasan R and Anderson KV.** The role of easter, an apparent serine protease, in organizing the dorsal-ventral pattern of the *Drosophila* embryo. *Cell* 56: 391–400, 1989.
50. **Cheatham TE III and Kollman PA.** Molecular dynamics simulation of nucleic acids. *Annu Rev Phys Chem* 51: 435–471, 2000.
51. **Chiu TK, Kaczor-Grzeskowiak M, and Dickerson RE.** Absence of minor groove monovalent cations in the crosslinked dodecamer C-G-C-G-A-A-T-T-C-G-C-G. *J Mol Biol* 292: 589–608, 1999.
52. **Ciszak EM, Korotchkina LG, Dominiak PM, Sidhu S, and Patel MS.** Structural basis for flip-flop action of thiamin pyrophosphate-dependent enzymes revealed by human pyruvate dehydrogenase. *J Biol Chem* 278: 21240–21246, 2003.
53. **Cohn M and Monod J.** Purification and properties of the beta-galactosidase (lactase) of *Escherichia coli*. *Biochim Biophys Acta* 7: 153–174, 1951.
54. **Collins KD.** Charge density-dependent strength of hydration and biological structure. *Biophys J* 72: 65–76, 1997.
55. **Collins KD.** Ion hydration: implications for cellular function, polyelectrolytes, and protein crystallization. *Biophys Chem* 119: 271–281, 2006.
56. **Collins KD.** Sticky ions in biological systems. *Proc Natl Acad Sci USA* 92: 5553–5557, 1995.
57. **Conn GL, Gittis AG, Lattman EE, Misra VK, and Draper DE.** A compact RNA tertiary structure contains a buried backbone-K^+ complex. *J Mol Biol* 318: 963–973, 2002.
58. **Costenaro L, Zaccai G, and Ebel C.** Link between protein-solvent and weak protein-protein interactions gives insight into halophilic adaptation. *Biochemistry* 41: 13245–13252, 2002.
59. **Cowan SW, Schirmer T, Rummel G, Steiert M, Ghosh R, Pauptit RA, Jansonius JN, and Rosenbusch JP.** Crystal structures explain functional properties of two *E. coli* porins. *Nature* 358: 727–733, 1992.
60. **Cram DJ.** The design of molecular hosts, guests, and their complexes. *Science* 240: 760–767, 1988.
61. **Dang OD, Vindigni A, and Di Cera E.** An allosteric switch controls the procoagulant and anticoagulant activities of thrombin. *Proc Natl Acad Sci USA* 92: 5977–5981, 1995.
62. **Dang QD and Di Cera E.** Residue 225 determines the Na(+)-induced allosteric regulation of catalytic activity in serine proteases. *Proc Natl Acad Sci USA* 93: 10653–10656, 1996.
63. **Dang QD, Guinto ER, and Di Cera E.** Rational engineering of activity and specificity in a serine protease. *Nat Biotechnol* 15: 146–149, 1997.
64. **De Filippis V, De Dea E, Lucatello F, and Frasson R.** Effect of Na^+ binding on the conformation, stability and molecular recognition properties of thrombin. *Biochem J* 390: 485–492, 2005.
65. **Degen SJ, McDowell SA, Sparks LM, and Scharrer I.** Prothrombin Frankfurt: a dysfunctional prothrombin characterized by substitution of Glu-466 by Ala. *Thromb Haemost* 73: 203–209, 1995.
66. **DeLaBarre B, Thompson PR, Wright GD, and Berghuis AM.** Crystal structures of homoserine dehydrogenase suggest a novel catalytic mechanism for oxidoreductases. *Nat Struct Biol* 7: 238–244, 2000.
67. **Denisov VP and Halle B.** Sequence-specific binding of counterions to B-DNA. *Proc Natl Acad Sci USA* 97: 629–633, 2000.
68. **Denton DA, McKinley MJ, and Weisinger RS.** Hypothalamic integration of body fluid regulation. *Proc Natl Acad Sci USA* 93: 7397–7404, 1996.
69. **De Wardener HE.** The hypothalamus and hypertension. *Physiol Rev* 81: 1599–1658, 2001.
70. **Di Cera E.** A structural perspective on enzymes activated by monovalent cations. *J Biol Chem* 281: 1305–1308, 2006.
71. **Di Cera E.** Thrombin interactions. *Chest* 124: 11S–17S, 2003.
72. **Di Cera E, Dang QD, and Ayala YM.** Molecular mechanisms of thrombin function. *Cell Mol Life Sci* 53: 701–730, 1997.
73. **Di Cera E, Guinto ER, Vindigni A, Dang QD, Ayala YM, Wuyi M, and Tulinsky A.** The Na^+ binding site of thrombin. *J Biol Chem* 270: 22089–22092, 1995.
74. **Di Cera E, Hopfner KP, and Dang QD.** Theory of allosteric effects in serine proteases. *Biophys J* 70: 174–181, 1996.
75. **Dill KA, Truskett TM, Vlachy V, and Hribar-Lee B.** Modeling water, the hydrophobic effect, and ion solvation. *Annu Rev Biophys Biomol Struct* 34: 173–199, 2005.
76. **Dima RI and Thirumalai D.** Determination of network of residues that regulate allostery in protein families using sequence analysis. *Protein Sci* 15: 258–268, 2006.
77. **Dionisi HM, Alvarez CV, and Viale AM.** Alkali metal ions protect mitochondrial rhodanese against thermal inactivation. *Arch Biochem Biophys* 361: 202–206, 1999.
78. **Dougherty DA.** Cation-pi interactions in chemistry and biology: a new view of benzene, Phe, Tyr, and Trp. *Science* 271: 163–168, 1996.
79. **Doyle DA, Morais Cabral J, Pfuetzner RA, Kuo A, Gulbis JM, Cohen SL, Chait BT, and MacKinnon R.** The structure of the potassium channel: molecular basis of K^+ conduction and selectivity. *Science* 280: 69–77, 1998.
80. **Dwyer MA, Looger LL, and Hellinga HW.** Computational design of a Zn^{2+} receptor that controls bacterial gene expression. *Proc Natl Acad Sci USA* 100: 11255–11260, 2003.
81. **Dym O, Mevarech M, and Sussman JL.** Structural features that stabilize halophilic malate dehydrogenase from an archaebacterium. *Science* 267: 1344–1346, 1995.
82. **Ebel C and Zaccai G.** Crowding in extremophiles: linkage between solvation and weak protein-protein interactions, stability and dynamics, provides insight into molecular adaptation. *J Mol Recogn* 17: 382–389, 2004.
83. **Eisenman G and Horn R.** Ionic selectivity revisited: the role of kinetic and equilibrium processes in ion permeation through channels. *J Membr Biol* 76: 197–225, 1983.
84. **Elber R and Karplus M.** Multiple conformational states of proteins: a molecular dynamics analysis of myoglobin. *Science* 235: 318–321, 1987.
85. **Esmon CT.** The protein C pathway. *Chest* 124: 26S–32S, 2003.
86. **Evans HJ and Sorger GJ.** Role of mineral elements with emphasis on the univalent cations. *Annu Rev Plant Physiol* 17: 47–76, 1966.
87. **Evarsson A, Chuang JL, Wynn RM, Turley S, Chuang DT, and Hol WG.** Crystal structure of human branched-chain alpha-ketoacid dehydrogenase and the molecular basis of multienzyme complex deficiency in maple syrup urine disease. *Structure* 8: 277–291, 2000.
88. **Farries TC and Atkinson JP.** Evolution of the complement system. *Immunol Today* 12: 295–300, 1991.
89. **Finney LA and O'Halloran TV.** Transition metal speciation in the cell: insights from the chemistry of metal ion receptors. *Science* 300: 931–936, 2003.
90. **Firsov D, Gautschi I, Merillat AM, Rossier BC, and Schild L.** The heterotetrameric architecture of the epithelial sodium channel (ENaC). *EMBO J* 17: 344–352, 1998.

91. **Fisher M, Pick U, and Zamir A.** A salt-induced 60-kilodalton plasma membrane protein plays a potential role in the extreme halotolerance of the alga *Dunaliella*. *Plant Physiol* 106: 1359–1365, 1994.
92. **Fjaervik E and Zotchev SB.** Biosynthesis of the polyene macrolide antibiotic nystatin in *Streptomyces noursei*. *Appl Microbiol Biotechnol* 67: 436–443, 2005.
93. **Flaherty KM, DeLuca-Flaherty C, and McKay DB.** Three-dimensional structure of the ATPase fragment of a 70K heat-shock cognate protein. *Nature* 346: 623–628, 1990.
94. **Flowers TJ and Yeo AR.** Breeding for salinity resistance in crop plants: where next? *Austr J Plant Physiol* 22: 875–884, 1995.
95. **Fodor AA and Aldrich RW.** Influence of conservation on calculations of amino acid covariance in multiple sequence alignments. *Proteins Struct Funct Genet* 56: 211–221, 2004.
96. **Fodor AA and Aldrich RW.** On evolutionary conservation of thermodynamic coupling in proteins. *J Biol Chem* 279: 19046–19050, 2004.
97. **Franks F.** Protein stability: the value of "old literature." *Biophys Chem* 96: 117–127, 2002.
98. **Frauenfelder H, Parak F, and Young RD.** Conformational substates in proteins. *Annu Rev Biophys Biophys Chem* 17: 451–479, 1988.
99. **Freda BJ, Davidson MB, and Hall PM.** Evaluation of hyponatremia: a little physiology goes a long way. *Cleve Clin J Med* 71: 639–650, 2004.
100. **Friedman PA and Gesek FA.** Cellular calcium transport in renal epithelia: measurement, mechanisms, and regulation. *Physiol Rev* 75: 429–471, 1995.
101. **Frohlich ED and Varagic J.** The role of sodium in hypertension is more complex than simply elevating arterial pressure. *Nat Clin Pract Cardiovasc Med* 1: 24–30, 2004.
102. **Frolow F, Harel M, Sussman JL, Mevarech M, and Shoham M.** Insights into protein adaptation to a saturated salt environment from the crystal structure of a halophilic 2Fe-2S ferredoxin. *Nat Struct Biol* 3: 452–458, 1996.
103. **Fuller PJ and Young MJ.** Mechanisms of mineralocorticoid action. *Hypertension* 46: 1227–1235, 2005.
104. **Funahashi J, Takano K, Yamagata Y, and Yutani K.** Positive contribution of hydration structure on the surface of human lysozyme to the conformational stability. *J Biol Chem* 277: 21792–21800, 2002.
105. **Gallagher DT, Monbouquette HG, Schröder I, Robinson H, Holden MJ, and Smith NN.** Structure of alanine dehydrogenase from Archaeoglobus: active site analysis and relation to bacterial cyclodeaminases and mammalian mu crystallin. *J Mol Biol* 342: 119–130, 2004.
106. **Gan L, Petsko GA, and Hedstrom L.** Crystal structure of a ternary complex of *Tritrichomonas foetus* inosine 5′-monophosphate dehydrogenase: NAD^+ orients the active site loop for catalysis. *Biochemistry* 41: 13309–13317, 2002.
107. **Garty H and Palmer LG.** Epithelial sodium channels: function, structure and regulation. *Physiol Revs* 77: 359–396, 1997.
108. **Gaxiola RA, Rao R, Sherman A, Grisafi P, Alper SL, and Fink GR.** The *Arabidopsis thaliana* proton transporters, AtNhx1 and Avp1, can function in cation detoxification in yeast. *Proc Natl Acad Sci USA* 96: 1480–1485, 1999.
109. **Gerstein M and Krebs W.** A database of macromolecular motions. *Nucleic Acids Res* 26: 4280–4290, 1998.
110. **Gething MJ and Sambrook J.** Protein folding in the cell. *Nature* 355: 33–45, 1992.
111. **Gibbs CS, Coutre SE, Tsiang M, Li WX, Jain AK, Dunn KE, Law VS, Mao CT, Matsumura SY, Mejza SJ, Paborsky LR, and Leung LLK.** Conversion of thrombin into an anticoagulant by protein engineering. *Nature* 378: 413–416, 1995.
112. **Gonzalez B, Pajares MA, Hermoso JA, Alvarez L, Garrido F, Sufrin JR, and Sanz-Aparicio J.** The crystal structure of tetrameric methionine adenosyltransferase from rat liver reveals the methionine-binding site. *J Mol Biol* 300: 363–375, 2000.
113. **Gonzalez CB and Figueroa CD.** Vasopressin and bradykinin receptors in the kidney: implications for tubular function. *Biol Res* 32: 63–76, 1999.
114. **Goodman JL, Wang S, Alam S, Ruzicka FJ, Frey PA, and Wedekind JE.** Ornithine cyclodeaminase: structure, mechanism of action, and implications for the α-crystallin family. *Biochemistry* 43: 13883–13891, 2004.
115. **Grant PJ, Tate GM, Hughes JR, Davies JA, and Prentice CR.** Does hypernatraemia promote thrombosis? *Thromb Res* 40: 393–399, 1985.
116. **Greasley SE, Horton P, Ramcharan J, Beardsley GP, Benkovic SJ, and Wilson IA.** Crystal structure of a bifunctional transformylase and cyclohydrolase enzyme in purine biosynthesis. *Nat Struct Biol* 8: 402–406, 2001.
117. **Grenthe I and Plyasunov A.** On the use of semiempirical electrolyte theories for the modeling of solution chemical data. *Pure Appl Chem* 69: 951–958, 1997.
118. **Griffon N and Di Stasio E.** Thermodynamics of Na^+ binding to coagulation serine proteases. *Biophys Chem* 90: 89–96, 2001.
119. **Gruber A, Cantwell AM, Di Cera E, and Hanson SR.** The thrombin mutant W215A/E217A shows safe and potent anticoagulant and antithrombotic effects in vivo. *J Biol Chem* 277: 27581–27584, 2002.
120. **Gruber A, Fernandez JA, Bush L, Marzec U, Griffin JH, Hanson SR, and Di Cera E.** Limited generation of activated protein C during infusion of the protein C activator thrombin analog W215A/E217A in primates. *J Thromb Haemost* 4: 392–397, 2006.
121. **Guinto ER, Caccia S, Rose T, Futterer K, Waksman G, and Di Cera E.** Unexpected crucial role of residue 225 in serine proteases. *Proc Natl Acad Sci USA* 96: 1852–1857, 1999.
122. **Guinto ER and Di Cera E.** Large heat capacity change in a protein-monovalent cation interaction. *Biochemistry* 35: 8800–8804, 1996.
123. **Gunasekaran K, Ma B, and Nussinov R.** Is allostery an intrinsic property of all dynamic proteins? *Proteins Struct Funct Genet* 57: 433–443, 2004.
124. **Hall DR, Bond CS, Leonard GA, Watt CI, Berry A, and Hunter WN.** Structure of tagatose-1,6-bisphosphate aldolase. Insight into chiral discrimination, mechanism, and specificity of class II aldolases. *J Biol Chem* 277: 22018–22024, 2002.
125. **Hall DR, Leonard GA, Reed CD, Watt CI, Berry A, and Hunter WN.** The crystal structure of *Escherichia coli* class II fructose-1,6-bisphosphate aldolase in complex with phosphoglycolohydroxamate reveals details of mechanism and specificity. *J Mol Biol* 287: 383–394, 1999.
126. **Halle B and Denisov VP.** Water and monovalent ions in the minor groove of B-DNA oligonucleotides as seen by NMR. *Biopolymers* 48: 210–233, 1998.
127. **Hampel A and Cowan JA.** A unique mechanism for RNA catalysis: the role of metal cofactors in hairpin ribozyme cleavage. *Chem Biol* 4: 513–517, 1997.
128. **Harding MM.** The architecture of metal coordination groups in proteins. *Acta Crystallogr D Biol Crystallogr* 60: 849–859, 2004.
129. **Harding MM.** Geometry of metal-ligand interactions in proteins. *Acta Crystallogr D Biol Crystallogr* 57: 401–411, 2001.
130. **Harding MM.** Metal-ligand geometry relevant to proteins and in proteins: sodium and potassium. *Acta Crystallogr D Biol Crystallogr* 58: 872–874, 2002.
131. **Harel M, Shoham M, Frolow F, Eisenberg H, Mevarech M, Yonath A, and Sussman JL.** Crystallization of halophilic malate dehydrogenase from *Halobacterium marismortui*. *J Mol Biol* 200: 609–610, 1988.
132. **Harold FM and Baarda JR.** Gramicidin, valinomycin, and cation permeability of *Streptococcus faecalis*. *J Bacteriol* 94: 53–60, 1967.
133. **Harris JL, Backes BJ, Leonetti F, Mahrus S, Ellman JA, and Craik CS.** Rapid and general profiling of protease specificity by using combinatorial fluorogenic substrate libraries. *Proc Natl Acad Sci USA* 97: 7754–7759, 2000.
134. **Häse CC and Barquera B.** Role of sodium bioenergetics in *Vibrio cholerae*. *Biochim Biophys Acta* 1505: 169–178, 2001.
135. **Hase CC, Fedorova ND, Galperin MY, and Dibrov PA.** Sodium ion cycle in bacterial pathogens: evidence from cross-genome comparisons. *Microbiol Mol Biol Rev* 65: 353–370, 2001.
136. **He H, Mortellaro MA, Leiner MJ, Young ST, Fraatz RJ, and Tusa JK.** A fluorescent chemosensor for sodium based on photoinduced electron transfer. *Anal Chem* 75: 549–555, 2003.

137. **Hedstrom L.** Serine protease mechanism and specificity. *Chem Rev* 102: 4501–4524, 2002.
138. **Hedstrom L.** Trypsin: a case study in the structural determinants of enzyme specificity. *Biol Chem* 377: 465–470, 1996.
139. **Hedstrom L, Farr-Jones S, Kettner CA, and Rutter WJ.** Converting trypsin to chymotrypsin: ground-state binding does not determine substrate specificity. *Biochemistry* 33: 8764–8769, 1994.
140. **Hedstrom L, Perona JJ, and Rutter WJ.** Converting trypsin to chymotrypsin: residue 172 is a substrate specificity determinant. *Biochemistry* 33: 8757–8763, 1994.
141. **Hedstrom L, Szilagyi L, and Rutter WJ.** Converting trypsin to chymotrypsin: the role of surface loops. *Science* 255: 1249–1253, 1992.
142. **Henriksen RA, Dunham CK, Miller LD, Casey JT, Menke JB, Knupp CL, and Usala SJ.** Prothrombin Greenville, Arg517→Gln, identified in an individual heterozygous for dysprothrombinemia. *Blood* 91: 2026–2031, 1998.
143. **Hill TL.** *Free Energy Transduction in Biology*. New York: Academic, 1977.
144. **Hladky SB and Haydon DA.** Ion transfer across lipid membranes in the presence of gramicidin A. I. Studies of the unit conductance channel. *Biochim Biophys Acta* 274: 294–312, 1972.
145. **Hochachka PW and Somero GN.** *Biochemical Adaptation*. Princeton, NJ: Princeton Univ. Press, 1984.
146. **Hogberg-Raibaud A, Raibaud O, and Goldberg ME.** Kinetic and equilibrium studies on the activation of *Escherichia coli* K12 tryptophanase by pyridoxal 5′-phosphate and monovalent cations. *J Biol Chem* 250: 3352–3358, 1975.
147. **Hohenester E, Keller JW, and Jansonius JN.** An alkali metal ion size-dependent switch in the active site structure of dialkylglycine decarboxylase. *Biochemistry* 33: 13561–13570, 1994.
148. **Holyoak T, Kettner CA, Petsko GA, Fuller RS, and Ringe D.** Structural basis for differences in substrate selectivity in Kex2 and furin protein convertases. *Biochemistry* 43: 2412–2421, 2004.
149. **Horovitz A, Fridmann Y, Kafri G, and Yifrach O.** Review: allostery in chaperonins. *J Struct Biol* 135: 104–114, 2001.
150. **Hribar B, Southall NT, Vlachy V, and Dill KA.** How ions affect the structure of water. *J Am Chem Soc* 124: 12302–12311, 2002.
151. **Hu X, Machius M, and Yang W.** Monovalent cation dependence and preference of GHKL ATPases and kinases. *FEBS Lett* 544: 268–273, 2003.
152. **Hud NV, Sklenár V, and Feigon J.** Localization of ammonium ions in the minor groove of DNA duplexes in solution and the origin of DNA A-tract bending. *J Mol Biol* 286: 651–660, 1999.
153. **Hummer G, Schotte F, and Anfinrud PA.** Unveiling functional protein motions with picosecond x-ray crystallography and molecular dynamics simulations. *Proc Natl Acad Sci USA* 101: 15330–15334, 2004.
154. **Ibers JA and Holm RH.** Modeling coordination sites in metallobiomolecules. *Science* 209: 223–235, 1980.
155. **Ishikawa K, Matsui I, Payan F, Cambillau C, Ishida H, Kawarabayasi Y, Kikuchi H, and Roussel A.** A hyperthermostable D-ribose-5-phosphate isomerase from *Pyrococcus horikoshii* characterization and three-dimensional structure. *Structure* 10: 877–886, 2002.
156. **Isupov MN, Antson AA, Dodson EJ, Dodson GG, Dementieva IS, Zakomirdina LN, Wilson KS, Dauter Z, Lebedev AA, and Harutyunyan EH.** Crystal structure of tryptophanase. *J Mol Biol* 276: 603–623, 1998.
157. **Johnson DJ, Adams TE, Li W, and Huntington JA.** Crystal structure of wild-type human thrombin in the Na^+-free state. *Biochem J* 392: 21–28, 2005.
158. **Jozic D, Bourenkov G, Lim NH, Visse R, Nagase H, Bode W, and Maskos K.** X-ray structure of human proMMP-1: new insights into procollagenase activation and collagen binding. *J Biol Chem* 280: 9578–9585, 2005.
159. **Jude AR, Greathouse DV, Koeppe RE II, Providence LL, and Andersen OS.** Modulation of gramicidin channel structure and function by the aliphatic "spacer" residues 10, 12, and 14 between the tryptophans. *Biochemistry* 38: 1030–1039, 1999.
160. **Jude AR, Providence LL, Schmutzer SE, Shobana S, Greathouse DV, Andersen OS, and Koeppe R II.** Peptide backbone chemistry and membrane channel function: effects of a single amide-to-ester replacement on gramicidin channel structure and function. *Biochemistry* 40: 1460–1472, 2001.
161. **Juers DH, Heightman TD, Vasella A, McCarter JD, Mackenzie L, Withers SG, and Matthews BW.** A structural view of the action of *Escherichia coli* (lacZ) beta-galactosidase. *Biochemistry* 40: 14781–14794, 2001.
162. **Juers DH, Jacobson RH, Wigley D, Zhang XJ, Huber RE, Tronrud DE, and Matthews BW.** High resolution refinement of beta-galactosidase in a new crystal form reveals multiple metal-binding sites and provides a structural basis for alpha-complementation. *Protein Sci* 9: 1685–1699, 2000.
163. **Jurica MS, Mesecar A, Heath PJ, Shi W, Nowak T, and Stoddard BL.** The allosteric regulation of pyruvate kinase by fructose-1,6-bisphosphate. *Structure* 6: 195–210, 1998.
164. **Kabsch W, Mannherz HG, Suck D, Pai EF, and Holmes KC.** Atomic structure of the actin:DNase I complex. *Nature* 347: 37–44, 1990.
165. **Kachmar JF and Boyer PD.** Kinetic analysis of enzyme reactions. II. The potassium activation and calcium inhibition of pyruvic phosphoferase. *J Biol Chem* 200: 669–682, 1953.
166. **Kamata K, Mitsuya M, Nishimura T, Eiki J, and Nagata Y.** Structural basis for allosteric regulation of the monomeric allosteric enzyme human glucokinase. *Structure* 12: 429–438, 2004.
167. **Kato M, Chuang JL, Tso SC, Wynn RM, and Chuang DT.** Crystal structure of pyruvate dehydrogenase kinase 3 bound to lipoyl domain 2 of human pyruvate dehydrogenase complex. *EMBO J* 24: 1763–1774, 2005.
168. **Kern D and Zuiderweg ERP.** The role of dynamics in allosteric regulation. *Curr Opin Struct Biol* 13: 748–757, 2003.
169. **Kilbourn BT, Dunitz JD, Pioda LA, and Simon W.** Structure of the K^+ complex with nonactin, a macrotetrolide antibiotic possessing highly specific K^+ transport properties. *J Mol Biol* 30: 559–563, 1967.
170. **Koeppe RE II, Greathouse DV, Providence LL, Shobana S, and Andersen OS.** Design and characterization of gramicidin channels with side chain or backbone mutations. *Novartis Found Symp* 225: 44–61, 1999.
171. **Kolatkar AR, Leung AK, Isecke R, Brossmer R, Drickamer K, and Weis WI.** Mechanism of *N*-acetylgalactosamine binding to a C-type animal lectin carbohydrate-recognition domain. *J Biol Chem* 273: 19502–19508, 1998.
172. **Komoto J, Yamada T, Takata Y, Markham GD, and Takusagawa F.** Crystal structure of the *S*-adenosylmethionine synthetase ternary complex: a novel catalytic mechanism of *S*-adenosylmethionine synthesis from ATP and Met. *Biochemistry* 43: 1821–1831, 2004.
173. **Korzhnev DM, Neudecker P, Mittermaier A, Orekhov VY, and Kay LE.** Multiple-site exchange in proteins studied with a suite of six NMR relaxation dispersion experiments: an application to the folding of a Fyn SH3 domain mutant. *J Am Chem Soc* 127: 15602–15611, 2005.
174. **Kosari F, Sheng S, Li J, Mak DO, Foskett JK, and Kleyman TR.** Subunit stoichiometry of the epithelial sodium channel. *J Biol Chem* 273: 13469–13474, 1998.
175. **Krem MM and Di Cera E.** Evolution of enzyme cascades from embryonic development to blood coagulation. *Trends Biochem Sci* 27: 67–74, 2002.
176. **Krem MM and Di Cera E.** Molecular markers of serine protease evolution. *EMBO J* 20: 3036–3045, 2001.
177. **Krem MM, Prasad S, and Di Cera E.** Ser(214) is crucial for substrate binding to serine proteases. *J Biol Chem* 277: 40260–40264, 2002.
178. **Krishnaswamy S.** Exosite-driven substrate specificity and function in coagulation. *J Thromb Haemost* 3: 54–67, 2005.
179. **Kumar S and Berl T.** Sodium. *Lancet* 352: 220–228, 1998.
180. **Kung C.** A possible unifying principle for mechanosensation. *Nature* 436: 647–654, 2005.
181. **Kunz W, Henle J, and Ninham BW.** 'Zur Lehre von der Wirkung der Salze' (about the science of the effect of salts): Franz Hofmeister's historical papers. *Curr Opin Colloid Interface Sci* 9: 19–37, 2004.
182. **Kurlansky M.** *Salt: A World History*. Toronto, Canada: Random House, 2002.

183. **Lai MT, Di Cera E, and Shafer JA.** Kinetic pathway for the slow to fast transition of thrombin. Evidence of linked ligand binding at structurally distinct domains. *J Biol Chem* 272: 30275–30282, 1997.
184. **Laine-Cessac P and Allain P.** Kinetic studies of the effects of K^+, Na^+ and Li^+ on the catalytic activity of human erythrocyte pyridoxal kinase. *Enzyme Protein* 49: 291–304, 1996.
185. **Larsen TM, Benning MM, Rayment I, and Reed GH.** Structure of the bis(Mg2+)-ATP-oxalate complex of the rabbit muscle pyruvate kinase at 2.1 A resolution: ATP binding over a barrel. *Biochemistry* 37: 6247–6255, 1998.
186. **Larsen TM, Laughlin LT, Holden HM, Rayment I, and Reed GH.** Structure of rabbit muscle pyruvate kinase complexed with Mn^{2+}, K^+, and pyruvate. *Biochemistry* 33: 6301–6309, 1994.
187. **Laughlin LT and Reed GH.** The monovalent cation requirement of rabbit muscle pyruvate kinase is eliminated by substitution of lysine for glutamate 117. *Arch Biochem Biophys* 348: 262–267, 1997.
188. **Lee JH, Van Montagu M, and Verbruggen N.** A highly conserved kinase is an essential component for stress tolerance in yeast and plant cells. *Proc Natl Acad Sci USA* 96: 5873–5877, 1999.
189. **Lehn JM.** Supramolecular chemistry: receptors, catalysts, and carriers. *Science* 227: 849–856, 1985.
190. **Li MH, Kwok F, Chang WR, Lau CK, Zhang JP, Lo SC, Jiang T, and Liang DC.** Crystal structure of brain pyridoxal kinase, a novel member of the ribokinase superfamily. *J Biol Chem* 277: 46385–46390, 2002.
191. **Liao DI, Dotson G, Turner I Jr, Reiss L, and Emptage M.** Crystal structure of substrate free form of glycerol dehydratase. *J Inorg Biochem* 93: 84–91, 2003.
192. **Lifton RP, Wilson FH, Choate KA, and Geller DS.** Salt and blood pressure: new insight from human genetic studies. *Cold Spring Harbor Symp Quant Biol* 67: 445–450, 2002.
193. **Lijk LJ, Torfs CA, Kalk KH, De Maeyer MC, and Hol WG.** Differences in the binding of sulfate, selenate and thiosulfate ions to bovine liver rhodanese, and a description of a binding site for ammonium and sodium ions. An X-ray diffraction study. *Eur J Biochem* 142: 399–408, 1984.
194. **Lockless SW and Ranganathan R.** Evolutionarily conserved pathways of energetic connectivity in protein families. *Science* 286: 295–299, 1999.
195. **Lutz WK, Wipf HK, and Simon W.** Alkali-cation specificity and carrier qualities of the antibiotics nigericin and monensin. *Helv Chim Acta* 53: 1741–1746, 1970.
196. **Maathuis FJM and Amtmann A.** K^+ nutrition and Na^+ toxicity: the basis of cellular K^+/Na^+ ratios. *Ann Botany* 84: 123–133, 1999.
197. **Machius M, Chuang JL, Wynn RM, Tomchick DR, and Chuang DT.** Structure of rat BCKD kinase: nucleotide-induced domain communication in a mitochondrial protein kinase. *Proc Natl Acad Sci USA* 98: 11218–11223, 2001.
198. **Machius M, Declerck N, Huber R, and Wiegand G.** Activation of *Bacillus licheniformis* alpha-amylase through a disorder→order transition of the substrate-binding site mediated by a calcium-sodium-calcium metal triad. *Structure* 6: 281–292, 1998.
199. **Machius M, Wiegand G, and Huber R.** Crystal structure of calcium-depleted *Bacillus licheniformis* alpha-amylase at 2.2 A resolution. *J Mol Biol* 246: 545–559, 1995.
200. **Madern D, Ebel C, and Zaccai G.** Halophilic adaptation of enzymes. *Extremophiles* 4: 91–98, 2000.
201. **Maeda T, Takekawa M, and Saito H.** Activation of yeast PBS2 MAPKK by MAPKKKs or by binding of an SH3-containing osmosensor. *Science* 269: 554–558, 1995.
202. **Maeda T, Wurgler-Murphy SM, and Saito H.** A two-component system that regulates an osmosensing MAP kinase cascade in yeast. *Nature* 369: 242–245, 1994.
203. **Mäler L, Blankenship J, Rance M, and Chazin WJ.** Site-site communication in the EF-hand Ca^{2+}-binding protein calbindin D(9k). *Nature Struct Biol* 7: 245–250, 2000.
204. **Mamat B, Roth A, Grimm C, Ermler U, Tziatzios C, Schubert D, Thauer RK, and Shima S.** Crystal structures and enzymatic properties of three formyltransferases from archaea: environmental adaptation and evolutionary relationship. *Protein Sci* 11: 2168–2178, 2002.
205. **Mann KG.** Thrombin formation. *Chest* 124: 4S–10S, 2003.
206. **Marcus F and Hosey MM.** Purification and properties of liver fructose 1,6-bisphosphatase from C57BL/KsJ normal and diabetic mice. *J Biol Chem* 255: 2481–2486, 1980.
207. **Maret W.** Zinc coordination environments in proteins determine zinc functions. *J Trace Elem Med Biol* 19: 7–12, 2005.
208. **Martin VV, Rothe A, and Gee KR.** Fluorescent metal ion indicators based on benzoannelated crown systems: a green fluorescent indicator for intracellular sodium ions. *Bioorg Med Chem Lett* 15: 1851–1855, 2005.
209. **Marvin JS and Hellinga HW.** Manipulation of ligand binding affinity by exploitation of conformational coupling. *Nature Struct Biol* 8: 795–798, 2001.
210. **Mather T, Oganessyan V, Hof P, Huber R, Foundling S, Esmon C, and Bode W.** The 2.8 A crystal structure of Gla-domainless activated protein C. *EMBO J* 15: 6822–6831, 1996.
211. **Meier T, Polzer P, Diederichs K, Welte W, and Dimroth P.** Structure of the rotor ring of F-Type Na^+-ATPase from *Ilyobacter tartaricus*. *Science* 308: 659–662, 2005.
212. **Meneton P, Jeunemaitre X, de Wardener HE, and MacGregor GA.** Links between dietary salt intake, renal salt handling, blood pressure, and cardiovascular diseases. *Physiol Rev* 85: 679–715, 2005.
213. **Mengwasser KE, Bush LA, Shih P, Cantwell AM, and Di Cera E.** Hirudin binding reveals key determinants of thrombin allostery. *J Biol Chem* 280: 23997–27003, 2005.
214. **Mesecar AD and Nowak T.** Metal-ion-mediated allosteric triggering of yeast pyruvate kinase. 1. A multidimensional kinetic linked-function analysis. *Biochemistry* 36: 6792–6802, 1997.
215. **Mesecar AD and Nowak T.** Metal-ion-mediated allosteric triggering of yeast pyruvate kinase. 2. A multidimensional thermodynamic linked-function analysis. *Biochemistry* 36: 6803–6813, 1997.
216. **Minke B and Cook B.** TRP channel proteins and signal transduction. *Physiol Rev* 82: 429–472, 2002.
217. **Minta A and Tsien RY.** Fluorescent indicators for cytosolic sodium. *J Biol Chem* 264: 19449–19457, 1989.
218. **Miyata T, Aruga R, Umeyama H, Bezeaud A, Guillin MC, and Iwanaga S.** Prothrombin salakta: substitution of glutamic acid-466 by alanine reduces the fibrinogen clotting activity and the esterase activity. *Biochemistry* 31: 7457–7462, 1992.
219. **Mohri F.** A new relation between bond valence and bond distance. *Acta Crystallogr B* 56: 626–638, 2000.
220. **Monnaie D, Arosio D, Griffon N, Rose T, Rezaie AR, and Di Cera E.** Identification of a binding site for quaternary amines in factor Xa. *Biochemistry* 39: 5349–5354, 2000.
221. **Monod J, Changeux JP, and Jacob F.** Allosteric proteins and cellular control systems. *J Mol Biol* 6: 306–329, 1963.
222. **Morgunova E, Tuuttila A, Bergmann U, Isupov M, Lindqvist Y, Schneider G, and Tryggvason K.** Structure of human pro-matrix metalloproteinase-2: activation mechanism revealed. *Science* 284: 1667–1670, 1999.
223. **Mudd SH and Cantoni GL.** Activation of methionine for transmethylation. III. The methionine-activating enzyme of Bakers' yeast. *J Biol Chem* 231: 481–492, 1958.
224. **Murata K, Mitsuoka K, Hiral T, Walz T, Agre P, Heymann JB, Engel A, and Fujiyoshi Y.** Structural determinants of water permeation through aquaporin-1. *Nature* 407: 599–605, 2000.
225. **Murata T, Yamato I, Kakinuma Y, Leslie AG, and Walker JE.** Structure of the rotor of the V-type Na^+-ATPase from *Enterococcus hirae*. *Science* 308: 654–659, 2005.
226. **Myers VB and Haydon DA.** Ion transfer across lipid membranes in the presence of gramicidin A. II. The ion selectivity. *Biochim Biophys Acta* 274: 313–322, 1972.
227. **Myles T, Yun TH, Hall SW, and Leung LL.** An extensive interaction interface between thrombin and factor V is required for factor V activation. *J Biol Chem* 276: 25143–25149, 2001.
228. **Nakamura RL, Anderson JA, and Gaber RF.** Determination of key structural requirements of a K^+ channel pore. *J Biol Chem* 272: 1011–1018, 1997.
229. **Nayal M and Di Cera E.** Valence screening of water in protein crystals reveals potential Na^+ binding sites. *J Mol Biol* 256: 228–234, 1996.
230. **Neupert-Laves K and Dobler M.** The crystal structure of a K^+ complex of valinomycin. *Helv Chim Acta* 58: 432–442, 1975.

231. **Neurath H.** Evolution of proteolytic enzymes. *Science* 224: 350–357, 1984.
232. **Nielsen S, Frokiaer J, Marples D, Kwon TH, Agre P, and Knepper MA.** Aquaporins in the kidney: from molecules to medicine. *Physiol Rev* 82: 205–244, 2002.
233. **Nocek B, Chang C, Li H, Lezondra L, Holzle D, Collart F, and Joachimiak A.** Crystal structures of 1-pyrroline-5-carboxylate reductase from human pathogens *Neisseria meningitides* and *Streptococcus pyogenes*. *J Mol Biol* 354: 91–106, 2005.
234. **Nogami K, Zhou Q, Myles T, Leung LL, Wakabayashi H, and Fay PJ.** Exosite-interactive regions in the A1 and A2 domains of factor VIII facilitate thrombin-catalyzed cleavage of heavy chain. *J Biol Chem* 280: 18476–18487, 2005.
235. **Nonaka T, Fujihashi M, Kita A, Hagihara H, Ozaki K, Ito S, and Miki K.** Crystal structure of calcium-free alpha-amylase from Bacillus sp. strain KSM-K38 (AmyK38) and its sodium ion binding sites. *J Biol Chem* 278: 24818–24824, 2003.
236. **Noskov SY, Berneche S, and Roux B.** Control of ion selectivity in potassium channels by electrostatic and dynamic properties of carbonyl ligands. *Nature* 431: 830–834, 2004.
237. **O'Brien MC and McKay DB.** How potassium affects the activity of the molecular chaperone Hsc70. I. Potassium is required for optimal ATPase activity. *J Biol Chem* 270: 2247–2250, 1995.
238. **Ogunjimi AA, Briant DJ, Pece-Barbara N, Le Roy C, Di Guglielmo GM, Kavsak P, Rasmussen RK, Seet BT, Sicheri F, and Wrana JL.** Regulation of Smurf2 ubiquitin ligase activity by anchoring the E2 to the HECT domain. *Mol Cell* 19: 297–308, 2005.
239. **Oria-Hernandez J, Cabrera N, Perez-Montfort R, and Ramirez-Silva L.** Pyruvate kinase revisited: the activating effect of K^+. *J Biol Chem* 280: 37924–37929, 2005.
240. **Orthner CL and Kosow DP.** The effect of metal ions on the amidolytic acitivity of human factor Xa (activated Stuart-Prower factor). *Arch Biochem Biophys* 185: 400–406, 1978.
241. **Orthner CL and Kosow DP.** Evidence that human alpha-thrombin is a monovalent cation-activated enzyme. *Arch Biochem Biophys* 202: 63–75, 1980.
242. **Owen WG, Bichler J, Ericson D, and Wysokinski W.** Gating of thrombin in platelet aggregates by pO2-linked lowering of extracellular Ca^{2+} concentration. *Biochemistry* 34: 9277–9281, 1995.
243. **Padmanabhan K, Padmanabhan KP, Tulinsky A, Park CH, Bode W, Huber R, Blankenship DT, Cardin AD, and Kisiel W.** Structure of human des(1–45) factor Xa at 2.2 A resolution. *J Mol Biol* 232: 947–966, 1993.
244. **Page M, MacGillivray RTA, and Di Cera E.** Determinants of specificity in coagulation proteases. *J Thromb Haemost* 3: 2401–2408, 2005.
245. **Page MJ, Bleackley MR, Wong S, MacGillivray RTA, and Di Cera E.** Conversion of trypsin into a Na^+ activated enzyme. *Biochemistry* 45: 2987–2993, 2006.
246. **Paoli M, Anderson BF, Baker HM, Morgan WT, Smith A, and Baker EN.** Crystal structure of hemopexin reveals a novel high-affinity heme site formed between two β-propeller domains. *Nature Struct Biol* 6: 926–931, 1999.
247. **Papaconstantinou ME, Carrell CJ, Pineda AO, Bobofchak KM, Mathews FS, Flordellis CS, Maragoudakis ME, Tsopanoglou NE, and Di Cera E.** Thrombin functions through its RGD sequence in a non-canonical conformation. *J Biol Chem* 280: 29393–29396, 2005.
248. **Pardo JM, Reddy MP, Yang S, Maggio A, Huh GH, Matsumoto T, Coca MA, Paino-D'Urzo M, Koiwa H, Yun DJ, Watad AA, Bressan RA, and Hasegawa PM.** Stress signaling through Ca^{2+}/calmodulin-dependent protein phosphatase calcineurin mediates salt adaptation in plants. *Proc Natl Acad Sci USA* 95: 9681–9686, 1998.
249. **Patthy L.** Evolution of the proteases of blood coagulation and fibrinolysis by assembly from modules. *Cell* 41: 657–663, 1985.
250. **Patthy L.** Genome evolution and the evolution of exon-shuffling—a review. *Gene* 238: 103–114, 1999.
251. **Pauling L.** *The Nature of the Chemical Bond*. New York: Cornell Univ. Press, 1960.
252. **Pearson RG.** Hard and soft acids and bases: the evolution of a chemical concept. *Coordination Chem Rev* 100: 403–425, 1990.
253. **Pedersen CJ.** Ionic complexes of macrocyclic polyethers. *Federation Proc* 27: 1305–1309, 1968.
254. **Peracchi A, Mozzarelli A, and Rossi GL.** Monovalent cations affect dynamic and functional properties of the tryptophan synthase alpha 2 beta 2 complex. *Biochemistry* 34: 9459–9465, 1995.
255. **Perez-Miller SJ and Hurley TD.** Coenzyme isomerization is integral to catalysis in aldehyde dehydrogenase. *Biochemistry* 42: 7100–7109, 2003.
256. **Perona JJ and Craik CS.** Evolutionary divergence of substrate specificity within the chymotrypsin-like serine protease fold. *J Biol Chem* 272: 29987–29990, 1997.
257. **Perona JJ, Hedstrom L, Rutter WJ, and Fletterick RJ.** Structural origins of substrate discrimination in trypsin and chymotrypsin. *Biochemistry* 34: 1489–1499, 1995.
258. **Petrovan RJ and Ruf W.** Role of residue Phe225 in the cofactor-mediated, allosteric regulation of the serine protease coagulation factor VIIa. *Biochemistry* 39: 14457–14463, 2000.
259. **Pflughoeft KJ, Kierek K, and Watnick PI.** Role of ectoine in *Vibrio cholerae* osmoadaptation. *Appl Environ Microbiol* 69: 5919–5927, 2003.
260. **Phillies GDJ, Asher IM, and Stanley HE.** Monovalent and divalent cation complexes of the ionophorous antibiotics nonactin, monactin and dinactin. *Biophys J* 16: 81A, 1976.
261. **Pineda AO, Cantwell AM, Bush LA, Rose T, and Di Cera E.** The thrombin epitope recognizing thrombomodulin is a highly cooperative hot spot in exosite I. *J Biol Chem* 277: 32015–32019, 2002.
262. **Pineda AO, Carrell CJ, Bush LA, Prasad S, Caccia S, Chen ZW, Mathews FS, and Di Cera E.** Molecular dissection of Na^+ binding to thrombin. *J Biol Chem* 279: 31842–31853, 2004.
263. **Pinkerton M, Steinrauf LK, and Dawkins P.** The molecular structure and some transport properties of valinomycin. *Biochem Biophys Res Commun* 35: 512–518, 1969.
264. **Pitzer KS.** *Activity Coefficients in Electrolyte Solutions*. Boca Raton, FL: CRC, 1991.
265. **Posas F, Chambers JR, Heyman JA, Hoeffler JP, de Nadal E, and Arino J.** The transcriptional response of yeast to saline stress. *J Biol Chem* 275: 17249–17255, 2000.
266. **Posas F, Wurgler-Murphy SM, Maeda T, Witten EA, Thai TC, and Saito H.** Yeast HOG1 MAP kinase cascade is regulated by a multistep phosphorelay mechanism in the SLN1-YPD1-SSK1 "two-component" osmosensor. *Cell* 86: 865–875, 1996.
267. **Prasad S, Cantwell AM, Bush LA, Shih P, Xu H, and Di Cera E.** Residue Asp-189 controls both substrate binding and the monovalent cation specificity of thrombin. *J Biol Chem* 279: 10103–10108, 2004.
268. **Prasad S, Wright KJ, Roy DB, Bush LA, Cantwell AM, and Di Cera E.** Redesigning the monovalent cation specificity of an enzyme. *Proc Natl Acad Sci USA* 100: 13785–13790, 2003.
269. **Premkumar L, Greenblatt HM, Bageshwar UK, Savchenko T, Gokhman I, Sussman JL, and Zamir A.** Three-dimensional structure of a halotolerant algal carbonic anhydrase predicts halotolerance of a mammalian homolog. *Proc Natl Acad Sci USA* 102: 7493–7498, 2005.
270. **Pressman BC.** Biological applications of ionophores. *Annu Rev Biochem* 45: 501–530, 1976.
271. **Prodromou C, Roe SM, O'Brien R, Ladbury JE, Piper PW, and Pearl LH.** Identification and structural characterization of the ATP/ADP-binding site in the Hsp90 molecular chaperone. *Cell* 90: 65–75, 1997.
272. **Proft M and Serrano R.** Repressors and upstream repressing sequences of the stress-regulated ENA1 gene in *Saccharomyces cerevisiae*: bZIP protein Sko1p confers HOG-dependent osmotic regulation. *Mol Cell Biol* 19: 537–546, 1999.
273. **Prosise GL and Luecke H.** Crystal structures of *Tritrichomonas foetus* inosine monophosphate dehydrogenase in complex with substrate, cofactor and analogs: a structural basis for the random-in ordered-out kinetic mechanism. *J Mol Biol* 326: 517–527, 2003.
274. **Prosise GL, Wu JZ, and Luecke H.** Crystal structure of *Tritrichomonas foetus* inosine monophosphate dehydrogenase in complex with the inhibitor ribavirin monophosphate reveals a catalysis-dependent ion-binding site. *J Biol Chem* 277: 50654–50659, 2002.

275. **Ratnoff OD.** The evolution of hemostatic mechanisms. *Perspect Biol Med* 31: 4–33, 1987.
276. **Rawlings ND, Tolle DP, and Barrett AJ.** MEROPS: the peptidase database. *Nucleic Acids Res* 32: D160–164, 2004.
277. **Reed LJ, Damuni Z, and Merryfield ML.** Regulation of mammalian pyruvate and branched-chain alpha-keto acid dehydrogenase complexes by phosphorylation-dephosphorylation. *Curr Top Cell Regul* 27: 41–49, 1985.
278. **Rep M, Reiser V, Gartner U, Thevelein JM, Hohmann S, Ammerer G, and Ruis H.** Osmotic stress-induced gene expression in *Saccharomyces cerevisiae* requires Msn1p and the novel nuclear factor Hot1p. *Mol Cell Biol* 19: 5474–5485, 1999.
279. **Rezaie AR and He X.** Sodium binding site of factor Xa: role of sodium in the prothrombinase complex. *Biochemistry* 39: 1817–1825, 2000.
280. **Rezaie AR and Kittur FS.** The critical role of the 185–189-loop in the factor Xa interaction with Na^+ and factor Va in the prothrombinase complex. *J Biol Chem* 279: 48262–48269, 2004.
281. **Rhee S, Parris KD, Ahmed SA, Miles EW, and Davies DR.** Exchange of K^+ or Cs^+ for Na^+ induces local and long-range changes in the three-dimensional structure of the tryptophan synthase alpha2beta2 complex. *Biochemistry* 35: 4211–4221, 1996.
282. **Riddell FG and Tompsett SJ.** The transport of Na^+ and K^+ ions through phospholipid bilayers mediated by the antibiotics salinomycin and narasin studied by ^{23}Na- and ^{39}K-NMR spectroscopy. *Biochim Biophys Acta* 1024: 193–197, 1990.
283. **Rios G, Ferrando A, and Serrano R.** Mechanisms of salt tolerance conferred by overexpression of the HAL1 gene in *Saccharomyces cerevisiae*. *Yeast* 13: 515–528, 1997.
284. **Rizzuto R and Pozzan T.** Microdomains of intracellular Ca^{2+}: molecular determinants and functional consequences. *Physiol Rev* 86: 369–408, 2006.
285. **Rockwell NC and Fuller RS.** Specific modulation of Kex2/furin family proteases by potassium. *J Biol Chem* 277: 17531–17537, 2002.
286. **Rode BM, Schwenk CF, Hofer TS, and Randolf BR.** Coordination and ligand exchange dynamics of solvated metal ions. *Coordination Chem Rev* 249: 2993–3006, 2005.
287. **Romani A, Marfella C, and Scarpa A.** Cell magnesium transport and homeostasis: role of intracellular compartments. *Miner Electrolyte Metab* 19: 282–289, 1993.
288. **Rouy S, Vidaud D, Alessandri JL, Dautzenberg MD, Venisse L, Guillin MC, and Bezeaud A.** Prothrombin Saint-Denis: a natural variant with a point mutation resulting in Asp to Glu substitution at position 552 in prothrombin. *Br J Haematol* 132: 770–773, 2006.
289. **Roy DB, Rose T, and Di Cera E.** Replacement of thrombin residue G184 with Lys or Arg fails to mimic Na^+ binding. *Proteins* 43: 315–318, 2001.
290. **Sarges R, and Witkop B.** Gramicidin A. V. The structure of valine- and isoleucine-gramicidin A. *J Am Chem Soc* 87: 2011–2020, 1965.
291. **Scharer K, Morgenthaler M, Paulini R, Obst-Sander U, Banner DW, Schlatter D, Benz J, Stihle M, and Diederich F.** Quantification of cation-pi interactions in protein-ligand complexes: crystal-structure analysis of Factor Xa bound to a quaternary ammonium ion ligand. *Angew Chem Int Ed Engl* 44: 4400–4404, 2005.
292. **Schechter I and Berger A.** On the size of the active site in proteases. I. Papain. *Biochem Biophys Res Commun* 27: 157–162, 1967.
293. **Schmidt AE, Padmanabhan K, Underwood MC, Bode W, Mather T, and Bajaj SP.** Thermodynamic linkage between the S1 site, the Na^+ site, and the Ca^{2+} site in the protease domain of human activated protein C (APC). Sodium ion in the APC crystal structure is coordinated to four carbonyl groups from two separate loops. *J Biol Chem* 277: 28987–28995, 2002.
294. **Schmidt AE, Stewart JE, Mathur A, Krishnaswamy S, and Bajaj SP.** Na^+ site in blood coagulation factor IXa: effect on catalysis and factor VIIIa binding. *J Mol Biol* 350: 78–91, 2005.
295. **Schmitt AP and McEntee K.** Msn2p, a zinc finger DNA-binding protein, is the transcriptional activator of the multistress response in *Saccharomyces cerevisiae*. *Proc Natl Acad Sci USA* 93: 5777–5782, 1996.
296. **Sheng S, Perry CJ, Kashlan OB, and Kleyman TR.** Side chain orientation of residues lining the selectivity filter of epithelial Na^+ channels. *J Biol Chem* 280: 8513–8522, 2005.
297. **Shi N, Ye S, Alam A, Chen L, and Jiang Y.** Atomic structure of a Na(+)- and K(+)-conducting channel. *Nature*. In press.
298. **Shibata N, Masuda J, Morimoto Y, Yasuoka N, and Toraya T.** Substrate-induced conformational change of a coenzyme B12-dependent enzyme: crystal structure of the substrate-free form of diol dehydratase. *Biochemistry* 41: 12607–12617, 2002.
299. **Shibata N, Masuda J, Tobimatsu T, Toraya T, Suto K, Morimoto Y, and Yasuoka N.** A new mode of B12 binding and the direct participation of a potassium ion in enzyme catalysis: X-ray structure of diol dehydratase. *Structure* 7: 997–1008, 1999.
300. **Silva FP, Antunes OAC, de Alecastro RB, and De Simone SG.** The Na^+ binding channel of human coagulation proteases: novel insights on the structure and allosteric modulation revealed by molecular surface analysis. *Biophys Chem* 119: 282–294, 2006.
301. **Sintchak MD, Fleming MA, Futer O, Raybuck SA, Chambers SP, Caron PR, Murcko MA, and Wilson KP.** Structure and mechanism of inosine monophosphate dehydrogenase in complex with the immunosuppressant mycophenolic acid. *Cell* 85: 921–930, 1996.
302. **Smith GA, Hesketh TR, and Metcalfe JC.** Design and properties of a fluorescent indicator of intracellular free Na^+ concentration. *Biochem J* 250: 227–232, 1988.
303. **Smith LC, Clow LA, and Terwilliger DP.** The ancestral complement system in sea urchins. *Immunol Rev* 180: 16–34, 2001.
304. **Snyder PM.** Minireview: regulation of epithelial Na^+ channel trafficking. *Endocrinology* 146: 5079–5085, 2005.
305. **Somoza JR, Skene RJ, Katz BA, Mol C, Ho JD, Jennings AJ, Luong C, Arvai A, Buggy JJ, Chi E, Tang J, Sang BC, Verner E, Wynands R, Leahy EM, Dougan DR, Snell G, Navre M, Knuth MW, Swanson RV, McRee DE, and Tari LW.** Structural snapshots of human HDAC8 provide insights into the class I histone deacetylases. *Structure* 12: 1325–1334, 2004.
306. **Sorokin DY and Kuenen JG.** Chemolithotrophic haloalkaliphiles from soda lakes. *FEMS Microbiol Ecol* 52: 287–295, 2005.
307. **Sriram M, Osipiuk J, Freeman B, Morimoto R, and Joachimiak A.** Human Hsp70 molecular chaperone binds two calcium ions within the ATPase domain. *Structure* 5: 403–414, 1997.
308. **Stanchev h Philips M, Villoutreix BO, Aksglaede L, Lethagen S, and Thorsen S.** Prothrombin deficiency caused by compound heterozygosity for two novel mutations in the prothrombin gene associated with a bleeding tendency. *Thromb Haemost* 95: 195–198, 2006.
309. **Steiner SA, Amphlett GW, and Castellino FJ.** Stimulation of the amidase and esterase activity of activated bovine plasma protein C by monovalent cations. *Biochem Biophys Res Commun* 94: 340–347, 1980.
310. **Steiner SA and Castellino FJ.** Effect of monovalent cations on the pre-steady-state kinetic parameters of the plasma protease bovine activated protein C. *Biochemistry* 24: 1136–1141, 1985.
311. **Steiner SA and Castellino FJ.** Kinetic mechanism for stimulation by monovalent cations of the amidase activity of the plasma protease bovine activated protein C. *Biochemistry* 24: 609–617, 1985.
312. **Steiner SA and Castellino FJ.** Kinetic studies of the role of monovalent cations in the amidolytic activity of activated bovine plasma protein C. *Biochemistry* 21: 4609–4614, 1982.
313. **Süel GM, Lockless SW, Wall MA, and Ranganathan R.** Evolutionarily conserved networks of residues mediate allosteric communication in proteins. *Nature Struct Biol* 10: 59–69, 2003.
314. **Suelter CH.** Enzymes activated by monovalent cations. *Science* 168: 789–795, 1970.
315. **Sun WY, Smirnow D, Jenkins ML, and Degen SJ.** Prothrombin Scranton: substitution of an amino acid residue involved in the binding of Na^+ (LYS-556 to THR) leads to dysprothrombinemia. *Thromb Haemost* 85: 651–654, 2001.
316. **Sundararaju B, Antson AA, Phillips RS, Demidkina TV, Barbolina MV, Gollnick P, Dodson GG, and Wilson KS.** The crystal structure of *Citrobacter freundii* tyrosine phenol-lyase complexed with 3-(4′-hydroxyphenyl)propionic acid, together with site-di-

rected mutagenesis and kinetic analysis, demonstrates that arginine 381 is required for substrate specificity. *Biochemistry* 36: 6502–6510, 1997.
317. **Sundararaju B, Chen H, Shilcutt S, and Phillips RS.** The role of glutamic acid-69 in the activation of *Citrobacter freundii* tyrosine phenol-lyase by monovalent cations. *Biochemistry* 39: 8546–8555, 2000.
318. **Suttner SW and Boldt J.** Natriuretic peptide system: physiology and clinical utility. *Curr Opin Crit Care* 10: 336–341, 2004.
319. **Szwajkajzer D and Carey J.** Molecular and biological constraints on ligand-binding affinity and specificity. *Biopolymers Biospectrosc Sect* 44: 181–198, 1997.
320. **Tainer JA, Roberts VA, and Getzoff ED.** Protein metal-binding sites. *Curr Opin Biotechnol* 3: 378–387, 1992.
321. **Takusagawa F, Kamitori S, and Markham GD.** Structure and function of *S*-adenosylmethionine synthetase: crystal structures of *S*-adenosylmethionine synthetase with ADP, BrADP, and PPi at 28 angstroms resolution. *Biochemistry* 35: 2586–2596, 1996.
322. **Takusagawa F, Kamitori S, Misaki S, and Markham GD.** Crystal structure of *S*-adenosylmethionine synthetase. *J Biol Chem* 271: 136–147, 1996.
323. **Teplitsky A, Shulami S, Moryles S, Shoham Y, and Shoham G.** Crystallization and preliminary X-ray analysis of an intracellular xylanase from *Bacillus stearothermophilus* T-6. *Acta Crystallogr D Biol Crystallogr* 56: 181–184, 2000.
324. **Toney MD, Hohenester E, Cowan SW, and Jansonius JN.** Dialkylglycine decarboxylase structure: bifunctional active site and alkali metal sites. *Science* 261: 756–759, 1993.
325. **Toney MD, Hohenester E, Keller JW, and Jansonius JN.** Structural and mechanistic analysis of two refined crystal structures of the pyridoxal phosphate-dependent enzyme dialkylglycine decarboxylase. *J Mol Biol* 245: 151–179, 1995.
326. **Toraya T, Sugimoto Y, Tamao Y, Shimizu S, and Fukui S.** Propanediol dehydratase system. Role of monovalent cations in binding of vitamin B12 coenzyme or its analogs to apoenzyme. *Biochemistry* 10: 3475–3484, 1971.
327. **Tsiang M, Jain AK, Dunn KE, Rojas ME, Leung LL, and Gibbs CS.** Functional mapping of the surface residues of human thrombin. *J Biol Chem* 270: 16854–16863, 1995.
328. **Turk BE, Huang LL, Piro ET, and Cantley LC.** Determination of protease cleavage site motifs using mixture-based oriented peptide libraries. *Nat Biotechnol* 19: 661–667, 2001.
329. **Underwood MC, Zhong D, Mathur A, Heyduk T, and Bajaj SP.** Thermodynamic linkage between the S1 site, the Na^+ site, and the Ca^{2+} site in the protease domain of human coagulation factor Xa. Studies on catalytic efficiency and inhibitor binding. *J Biol Chem* 275: 36876–36884, 2000.
330. **Vanhooke JL, Thoden JB, Brunhuber NMW, Blanchard JS, and Holden HM.** Phenylalanine dehydrogenase from Rhodococcus sp. M4: high-resolution X-ray analyses of inhibitory ternary complexes reveal key features in the oxidative deamination mechanism. *Biochemistry* 38: 2326–2339, 1999.
331. **Vargas C, Kallimanis A, Koukkou AI, Calderon MI, Canovas D, Iglesias-Guerra F, Drainas C, Ventosa A, and Nieto JJ.** Contribution of chemical changes in membrane lipids to the osmoadaptation of the halophilic bacterium *Chromohalobacter salexigens*. *Syst Appl Microbiol* 28: 571–581, 2005.
332. **Vargas C and Nieto JJ.** Genetic tools for the manipulation of moderately halophilic bacteria of the family Halomonadaceae. *Methods Mol Biol* 267: 183–208, 2004.
333. **Veatch WR and Blout ER.** The aggregation of gramicidin A in solution. *Biochemistry* 13: 5257–5264, 1974.
334. **Veatch WR, Fossel ET, and Blout ER.** The conformation of gramicidin A. *Biochemistry* 13: 5249–5256, 1974.
335. **Venekei I, Szilagyi L, Graf L, and Rutter WJ.** Attempts to convert chymotrypsin to trypsin. *FEBS Lett* 383: 143–147, 1996.
336. **Viitanen PV, Lubben TH, Reed J, Goloubinoff P, O'Keefe DP, and Lorimer GH.** Chaperonin-facilitated refolding of ribulosebisphosphate carboxylase and ATP hydrolysis by chaperonin 60 (groEL) are K^+ dependent. *Biochemistry* 29: 5665–5671, 1990.
337. **Villeret V, Huang S, Fromm HJ, and Lipscomb WN.** Crystallographic evidence for the action of potassium, thallium, and lithium ions on fructose-1,6-bisphosphatase. *Proc Natl Acad Sci USA* 92: 8916–8920, 1995.
338. **Vindigni A and Di Cera E.** Role of P225 and the C136–C201 disulfide bond in tissue plasminogen activator. *Protein Sci* 7: 1728–1737, 1998.
339. **Voisin DL and Bourque CW.** Integration of sodium and osmosensory signals in vasopressin neurons. *Trends Neurosci* 25: 199–205, 2002.
340. **Vreeland RH.** Mechanisms of halotolerance in microorganisms. *Crit Rev Microbiol* 14: 311–356, 1987.
341. **Wallace BA, Veatch WR, and Blout ER.** Conformation of gramicidin A in phospholipid vesicles: circular dichroism studies of effects of ion binding, chemical modification, and lipid structure. *Biochemistry* 20: 5754–5760, 1981.
342. **Walz T, Hirai T, Murata K, Heymann JB, Mitsuoka K, Fujiyoshi Y, Smith BL, Agre P, and Engel A.** The three-dimensional structure of aquaporin-1. *Nature* 387: 624–627, 1997.
343. **Wang D, Bode W, and Huber R.** Bovine chymotrypsinogen A X-ray crystal structure analysis and refinement of a new crystal form at 1.8 A resolution. *J Mol Biol* 185: 595–624, 1985.
344. **Wang J and Boisvert DC.** Structural basis for GroEL-assisted protein folding from the crystal structure of (GroEL-KMgATP)14 at 2.0 A resolution. *J Mol Biol* 327: 843–855, 2003.
345. **Weinstein S, Wallace BA, Blout ER, Morrow JS, and Veatch W.** Conformation of gramicidin A channel in phospholipid vesicles: a ^{13}C and ^{19}F nuclear magnetic resonance study. *Proc Natl Acad Sci USA* 76: 4230–4234, 1979.
346. **Weinstein S, Wallace BA, Morrow JS, and Veatch WR.** Conformation of the gramicidin A transmembrane channel: a ^{13}C nuclear magnetic resonance study of ^{13}C-enriched gramicidin in phosphatidylcholine vesicles. *J Mol Biol* 143: 1–19, 1980.
347. **Weiss MS, Kreusch A, Schiltz E, Nestel U, Welte W, Weckesser J, and Schulz GE.** The structure of porin from *Rhodobacter capsulatus* at 1.8 A resolution. *FEBS Lett* 280: 379–382, 1991.
348. **Wells CM and Di Cera E.** Thrombin is a Na(+)-activated enzyme. *Biochemistry* 31: 11721–11730, 1992.
349. **Weyand M and Schlichting I.** Crystal structure of wild-type tryptophan synthase complexed with the natural substrate indole-3-glycerol phosphate. *Biochemistry* 38: 16469–16480, 1999.
350. **Wieland T and Faulstich H.** Amatoxins, phallotoxins, phallolysin, and antamanide: the biologically active components of poisonous Amanita mushrooms. *CRC Crit Rev Biochem* 5: 185–260, 1978.
351. **Wigley DB, Davies GJ, Dodson EJ, Maxwell A, and Dodson G.** Crystal structure of an N-terminal fragment of the DNA gyrase B protein. *Nature* 351: 624–629, 1991.
352. **Wilbanks SM and McKay DB.** How potassium affects the activity of the molecular chaperone Hsc70. II. Potassium binds specifically in the ATPase active site. *J Biol Chem* 270: 2251–2257, 1995.
353. **Wilbanks SM and McKay DB.** Structural replacement of active site monovalent cations by the epsilon-amino group of lysine in the ATPase fragment of bovine Hsc70. *Biochemistry* 37: 7456–7462, 1998.
354. **Woehl E and Dunn MF.** Mechanisms of monovalent cation action in enzyme catalysis: the first stage of the tryptophan synthase beta-reaction. *Biochemistry* 38: 7118–7130, 1999.
355. **Woehl E and Dunn MF.** Mechanisms of monovalent cation action in enzyme catalysis: the tryptophan synthase alpha-, beta-, and alpha beta-reactions. *Biochemistry* 38: 7131–7141, 1999.
356. **Woehl EU and Dunn MF.** Monovalent metal ions play an essential role in catalysis and intersubunit communication in the tryptophan synthase bienzyme complex. *Biochemistry* 34: 9466–9476, 1995.
357. **Woehl EU and Dunn MF.** The roles of Na^+ and K^+ in pyridoxal phosphate enzyme catalysis. *Coord Chem Rev* 144: 147–197, 1995.
358. **Wu Y, He Y, Moya IA, Qian X, and Luo Y.** Crystal structure of archaeal recombinase RADA: a snapshot of its extended conformation. *Mol Cell* 15: 423–435, 2004.
359. **Wu Y, Qian X, He Y, Moya IA, and Luo Y.** Crystal structure of an ATPase-active form of Rad51 homolog from Methanococcus voltae. Insights into potassium dependence. *J Biol Chem* 280: 722–728, 2005.

360. **Wynn RM, Kato M, Machius M, Chuang JL, Li J, Tomchick DR, and Chuang DT.** Molecular mechanism for regulation of the human mitochondrial branched-chain alpha-ketoacid dehydrogenase complex by phosphorylation. *Structure* 12: 2185–2196, 2004.
361. **Xu H, Bush LA, Pineda AO, Caccia S, and Di Cera E.** Thrombomodulin changes the molecular surface of interaction and the rate of complex formation between thrombin and protein C. *J Biol Chem* 280: 7956–7961, 2005.
362. **Xu J, McRae MA, Harron S, Rob B, and Huber RE.** A study of the relationships of interactions between Asp-201, Na^+ or K^+, and galactosyl C6 hydroxyl and their effects on binding and reactivity of beta-galactosidase. *Biochem Cell Biol* 82: 275–284, 2004.
363. **Yamada T, Komoto J, Takata Y, Ogawa H, Pitot HC, and Takusagawa F.** Crystal structure of serine dehydratase from rat liver. *Biochemistry* 42: 12854–12865, 2003.
364. **Yamanishi M, Yunoki M, Tobimatsu T, Sato H, Matsui J, Dokiya A, Iuchi Y, Oe K, Suto K, Shibata N, Morimoto Y, Yasuoka N, and Toraya T.** The crystal structure of coenzyme B_{12}-dependent glycerol dehydratase in complex with cobalamin and propane-1,2-diol. *Eur J Biochem* 269: 4484–4494, 2002.
365. **Yamashita A, Singh SK, Kawate T, Jin Y, and Gouaux E.** Crystal structure of a bacterial homologue of Na^+/Cl^--dependent neurotransmitter transporters. *Nature* 437: 215–223, 2005.
366. **Yamashita MM, Wesson L, Eisenman G, and Eisenberg D.** Where metal ions bind in proteins. *Proc Natl Acad Sci USA* 87: 5648–5652, 1990.
367. **Yan Y, Harper S, Speicher DW, and Marmorstein R.** The catalytic mechanism of the ESA1 histone acetyltransferase involves a self-acetylated intermediate. *Nature Struct Biol* 9: 862–869, 2002.
368. **Yancey PH.** Organic osmolytes as compatible, metabolic and counteracting cytoprotectants in high osmolarity and other stresses. *J Exp Biol* 208: 2819–2830, 2005.
369. **Yancey PH, Rhea MD, Kemp KM, and Bailey DM.** Trimethylamine oxide, betaine and other osmolytes in deep-sea animals: depth trends and effects on enzymes under hydrostatic pressure. *Cell Mol Biol* 50: 371–376, 2004.
370. **Yang W, Lee HW, Hellinga H, and Yang JJ.** Structural analysis, identification, and design of calcium-binding sites in proteins. *Proteins* 47: 344–356, 2002.
371. **Yang Z, Zhang H, Hung HC, Kuo CC, Tsai LC, Yuan HS, Chou WY, Chang GG, and Tong L.** Structural studies of the pigeon cytosolic $NADP^+$-dependent malic enzyme. *Protein Sci* 11: 332–341, 2002.
372. **Yun TH, Baglia FA, Myles T, Navaneetham D, Lopez JA, Walsh PN, and Leung LL.** Thrombin activation of factor XI on activated platelets requires the interaction of factor XI and platelet glycoprotein Ib alpha with thrombin anion-binding exosites I and II, respectively. *J Biol Chem* 278: 48112–48119, 2003.
373. **Zhang Y, Dougherty M, Downs DM, and Ealick SE.** Crystal structure of an aminoimidazole riboside kinase from *Salmonella enterica*: implications for the evolution of the ribokinase superfamily. *Structure* 12: 1809–1821, 2004.
374. **Zhao H.** Effect of ions and other compatible solutes on enzyme activity, and its implication for biocatalysis using ionic liquids. *J Mol Catalysis* 37: 16–25, 2005.
375. **Zhou Y and MacKinnon R.** Ion binding affinity in the cavity of the KcsA potassium channel. *Biochemistry* 43: 4978–4982, 2004.
376. **Zhou Y and MacKinnon R.** The occupancy of ions in the K^+ selectivity filter: charge balance and coupling of ion binding to a protein conformational change underlie high conduction rates. *J Mol Biol* 333: 965–975, 2003.
377. **Zhou Y, Morais-Cabral JH, Kaufman A, and MacKinnon R.** Chemistry of ion coordination and hydration revealed by a K^+ channel-Fab complex at 2.0 A resolution. *Nature* 414: 43–48, 2001.
378. **Zhu JK.** Plant salt tolerance. *Trends Plant Sci* 6: 66–71, 2001.